Studies on sparse optimal control and passivity-based control for nonlinear mechanical systems

Kiyoshi Hamada

Studies on sparse optimal control and passivity-based control for nonlinear mechanical systems

Kiyoshi Hamada
Department of Aeronautics and Astronautics
Kyoto University

A thesis submitted for the degree of
Doctor of Engineering

2022

Abstract

When controlling a nonlinear mechanical system such as vehicles or artificial satellites, a combination of the feedforward control and feedback control is often adopted. The feedforward control is a method of calculating the control inputs in advance, and the optimal control is classified into this control method, for example. On the other hand, the feedback control is a method in which the control inputs are calculated sequentially based on the current state, and the stabilizing control, for example, is classified into this method. When controlling a vehicle, these two methods are combined as follows; the ideal trajectory from the current location to the destination is planned using the feedforward control, and then the position and attitude of the vehicle are controlled to follow the planned trajectory by the feedback control.

As these control techniques become more widespread, more difficult control objectives have been set in various projects in recent years, and there is a need to develop control methods that can cope with these objectives. For example, in the example mentioned above, it is required to generate a trajectory that is easy to follow and to control the position and posture so that there is no deviation from the generated trajectory while suppressing the wobbling. In order to achieve such difficult objectives, it is necessary to improve the performance of, for example, the optimal control method used for trajectory generation and the stabilizing control method for trajectory tracking.

This thesis focuses especially on sparse optimal control methods and passivity-based stabilizing control methods and makes some proposals to improve the performance of these control methods. The first part of this thesis deals with the sparse optimal control that is one of the feedforward control techniques and has the property that the control input is zero in large part, that is, sparse. While this method has the advantage of minimizing energy consumption, it has the problem that it is difficult to calculate the optimal input when the system is nonlinear. This thesis proposes several new methods for computing sparse optimal inputs to conquer this difficulty. The proposed methods provide conditions for computing the input reliably for a given control objective. This thesis also proposes an application of a sparse optimal control method to the problem of generating a trajectory that is easy to track. The second part of this thesis deals with the passivity-based stabilizing control, one of the feedback control methods. The passivity-based control stabilizes the system at the desired state by designing the controller so that the energy of the system monotonically decreases. This method is applicable to a wide range of nonlinear mechanical systems but has the problem that it is difficult to adjust the output response of the system. To solve this problem, this thesis proposes new passivity-based controllers that make it possible to tune the output response through a frequency analysis approach. Numerical simulations and experimental results listed in this thesis show that those proposals improve the practicality of the optimal control and stabilizing control techniques and thus make it possible to achieve challenging control objectives.

Acknowledgements

First of all, I would like to express my gratitude to Mori Manufacturing Research and Technology Foundation for financial support. Further, I would like to thank my patient supervisors, Professor Kenji Fujimoto and Associate Professor Ichiro Maruta, who have supported my research with valuable advice and guidance. I would also like to thank Prof. Jacquelien Scherpen at the University of Groningen for her helpful discussions, advice, and support on my research activities in the Netherlands. I am grateful to Prof. Kei Senda and Prof. Toshiyuki Otsuka for their various advice in preparing this thesis.

I would also like to express my deepest gratitude to Dr. Pablo Borja, who helped me with my research during my stay in the Netherlands. He patiently guided me with his superior intelligence and warm spirit. Without his help, I would not have been able to complete my Ph.D. program. I would also like to thank Anne Peters and her family for their support during my stay in the Netherlands. They were really kind to me and exposed me to new values. I am also grateful to Dr. Hamamoto and Mr. Nakamura at Kajima Technical Research Institute and Dr. Takei at Japan Aerospace Exploration Agency for their valuable discussions and suggestions. I would also like to thank my friends I met in this program, Assistant Professor Iori at Osaka University, Mr. Ito, Mr. Shengbing. Discussions with these excellent people motivated me to do research and gave me a lot of knowledge. I would also like to express my gratitude to Mr. Beppu and Mr. Kuyama, my friends from my undergraduate days. They have helped me both in private and public life. I would also like to thank the lab members, family, relatives, and many friends.

Finally, I would like to thank my grandfather and Mr. Fujioka for showing me the way to become a researcher, my friend Ms. Ayaka Kawashima for pushing me to study at Kyoto University, and Ms. Kazue Ueta and Mr. Kotaro Yamada for constantly encouraging me. Without them, I would not have been able to come this far.

Contents

List of Figures

Notation

Symbols	Meanings
$\mathbb{Z}_+$	Set of positive integers
$\mathbb{R}_+$	Set of positive real numbers
$0_{n\times m}$	Zero matrix of size $n \times m$
I_n	Identity matrix of size $n \times n$
b_i	The i-th element of a vector b
$B_{i,j}$	The (i, j)-th element of a matrix B
B_i	The (i, i)-th element of a matrix B
$\mathrm{diag}(B_i)_{i=1}^n$	A diagonal matrix B, where $(B_i)_{i=1}^n = (B_1, \cdots, B_n)$
$\lvert a\rvert$	Absolute value of a scalar a
$\lVert b\rVert$	The Euclidean norm of a vector b
$\lVert b\rVert_1$	ℓ^1-norm of a vector b
$\lVert b\rVert_\infty$	ℓ^∞-norm of a vector b
$\lVert b\rVert_B^2 := b^\top Bb$	The Euclidean norm of a vector b weighted by a matrix B
$\lVert B\rVert_p$	Induced norm of a matrix B with respect to the ℓ^p-norm
$\min(b)$	Minimum element of the vector b
$\max(b)$	Max element of the vector b
$\mathrm{null}(B)$	Null space of a matrix B
$\mathcal{L}\left[f(t)\right]$	Laplace transformation of a function $f(t) : \mathbb{R} \to \mathbb{R}^n$, $n \in \mathbb{Z}_+$
$f_i(x)$	The i-th component of a vector-valued function $f(x) : \mathbb{R}^n \to \mathbb{R}^m$, $n, m \in \mathbb{Z}_+$
$\nabla_x f(x)$	Vector-valued function whose i-th component is $\partial f(x)/\partial x_i$

Chapter 1

Introduction

When controlling nonlinear mechanical systems, we often combine the feedforward control and feedback control to achieve control objectives. For example, when controlling a vehicle, a trajectory is calculated in advance using feedforward control, and the position and posture of the vehicle are controlled to follow the trajectory using feedback control.

In recent years, control objectives have become more complex, and therefore, it is necessary to improve the performance of control methods. For example, in controlling a vehicle, it is required to achieve complex objectives such as generating a trajectory that is easy for the vehicle to follow and then controlling the vehicle to follow the trajectory without wobbling and deviation. To satisfy such complex requirements, it is essential to improve the performance of both feedforward and feedback control. With the aim of improving the performance of each control technique, this thesis focuses on the finite-time sparse optimal control, which is one of the feedforward control techniques, and the passivity-based stabilizing control, which is one of the feedback control techniques.

1.1 Numerical solution methods for sparse optimal control problems

Finite-time optimal control is one of the feedforward control methods, where the inputs are designed to minimize a given cost function. A wide range of control methods, such as robust optimal control [1, 2] and model predictive control [3, 4], is based on the optimal control method. In the application of the optimal control, it is necessary to calculate the input by solving an optimal control problem in advance. In recent years, the application of sparse optimal control to nonlinear mechanical systems has become popular, and research has been conducted on methods for calculating such optimal control inputs [5, 6, 7]. Sparse optimal control has the advantage of reducing fuel consumption because its input becomes sparse, i.e., zero in large part, but has the disadvantage that it is difficult to compute the input. The first part of this thesis is devoted to numerical solution methods for sparse optimal control problems to conquer this difficulty.

In the nonlinear case, finite-time optimal control problems are difficult to solve analytically, so most of those problems are solved numerically. Numerical solution methods for optimal control problems are basically classified into direct and indirect methods [8]. The direct method obtains a solution by directly updating the input and state variables so that the value of the evaluation function given in advance is minimized [9, 10, 11, 7, 12]. On the other hand, the indirect method converts the optimal control problem into a problem in finding solutions to ordinary differential equations by using first-order optimality conditions [13, 14, 15, 16, 17, 6]. The direct method has the advantage that constraints are easy to consider but has the disadvantage of the high space complexity, that is, the algorithm requires a lot of memory space for the computation. On the other hand, the indirect method has the advantage of reducing the space complexity by converting the original optimal control problem into an initial value problem, but it has the disadvantage of increasing the time complexity, the computer time required to execute the algorithm. This is because the algorithm in this method involves integral computation. Both methods are widely used, and various methods have been proposed in these frameworks in recent years. However, it is still difficult to solve nonlinear sparse optimal control problems with existing methods. This thesis proposes new numerical solution methods for solving difficult optimal control problems like sparse optimal control problems.

First, we propose a new continuation method based on the shooting method in the framework of the indirect method. The shooting method is often used to solve optimal control problems as initial value problems, and it has the advantage of reducing the space complexity. In the shooting method, an estimate of the solution is given first, and then the solution is obtained by updating the estimate. The problem is that if the difference between the given estimate and the true solution is not less than a certain value, that is, if the estimate is not within the convergence region, the result of the updates will not converge to the true solution. Especially in the case of difficult optimal control problems such as sparse optimal control problems, the convergence region becomes small and it becomes difficult to find the solution with the shooting method. To make up for this disadvantage, the shooting method is often combined with the continuation method. The continuation method considers a parametrized optimal control problem. The problem is designed so that its convergence region is relatively large when the parameter is zero and it matches the original problem when the parameter is one. The idea of the continuation method is to solve the problem iteratively while gradually changing the parameter from 0 to 1. The specific algorithm is as follows. First, a simple optimal control problem with the parameter 0 is solved, and its solution is saved. Since the convergence region of this problem is large, it is easy to find the solution. Then, modify the problem slightly by setting the parameter closer to 1 and solve the transformed problem using the previously obtained solution as the estimate. If the deformation of the parameter is small, it is expected that the solution to the problem before deformation and the solution to the problem after deformation will be close. Therefore, by performing the above procedure while repeating small deformations, it is possible to give an estimate that always falls within the convergence region. Various versions of continuation methods have been proposed [11, 18, 19, 20, 21, 22, 23, 24, 25], but in those existing methods, the relationship between how to deform the parameter and the closeness of the solutions before and after the deformation is unknown. Thus there are no clear guidelines for the deformation. To conquer this difficulty, we propose a locally deforming continuation method, in which the relationship between the deformation of the parameter and the closeness of the solutions is explicitly given. In the proposed method, the problem is transformed locally during the iterations of the continuation method, and the upper bound of the difference of the solutions before and after the deformation is given as a function of the continuation parameter. In other words, the proposed method shows how to deform the continuation parameter to bring the solutions before and after the deformation closer together.

Next, we propose a new numerical solution method in the framework of the direct method for the nonlinear sparse optimal control problem, which is one of the difficult optimal control problems. Several methods have been proposed for this problem [11, 7, 12, 6], but the convergence of the algorithms is not discussed much in those papers. Recently, for solving such problems, the sparse Newton method has been proposed [26], which guarantees the quadratic convergence of the algorithm. However, this method does not guarantee the ℓ^1-optimality of the inputs. In this thesis, we propose a modified version of this method that guarantees quadratic convergence of the algorithm and ℓ^1-optimality of the inputs.

Finally, an application of the sparse optimal control to a trajectory generation problem is presented to illustrate the importance of solving nonlinear sparse optimal control problems. In an autonomous driving system, a vehicle moves autonomously by tracking a trajectory generated beforehand, and thus generating a trajectory that is easy to follow is essential. A circular-clothoid trajectory is one of the trajectories that are easy to track, and a lot of trajectory planning methods use it [27, 28, 29]. In some conventional methods for generating a circular-clothoid trajectory [30, 31], a designer has to specify waypoints appropriately first. Then the trajectory is generated so that it passes through the specified waypoints. In addition, the velocity of the generated trajectory changes discontinuously at the turning points where the vehicle changes the direction of travel. This thesis proposes a new method to generate a circular-clothoid trajectory using the L^1/L^2-optimal control, one of the sparse optimal control techniques. The proposed method is superior in that it does not require specifying waypoints and that the velocity changes continuously at the turning point of the generated trajectory where the vehicle switches the direction of travel.

1.2 Tuning methods for passivity-based controllers

Passivity-based control (PBC) is one of the feedback control methods for nonlinear systems and has proven to be suitable to stabilize a variety of mechanical systems represented in the port-Hamiltonian (pH) framework [32, 33]. The second part of this thesis is devoted to the tuning method for PBC that stabilizes nonlinear mechanical pH systems.

The port-Hamilton framework is characterized by its explicit representation of physical phenomena and concepts such as energy, interconnection patterns, and dissipation, which may provide some intuition to ease the analysis of the system and the control design process. Due to the energy-based nature of the pH models, the PBC technique is often used to develop stabilizing controllers for pH systems [34]. In the PBC technique, the controller is designed by using the energy of the system as a Lyapunov function candidate according to the following steps. First, the energy of the system is shaped to move the equilibria of the closed-loop system to the target value, and then the damping is injected via the controller so that the shaped energy always decays except for at the designated equilibria. The advantage of the passivity-based control is that the stabilizing controller can be designed easily by this procedure. There are many applications of passivity-based control [35, 36, 37, 38, 39, 40, 41]. However, most of the existing PBC methods focus only on stabilization and do not provide clear guidance on how to adjust the gain of the controller. As an answer to this problem, this thesis proposes passivity-based controllers that can be interpreted as compensators such as lag compensators and lead-lag compensators. The proposed controller can be tuned in the frequency domain to reduce steady-state errors or suppress oscillations while ensuring the stability of the closed-loop system. The effectiveness of the proposed controllers is confirmed through experiments and numerical simulations on a planar manipulator.

1.3 Outline and contributions

This thesis is divided into two main parts. The first part focuses on the sparse optimal control, one of the feedforward control techniques, and consists of Chapters 2-4 that propose several numerical solution methods for the optimal control problems and some applications of sparse optimal control. These chapters deal with finite-time sparse optimal control problems for nonlinear systems with boundary conditions imposed on the initial and final states. In Chapter 2, a new continuation method, the locally deforming continuation method, is proposed in the framework of the indirect method. Chapter 3 proposes a new direct method, the modified sparse Newton method that ensures quadratic convergence and ℓ^1-optimality of the inputs, for sparse optimal control problems that are particularly difficult to solve. In Chapter 4, applications of sparsity-based optimal control methods are presented. The second part consists of Chapters 5 and 6 that propose new passivity-based controllers in the framework of feedback control techniques. In these chapters, we propose passivity-based compensators for nonlinear mechanical systems represented in the pH framework. In Chapter 5, we propose a passivity-based lag compensator that guarantees stability under input constraints without velocity measurements. In Chapter 6, we generalize the result of Chapter 5 and propose higher-order compensators based on passivity. The results obtained in these chapters improve the practicality of the feedforward and feedback control and enable the achievement of challenging control tasks. The remaining part of this section introduces the contributions of each chapter.

Chapter 2 - Locally deforming continuation method This chapter proposes a new continuation method based on the shooting method as a numerical solution method for optimal control problems. In the proposed method, the cost function of an optimal control problem is locally deformed to find the solution of the problem in a stable way. In addition, this chapter gives an analytical relation between the variation of the continuation parameter and the proximity of the solutions before and after deformation. The obtained relation provides guidelines on how to deform the continuation parameter. The effectiveness of this method is confirmed through numerical examples.

Chapter 3 - Modified sparse newton method This chapter proposes an algorithm classified into direct methods for solving nonlinear ℓ^1-optimal control problems based on a newton method. In the proposed algorithm, the inputs are updated according to the Newton method so that the boundary conditions are satisfied. Since the equation that an update direction must satisfy is underdetermined, there are multiple candidates for the direction. By choosing the direction that minimizes the ℓ^1-norm of the inputs among those candidates, the algorithm finds ℓ^1-optimal inputs satisfying the boundary conditions. The proposed algorithm has quadratic convergence. To demonstrate the effectiveness of the method, the proposed method is applied to a trajectory generation problem of a nonlinear system.

Chapter 4 - Circular-clothoid trajectory generation method This chapter introduces an example of the application of a kind of sparse optimal control. In this chapter, L^1/L^2-optimal control, a control method based on the sparse optimal control is applied to generate a vehicle trajectory whose curvature and velocity continuously change while both are piecewise constant in large part. The generated trajectory is called a circular-clothoid trajectory defined as the trajectory connecting circular curves with clothoid curves, which is easy to track. The effectiveness of the proposed method is confirmed through some examples.

Chapter 5 - Passivity-based lag-compensator with input saturation This chapter proposes a passivity-based control technique, where the resulting controllers can be interpreted as lag-compensators for nonlinear mechanical pH systems. The proposed method considers a dynamic controller whose frequency properties can be expressed in terms of a transfer function, that is, the controller gains can be tuned through a frequency analysis approach. The proposed controllers can reduce the steady-state error without velocity measurements, and they can cope with input saturation. The applicability of the proposed method is illustrated through some experiments with a planar manipulator.

Chapter 6 - Passivity-based high-order compensator This chapter generalizes the results of chapter 6 and proposes passivity-based control techniques, where the resulting controllers include the entire class of dynamic output feedback controllers that preserve the port-Hamiltonian structure and do not require velocity measurements. The proposed controller can be interpreted as a high-order compensator, and thus the gains can be tuned through a frequency analysis approach so that the steady-state errors and the oscillations are suppressed. The applicability of the proposed method is confirmed through a numerical simulation.

Chapter 7 - Conclusions In this chapter, we provide the conclusion and give suggestions for future works.

Chapter 2

Locally Deforming Continuation Method Based on a Shooting Method

This chapter proposes a new continuation method with a shooting method in the framework of the indirect method. In the indirect method, the optimal control problem is replaced by a two-point boundary value problem (TPBVP), and the TPBVP is solved numerically [13]. The shooting methods are one of the most popular indirect methods. Since the shooting methods solve the TPBVP as an initial value problem, the search parameters are only the initial values, and thus the computational complexity is very small. However, there is a disadvantage that the convergence region is small, and therefore a good estimate of the solution has to be given beforehand in the shooting methods. The continuation method is one of the ways to mitigate this difficulty.

The continuation method is a method to solve a difficult problem by iteratively deforming the problem continuously with a continuation parameter, and various methods have been proposed [11, 18, 19, 20, 21, 22, 23, 24, 25]. The idea of the method is to find a solution in a stable way by using the solution before deformation as an initial guess of the solution after deformation. In the method, an easy optimal control problem is set up and solved first. Next, the cost function of the easy problem is deformed slightly towards the original problem, and the deformed optimal control problem is solved by using the previously obtained solution as an initial guess. By repeating this procedure and transforming the problem into the original problem at the end, the solution of the original problem is obtained. If each deformation is small, the solutions before and after a deformation are expected to be close enough, hence the method can solve the original problem in a stable way. The continuation method is widely used for solving various difficult problems such as obstacle avoidance problems [42], model predictive control problems [43], and sparse optimal control problems like an L^1/L^2-optimal control problem [44]. However, there is no continuation method that is effective for all problems, and it is unclear how the change of the cost function affects the closeness of the solutions before and after the deformation in those conventional methods.

In this chapter, we propose a new continuation method, named a locally deforming continuation method, based on a shooting method. The idea of this method is to transform the cost function of the optimal control problem locally during the iterations of the continuation method. In addition, we provide a relation between the variation of the continuation parameter and the closeness of the solutions before and after the deformation in the form of an upper bound of the errors in the shooting method. This relation gives clear guidance on how to change the continuation parameter during the algorithm for stably solving relatively difficult problems.

The rest of this chapter is organized as follows. In Section 2.1, we introduce the problem formulation, and in Section 2.2, we briefly revisit some previous results. Next, Section 2.3 proposes the locally deforming continuation method and a modified shooting method, and the results of our method are illustrated in Section 2.4. We summarize this chapter in Section 2.5.

2.1 Problem setting

Here we treat the optimal control problem to find the input which minimizes the cost function

$$J = \int_0^{t_\mathrm{f}} l(x(t), u(t), t)\mathrm{d}t, \tag{2.1.1}$$

subject to the following dynamics and input constraints

$$\begin{aligned} &\frac{\mathrm{d}x(t)}{\mathrm{d}t} = f(x(t)) + g(x(t))u(t), && (2.1.2)\\ &x(0) = x^0,\ x(t_\mathrm{f}) = x^\mathrm{f}, && (2.1.3)\\ &|u_i(t)| \leq u_{\mathrm{b},i},\ (i = 1, \cdots, m), && (2.1.4)\end{aligned}$$

where $x \in \mathbb{R}^n$ is the state vector, $u \in \mathbb{R}^m$ is the input vector, $u_\mathrm{b} \in \mathbb{R}^m$ is a positive constant vector, $t_\mathrm{f} \in \mathbb{R}_+$ is a terminal time, $x^0 \in \mathbb{R}^n$ is an initial state vector, $x^\mathrm{f} \in \mathbb{R}^n$ is a terminal state vector, $f : \mathbb{R}^n \to \mathbb{R}^n$, $g : \mathbb{R}^n \to \mathbb{R}^{n\times m}$, and $l : \mathbb{R}^n \times \mathbb{R}^m \times \mathbb{R} \to \mathbb{R}_+$. In this chapter, it is assumed that l is continuously differentiable for x. This chapter also assumes that $f(x) + g(x)u$ is continuously differentiable for x and u. If the dynamics (2.1.2) is nonlinear, the input cannot be obtained analytically in general. There are several ways to solve the problem, and these methods are mainly classified into the direct method or the indirect method. In this study, we use a shooting method classified into the indirect method for solving this problem.

When the cost is the L^1 norm of the input, the problem becomes a sparse optimal control problem, and the resulting optimal control input is sparse, i.e., the L^0 norm of the input is much smaller than t_f [44]. However, in the case of nonlinear systems, problems such as L^1-optimal control problems are challenging to solve. The continuation method is one of the techniques to overcome this difficulty. The next section briefly reviews the conventional method.

2.2 Preliminaries

This section briefly reviews an existing indirect method to solve an optimal control problem with a shooting method.

2.2.1 Transformation of the optimal control problem

Define a Hamiltonian function as follows.

$$\begin{aligned} H(x(t),\lambda(t), u(t), t) &= l(x(t), u(t), t) \\ &\quad + \lambda(t)^\top (f(x(t)) + g(x(t))u(t)), \end{aligned} \tag{2.2.1}$$

It follows from Pontryagin's minimum principle that the optimal control problem with (2.1.1)-(2.1.4) is reduced to a problem of solving the following simultaneous differential equation

$$\frac{\mathrm{d}x(t)}{\mathrm{d}t} = \frac{\partial H(x(t), \lambda(t), u^*(t), t)}{\partial \lambda(t)}, \tag{2.2.2}$$

$$\frac{\mathrm{d}\lambda(t)}{\mathrm{d}t} = -\frac{\partial H(x(t), \lambda(t), u^*(t), t)}{\partial x(t)}, \tag{2.2.3}$$

$$u^*(t) = \underset{u(t)}{\mathrm{argmin}}\ H(x(t), \lambda(t), u(t), t), \tag{2.2.4}$$

$$\text{s.t.(2.1.3) and (2.1.4),}$$

with $\lambda(t) \in \mathbb{R}^n$ that is the costate of $x(t)$ [45, 46, 47]. This problem is called a TPBVP. Assume that (2.2.4) can be rewritten as the following by using a function of $x(t)$, $\lambda(t)$, and t.

$$u^*(t) = f_u(x(t), \lambda(t), t), \tag{2.2.5}$$

where $f_u : \mathbb{R}^n \times \mathbb{R}^n \times \mathbb{R} \to \mathbb{R}^m$ and $u^*(t)$ is Lebesgue measurable. In this case, the TPBVP is rewritten as follows with $\xi(t) = (x(t)^\top, \lambda(t)^\top)^\top$.

$$\begin{aligned} &\text{Find } x(t) \text{ and } \lambda(t),\ t \in [0, t_\mathrm{f}] \text{ satisfying} \\ &\frac{\mathrm{d}\xi}{\mathrm{d}t} = \left.\begin{pmatrix} \frac{\partial H(x,\lambda,u,t)}{\partial \lambda} \\ -\frac{\partial H(x,\lambda,u,t)}{\partial x} \end{pmatrix}\right|_{u=f_u(x,\lambda,t)} =: F(\xi, t), \\ &\text{(2.1.3) and (2.1.4).} \end{aligned} \tag{2.2.6}$$

Here the defined function F is $F : \mathbb{R}^{2n} \times [0, t_\mathrm{f}] \to \mathbb{R}^{2n}$. There are several ways to solve this TPBVP, such as the shooting methods and the collocation methods. Among them, the shooting methods have an advantage that the number of the search parameters is small. The next section briefly explains a standard shooting method.

2.2.2 Shooting method

If $x(0)$ and $\lambda(0)$ are given, $x(t), \lambda(t)$ satisfying (2.2.6) is uniquely determined. The shooting method takes advantage of this property and treats the TPBVP as an initial value problem. Since $x(0)$ is already given as the boundary condition, the method searches for $\lambda(0)$ that satisfies

$$\epsilon_x := x(t_\mathrm{f}) - x^\mathrm{f} = 0,\ \text{(2.2.6) and } \ x(0) = x^0. \tag{2.2.7}$$

Define the solution of the problem as $\lambda^*(0)$. In the algorithm, an initial guess of the solution $\lambda^*(0)$ is given as λ^g, and then update $\lambda(0)$ so that the error $\|\epsilon_x\|$ decreases. The difficulty of this method is that the error cannot be reduced to 0 if the initial guess λ^g is far from $\lambda^*(0)$. One of the way to mitigate this difficulty is to apply the continuation method. In the continuation method, a relatively easy optimal control problem is solved first. Then, the cost function is slightly changed towards the original problem, and solve the changed problem by using the previous solution as the initial guess. Since the previous solution is expected to be close to the solution of the current problem, the shooting method successfully finds the solution with the given initial guess. Iterating this procedure, and finally we can obtain the solution of the original problem. There are several continuation methods for solving an optimal control problem [11, 18, 19, 20, 21, 22, 23, 24, 25]. However, there is no continuation method that is effective for all problems, and it is unclear how the change of the cost function affects the closeness of the solutions before and after the deformation in those conventional methods.

This chapter proposes a new continuation method based on a shooting method and analyzes the relation between the variation of the continuation parameter and the deviation of the initial estimate from the solution. This relation gives a clear guidance on how to change the continuation parameter during the algorithm for stably solving relatively difficult problems. The next section explains the proposed method.

2.3 Proposed method

The proposed method solves the problem iteratively by successively transforming the problem from a relatively easy one to the original problem, in the same way as the existing methods. The characteristic feature of the proposed method is that the cost function is locally deformed during the iterations. Define the cost function of a relatively easy problem as

$$J_{\mathrm{E}} := \int_0^{t_{\mathrm{f}}} l^{\mathrm{E}}(x(t), u(t), t)\mathrm{d}t, \tag{2.3.1}$$

and define the cost function of the original problem as

$$J_{\mathrm{O}} := \int_0^{t_{\mathrm{f}}} l^{\mathrm{O}}(x(t), u(t), t)\mathrm{d}t, \tag{2.3.2}$$

with $l^{\mathrm{E}}(x(t), u(t), t) \in \mathbb{R}_+$ and $l^{\mathrm{O}}(x(t), u(t), t) \in \mathbb{R}_+$. Basically, the previous continuation method gradually changes the cost function by transforming the continuation parameter c from zero to one, where the cost function is defined as

$$\bar{J}_c := \int_0^{t_{\mathrm{f}}} (1-c)l^{\mathrm{E}}(x(t), u(t), t) + cl^{\mathrm{O}}(x(t), u(t), t)\mathrm{d}t. \tag{2.3.3}$$

In our new method, we define a cost function as

$$J_c := \int_0^{t_{\mathrm{f}}} l(x(t), u(t), t, c)\mathrm{d}t. \tag{2.3.4}$$

The function $l(x(t), u(t), t, c)$ is defined as

$$l(x(t), u(t), t, c) = \begin{cases} l^{\mathrm{E}}(x(t), u(t), t) & t \le c, \\ l^{\mathrm{C}}(x(t), u(t), t) & c \le t \le c+h, \\ l^{\mathrm{O}}(x(t), u(t), t) & c+h \le t, \end{cases} \tag{2.3.5}$$

with a scalar $h > 0$. Here $l^{\mathrm{C}}(x(t), u(t), t, c) \in \mathbb{R}_+$ satisfies

$$\begin{aligned} &l^{\mathrm{C}}(x(c), u(c), c) = l^{\mathrm{E}}(x(c), u(c), c), \\ &l^{\mathrm{C}}(x(c+h), u(c+h), c+h) = l^{\mathrm{O}}(x(c+h), u(c+h), c+h), \end{aligned}$$

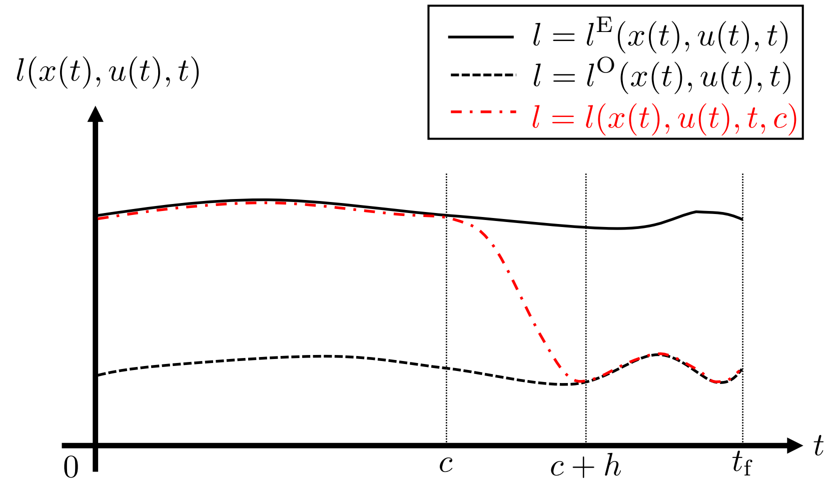

Figure 2.1: Cost function of the proposed method

and continuously differentiable for x. Figure 2.1 shows an example of the shape of $l^{\mathrm{E}}(x(t),u(t),t)$, $l^{\mathrm{O}}(x(t),u(t),t)$, and $l(x(t),u(t),t,c)$, where the horizontal axis is time and the vertical axis is the value of the function $l(x(t),u(t),t)$. The black solid line shows $l^{\mathrm{E}}(x(t),u(t),t)$, the black dotted line shows $l^{\mathrm{O}}(x(t),u(t),t)$, and the red dash-dotted line shows $l(x(t),u(t),t,c)$. Note that $J_c = J_{\mathrm{E}}$ when $c \geq t_{\mathrm{f}}$, and $J_c = J_{\mathrm{O}}$ when $c \leq -h$. Our new continuation method transforms the cost function locally by changing the value of c. Note that we assume that each optimal control problem transformed iteratively has a solution. In the following, we define the solution of the optimal control problem with the cost function (2.3.4) as $x^{J_c}(t)$, $\lambda^{J_c}(t)$, and $u^{J_c}(t)$ for $t \in [0, t_{\mathrm{f}}]$. The next section explains a shooting method used in the proposed continuation method. In the shooting method, the condition (2.2.7) is modified.

2.3.1 Modified shooting method

Define a Hamiltonian function as

$$\begin{aligned} H_c(x(t),&\lambda(t),u(t),t) = l(x(t),u(t),t,c) \\ &+ \lambda^{\top}(f(x(t)) + g(x(t))u(t)), \end{aligned} \tag{2.3.6}$$

for the optimal control problem defined in the previous section. Then, from the Pontryagin's minimum principle, $x(t)$, $\lambda(t)$, and $u(t)$ minimizing J_c satisfy

$$\frac{\mathrm{d}\xi}{\mathrm{d}t} = \left.\begin{pmatrix} \frac{\partial H_c(x,\lambda,u,t)}{\partial \lambda} \\ -\frac{\partial H_c(x,\lambda,u,t)}{\partial x} \end{pmatrix}\right|_{u=f_u^c(x,\lambda,t)} =: F_c(\xi,t), \tag{2.3.7}$$

(2.1.3) and (2.1.4).

with the function $f_u^c : \mathbb{R}^n \times \mathbb{R}^n \times \mathbb{R} \to \mathbb{R}^m$ derived from

$$u^*(t) = \underset{u(t)}{\operatorname{argmin}}\ H_c(x(t), \lambda(t), u(t), t). \tag{2.3.8}$$

Here we modify the shooting method in Section 2.2 as in the following definition.

Definition 2.3.1. *Modified shooting method: Find* $\lambda(0)$ *and* $\lambda(t_{\mathrm{f}})$ *that satisfy*

$$\|\epsilon_{J_c}(t_{\mathrm{mid}})\| = 0, \tag{2.3.9}$$

for the error $\epsilon_{J_c}(t_{\mathrm{mid}})$ *defined as*

$$\begin{aligned}\epsilon_{J_c}(t_{\mathrm{mid}}) :=& \int_0^{t_{\mathrm{mid}}} F_c(\xi_{c,+}(t), t)\mathrm{d}t + \xi(0)\\ &- \left(\int_{t_{\mathrm{f}}}^{t_{\mathrm{mid}}} F_c(\xi_{c,-}(t), t)\mathrm{d}t + \xi(t_{\mathrm{f}})\right),\end{aligned} \tag{2.3.10}$$

with

$$\xi(0) = \begin{pmatrix} x^0 \\ \lambda(0) \end{pmatrix},\ \xi(t_f) = \begin{pmatrix} x^{\mathrm{f}} \\ \lambda(t_{\mathrm{f}}) \end{pmatrix}. \tag{2.3.11}$$

Here $t_{\mathrm{mid}} \in [0, t_{\mathrm{f}}]$*, and* $\xi_{c,+}(t)$ *and* $\xi_{c,-}(t)$ *are defined as*

$$\xi_{c,+}(t) := \int_0^t F_c(\xi_{c,+}(s), s)\mathrm{d}s + \xi(0), \tag{2.3.12}$$

$$\xi_{c,-}(t) := \int_{t_{\mathrm{f}}}^t F_c(\xi_{c,-}(s), s)\mathrm{d}s + \xi(t_{\mathrm{f}}). \tag{2.3.13}$$

The difference between this method and the shooting method introduced in Section 2.2 is that there are two parameters to search for, not only $\lambda(0)$ but also $\lambda(t_{\mathrm{f}})$, and the boundary conditions are the continuity of $x(t)$ and $\lambda(t)$ at $t = t_{\mathrm{mid}}$. When the initial guess of the solution is different from the solution, $\|\epsilon_{J_c}(t_{\mathrm{mid}})\|$ takes a value greater than zero, and if the norm of the error is sufficiently small for the initial guess, the guess is expected to be close enough to the solution. We define the error for the initial guess as "initial error".

Definition 2.3.2. *Define the initial guess of* $\lambda(0)$ *and* $\lambda(t_{\mathrm{f}})$ *as* λ_0^{g} *and* $\lambda_{\mathrm{f}}^{\mathrm{g}}$*, respectively. The corresponding initial error* $\epsilon_{J_c}^{\mathrm{I}}(t_{\mathrm{mid}})$ *is defined as*

$$\epsilon_{J_c}(t_{\mathrm{mid}}) \textit{ given by } (2.3.10) \textit{ with } \xi(0) = \begin{pmatrix} x^0 \\ \lambda_0^{\mathrm{g}} \end{pmatrix},\ \xi(t_f) = \begin{pmatrix} x^{\mathrm{f}} \\ \lambda_{\mathrm{f}}^{\mathrm{g}} \end{pmatrix}.$$

In the next section, we explain the new continuation method and provides a clear relation between the variation of the continuation parameter c and the initial error $\|\epsilon_{J_c}^{\mathrm{I}}(t_{\mathrm{mid}})\|$.

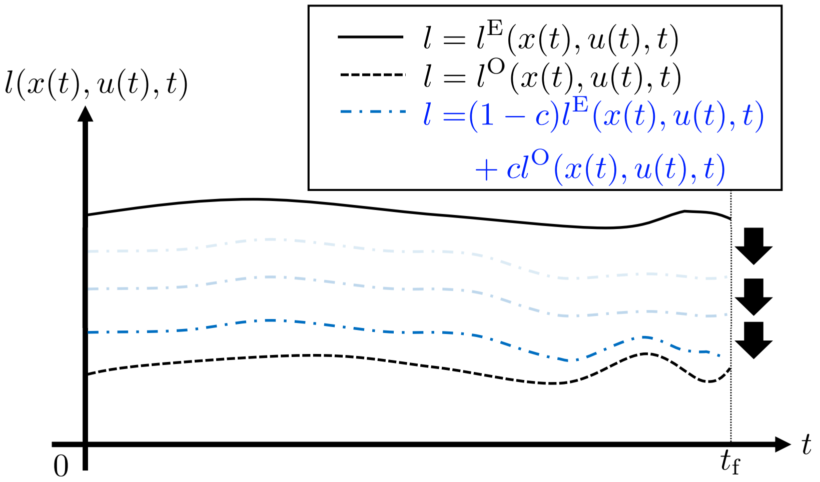
$l = l^{\mathrm{E}}(x(t), u(t), t)$
$l = l^{\mathrm{O}}(x(t), u(t), t)$
$l = (1-c)l^{\mathrm{E}}(x(t), u(t), t) + cl^{\mathrm{O}}(x(t), u(t), t)$
$l(x(t), u(t), t)$
0
t_{f}
t

Figure 2.2: Transition of the function $(1-c)l^{\mathrm{E}} + cl^{\mathrm{O}}$ in the algorithm of the existing continuation method for a given $x(t)$ and $u(t)$

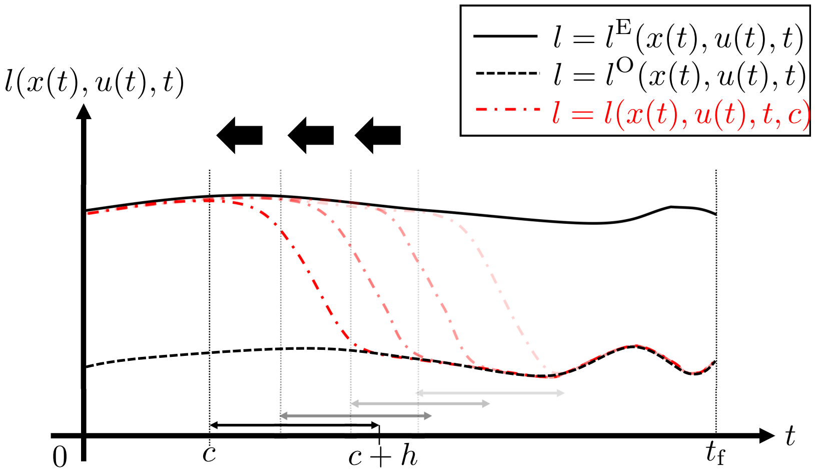
$l = l^{\mathrm{E}}(x(t), u(t), t)$
$l = l^{\mathrm{O}}(x(t), u(t), t)$
$l = l(x(t), u(t), t, c)$
$l(x(t), u(t), t)$
0
c
$c+h$
t_{f}
t

Figure 2.3: Transition of the function l in the algorithm of the locally deforming continuation method for a given $x(t)$ and $u(t)$

2.3.2 Locally deforming continuation method

The idea of the locally deforming continuation method is to transform the cost function locally. In the existing methods, the cost function is deformed by changing the continuation parameter c from 0 to 1 as in Fig. 2.2. On the other hand, the locally deforming continuation method locally changes the cost function by changing c from t_{f} to $-h$, where the function $l(x(t), u(t), t, c)$ changes as shown in Fig. 2.3. Both Figs. 2.2 and 2.3 are depicted in the same way as Fig. 2.1. The algorithm of the locally deforming continuation method with the modified shooting method is shown in Algorithm 1. Here t_{mid} is set as

$$t_{\mathrm{mid}} = f_{t_{\mathrm{mid}}}(c), \tag{2.3.14}$$

$$f_{t_{\mathrm{mid}}}(c) = \begin{cases} t_{\mathrm{f}} & c \geq t_f - h, \\ c + h & t_{\mathrm{f}} - h > c > -h, \\ 0 & -h \geq c, \end{cases} \tag{2.3.15}$$

The parameters $t_{\mathrm{f}}, x^0, x^{\mathrm{f}}, h, \delta$ are given before executing the algorithm, and assume that $x^{J_{\mathrm{E}}}(t)$, $u^{J_{\mathrm{E}}}(t)$, and $\lambda^{J_{\mathrm{E}}}(t)$ are obtained. Here h and δ are scalars satisfying $0 < \delta \leq h$, and δ represents the variation of the continuation parameter c. In the next section, we analyze the relation between δ and the initial error $\epsilon^{\mathrm{I}}_{J_c}(f_{t_{\mathrm{mid}}}(c))$ with respect to the proposed algorithm.

Algorithm 1 Locally deforming continuation method

```
Input: $t_{\mathrm{f}}, x^0, x^{\mathrm{f}}, h, \delta, x^{J_{\mathrm{E}}}(t), u^{J_{\mathrm{E}}}(t), \lambda^{J_{\mathrm{E}}}(t)$
Output: $x^{J_{\mathrm{O}}}(t), u^{J_{\mathrm{O}}}(t)$
$c \leftarrow t_{\mathrm{f}} - \delta$
loop
    $t_{\mathrm{mid}} \leftarrow f_{t_{\mathrm{mid}}}(c)$
    $\lambda^{\mathrm{g}}_0 \leftarrow \lambda^{J_{c+\delta}}(0)$, $\lambda^{\mathrm{g}}_{\mathrm{f}} \leftarrow \lambda^{J_{c+\delta}}(t_{\mathrm{f}})$
    Find $\lambda^{J_c}(0)$, $\lambda^{J_c}(t_{\mathrm{f}})$ by solving TPBVP (2.3.7) from the initial guess
    if $c \leq -h$ then
        return $x^{J_c}(t), u^{J_c}(t)$
    else
        $c \leftarrow c - \delta$
    end if
end loop
```

2.3.3 Analysis of the relation between δ and $\epsilon^{\mathrm{I}}_{J_c}(f_{t_{\mathrm{mid}}}(c))$

First, we prove the following lemmas for $\epsilon^{\mathrm{I}}_{J_c}(f_{t_{\mathrm{mid}}}(c))$ and then we introduce the relation between δ and $\epsilon^{\mathrm{I}}_{J_c}(f_{t_{\mathrm{mid}}}(c))$.

Lemma 2.3.1. *Select c so that $t_{\mathrm{f}} - h \leq c \leq t_{\mathrm{f}}$ and $t_{\mathrm{mid}} = f_{t_{\mathrm{mid}}}(c)$. Assume that $u^{J_c}(t), x^{J_c}(t)$, and $\lambda^{J_c}(t)$, $t \in [0, t_{\mathrm{f}}]$ are obtained. If we give λ^{g}_0 and $\lambda^{\mathrm{g}}_{\mathrm{f}}$ as $\lambda^{J_c}(0)$ and $\lambda^{J_c}(t_{\mathrm{f}})$ respectively, the initial error $\epsilon^{\mathrm{I}}_{J_{c-\delta}}(t_{\mathrm{mid}})$ for $J_{c-\delta}$ satisfies*

$$\epsilon^{\mathrm{I}}_{J_{c-\delta}}(t_{\mathrm{mid}}) = \int_{c-\delta}^{t_{\mathrm{f}}} F_{c-\delta}(\xi_{c-\delta,+}(t), t) - F_c(\xi_{c,+}(t), t) \, \mathrm{d}t. \tag{2.3.16}$$

Proof. It follows from (2.3.5) that

$$l(x(t),u(t),t,c)=l(x(t),u(t),t,c-\delta), \tag{2.3.17}$$

holds for $t\in[0,c-\delta]$, therefore

$$F_c(\xi_{c,+}(t),t)=F_{c-\delta}(\xi_{c-\delta,+}(t),t), \tag{2.3.18}$$

also holds for $t\in[0,c-\delta]$. Note that

$$\xi^{\mathrm{f}}=\int_0^{t_f}F_c(\xi_{c,+}(t),t)\mathrm{d}t+\xi^0, \tag{2.3.19}$$

with $\xi^{\mathrm{f}}:=({x^{\mathrm{f}}}^\top,\lambda^{J_c}(t_{\mathrm{f}})^\top)^\top$ and $\xi^0:=({x^0}^\top,\lambda^{J_c}(0)^\top)^\top$ holds for $\lambda^{J_c}(0)$ and $\lambda^{J_c}(t_{\mathrm{f}})$. Hence, for $\epsilon^{\mathrm{I}}_{J_{c-\delta}}(t_{\mathrm{mid}})$, (2.3.15), (2.3.18) and (2.3.19) lead

$$\begin{aligned}
\epsilon^{\mathrm{I}}_{J_{c-\delta}}(t_{\mathrm{mid}})&=\int_0^{t_{\mathrm{f}}}F_{c-\delta}(\xi_{c-\delta,+}(t),t)\mathrm{d}t+\xi^0\\
&-\left(\int_{t_{\mathrm{f}}}^{t_{\mathrm{f}}}F_{c-\delta}(\xi_{c-\delta,-}(t),t)\mathrm{d}t+\xi^{\mathrm{f}}\right)\\
&=\int_0^{t_{\mathrm{f}}}F_{c-\delta}(\xi_{c-\delta,+}(t),t)\mathrm{d}t+\xi^0-\xi^{\mathrm{f}}\\
&=\int_0^{t_{\mathrm{f}}}F_{c-\delta}(\xi_{c-\delta,+}(t),t)\mathrm{d}t+\xi^0-\left(\int_0^{t_{\mathrm{f}}}F_c(\xi_{c,+}(t),t)\mathrm{d}t+\xi^0\right)\\
&=\int_{c-\delta}^{t_{\mathrm{f}}}F_{c-\delta}(\xi_{c-\delta,+}(t),t)\mathrm{d}t+\int_0^{c-\delta}F_{c-\delta}(\xi_{c-\delta,+}(t),t)\mathrm{d}t\\
&-\left(\int_{c-\delta}^{t_{\mathrm{f}}}F_c(\xi_{c,+}(t),t)\mathrm{d}t+\int_0^{c-\delta}F_c(\xi_{c,+}(t),t)\mathrm{d}t\right)\\
&=\int_{c-\delta}^{t_{\mathrm{f}}}F_{c-\delta}(\xi_{c-\delta,+}(t),t)\mathrm{d}t-\int_{c-\delta}^{t_{\mathrm{f}}}F_c(\xi_{c,+}(t),t)\mathrm{d}t,
\end{aligned}$$

and this completes the proof. □

Lemma 2.3.2. *Select c so that $\delta\le c\le t_{\mathrm{f}}-h$ and $t_{\mathrm{mid}}=f_{t_{\mathrm{mid}}}(c)$. Assume that $u^{J_c}(t)$, $x^{J_c}(t)$, and $\lambda^{J_c}(t)$ are obtained. If we give λ^{g}_0 and $\lambda^{\mathrm{g}}_{\mathrm{f}}$ as $\lambda^{J_c}(0)$ and $\lambda^{J_c}(t_{\mathrm{f}})$ respectively, the initial error $\epsilon^{\mathrm{I}}_{J_{c-\delta}}(t_{\mathrm{mid}})$ for $J_{c-\delta}$ satisfies*

$$\epsilon^{\mathrm{I}}_{J_{c-\delta}}(t_{\mathrm{mid}})=\int_{c-\delta}^{c+h}F_{c-\delta}(\xi_{c-\delta,+}(t),t)-F_c(\xi_{c,+}(t),t)\mathrm{d}t \tag{2.3.20}$$

Proof. The proof of the lemma 2.3.2 is similar to the one of the lemma 2.3.1. It follows from (2.3.5) that

$$l(x(t),u(t),t,c)=l(x(t),u(t),t,c-\delta), \tag{2.3.21}$$

holds for $t \in [0, c-\delta]$ and $t \in [c+h, t_{\mathrm{f}}]$, therefore

$$F_c(\xi_{c,+}(t), t) = F_{c-\delta}(\xi_{c-\delta,+}(t), t), \tag{2.3.22}$$

also holds for $t \in [0, c-\delta]$ and

$$F_c(\xi_{c,-}(t), t) = F_{c-\delta}(\xi_{c-\delta,-}(t), t), \tag{2.3.23}$$

holds for $t \in [c+h, t_{\mathrm{f}}]$. Note that

$$\begin{aligned} \xi(t) &= \int_0^t F_c(\xi_{c,+}(t), t)\mathrm{d}t + \xi^0 \\ &= \int_{t_{\mathrm{f}}}^t F_c(\xi_{c,-}(t), t)\mathrm{d}t + \xi^{\mathrm{f}}, \end{aligned} \tag{2.3.24}$$

with $\xi^{\mathrm{f}} = (x^{\mathrm{f}\top}, \lambda^{J_c}(t_{\mathrm{f}})^\top)^\top$ and $\xi^0 = (x^{0\top}, \lambda^{J_c}(0)^\top)^\top$ holds for $\lambda^{J_c}(0)$ and $\lambda^{J_c}(t_{\mathrm{f}})$ from the assumption. Hence, it follows from (2.3.15) and (2.3.22)-(2.3.24) that

$$\begin{aligned} \epsilon^{\mathrm{I}}_{J_{c-\delta}}(t_{\mathrm{mid}}) &= \int_0^{c+h} F_{c-\delta}(\xi_{c-\delta,+}(t), t)\mathrm{d}t + \xi^0 \\ &\quad - \left(\int_{t_{\mathrm{f}}}^{c+h} F_{c-\delta}(\xi_{c-\delta,-}(t), t)\mathrm{d}t + \xi^{\mathrm{f}} \right) \\ &= \int_0^{c+h} F_{c-\delta}(\xi_{c-\delta,+}(t), t)\mathrm{d}t + \xi^0 - \left(\int_{t_{\mathrm{f}}}^{c+h} F_c(\xi_{c,-}(t), t)\mathrm{d}t + \xi^{\mathrm{f}} \right) \\ &= \int_0^{c+h} F_{c-\delta}(\xi_{c-\delta,+}(t), t)\mathrm{d}t + \xi^0 - \left(\int_0^{c+h} F_c(\xi_{c,+}(t), t)\mathrm{d}t + \xi^0 \right) \\ &= \int_{c-\delta}^{c+h} F_{c-\delta}(\xi_{c-\delta,+}(t), t)\mathrm{d}t + \int_0^{c-\delta} F_{c-\delta}(\xi_{c-\delta,+}(t), t)\mathrm{d}t \\ &\quad - \left(\int_{c-\delta}^{c+h} F_c(\xi_{c,+}(t), t)\mathrm{d}t + \int_0^{c-\delta} F_c(\xi_{c,+}(t), t)\mathrm{d}t \right) \\ &= \int_{c-\delta}^{c+h} F_{c-\delta}(\xi_{c-\delta,+}(t), t)\mathrm{d}t - \int_{c-\delta}^{c+h} F_c(\xi_{c,+}(t), t)\mathrm{d}t, \end{aligned}$$

and this completes the proof. □

Lemma 2.3.3. *Select c so that $-h \leq c \leq \delta$ and $t_{\mathrm{mid}} = f_{t_{\mathrm{mid}}}(c)$. Assume that $u^{J_c}(t)$, $x^{J_c}(t)$, and $\lambda^{J_c}(t)$ are obtained. If we give λ^{g}_0 and $\lambda^{\mathrm{g}}_{\mathrm{f}}$ as $\lambda^{J_c}(0)$ and $\lambda^{J_c}(t_{\mathrm{f}})$ respectively, the initial error $\epsilon^{\mathrm{I}}_{J_{c-\delta}}(t_{\mathrm{mid}})$ for $J_{c-\delta}$ satisfies*

$$\epsilon^{\mathrm{I}}_{J_{c-\delta}}(t_{\mathrm{mid}}) = \int_0^{c+h} F_{c-\delta}(\xi_{c-\delta,+}(t), t) - F_c(\xi_{c,+}(t), t)\mathrm{d}t \tag{2.3.25}$$

We omit the proof since it is proved in the same way as Lemma 2.3.1. In addition to Lemmas 2.3.1-2.3.3, under certain conditions, the following theorem holds.

Theorem 2.3.1. *Assume that $l(x(t), u(t), t, c) = l(u(t), t, c)$. Then the costate system of (2.3.7) can be written as*

$$\begin{aligned} \frac{\mathrm{d}\lambda(t)}{\mathrm{d}t} &= -\frac{\partial H_c(\xi(t), u(t), t)}{\partial x(t)}\bigg|_{u(t)=f_u^c(\xi(t),t)} \\ &= \tilde{f}(\xi(t)) + \tilde{g}(\xi(t)) f_u^c(\xi(t), t), \end{aligned} \tag{2.3.26}$$

with $\tilde{f} : \mathbb{R}^{2n} \to \mathbb{R}^n$, $\tilde{g} : \mathbb{R}^{2n} \to \mathbb{R}^{n\times m}$, and

$$\frac{\mathrm{d}x(t)}{\mathrm{d}t} = f(x(t)) + g(x(t)) f_u^c(\xi(t), t). \tag{2.3.27}$$

Assume that there exist constants α_1, α_2, $\beta_{1,i}$, and $\beta_{2,i}$, $i = 1, \cdots m$ such that

$$\|f(x_1) - f(x_2)\| \le \alpha_1 \|x_1 - x_2\|, \tag{2.3.28}$$

$$\|\tilde{f}(\xi_1) - \tilde{f}(\xi_2)\| \le \alpha_2 \|\xi_1 - \xi_2\|, \tag{2.3.29}$$

$$\|g_i(x^*(\tau))\| \le \beta_{1,i}, \tag{2.3.30}$$

$$\|\tilde{g}_i(\xi^*(\tau))\| \le \beta_{2,i}, \tag{2.3.31}$$

where $x_1,\ x_2 \in \mathbb{R}^n$, $\xi_1,\ \xi_2 \in \mathbb{R}^{2n}$, $\tau \in [\max(c-\delta, 0), \min(c+h, t_\mathrm{f})]$, g_i and $\tilde{g}_i$ are the column vectors of $g = (g_1, \cdots, g_m)$ and $\tilde{g} = (\tilde{g}_1, \cdots, \tilde{g}_m)$, and $x^*(\tau)$ and $\xi^*(\tau)$ are arbitrary vectors that satisfy (2.1.3), (2.3.26) and (2.3.27) for τ. Then, if we give λ_0^g and $\lambda_\mathrm{f}^\mathrm{g}$ as $\lambda^{J_c}(0)$ and $\lambda^{J_c}(t_\mathrm{f})$ respectively, for $t_\mathrm{mid} = f_{t_\mathrm{mid}}(c)$, $c \in [-h, t_\mathrm{f}]$, the following relation

$$\|\epsilon^\mathrm{I}_{J_{c-\delta}}(t_\mathrm{mid})\| \le \frac{2\sum_{i=1}^m (\beta_{1,i} + \beta_{2,i}) u_{b,i}}{\alpha} \left(e^{\alpha(h+\delta)} - 1\right). \tag{2.3.32}$$

with $\alpha = \alpha_1 + \alpha_2$ holds.

Proof. This proof refers the proof of Theorem 2.1 in [48]. Consider the case $\delta \le c \le$

$t_{\mathrm{f}} - h$ and define $\left({x_{c,+}}^\top, {\lambda_{c,+}}^\top\right)^\top := \xi_{c,+}$. Here $t_{\mathrm{mid}} = c + h$. For $t \in [c - \delta, c + h]$,

$$\begin{aligned}
&\frac{\mathrm{d}}{\mathrm{d}t}\|x_{c-\delta,+} - x_{c,+}\| + \frac{\mathrm{d}}{\mathrm{d}t}\|\lambda_{c-\delta,+} - \lambda_{c,+}\| \\
\leq& \|\dot{x}_{c-\delta,+} - \dot{x}_{c,+}\| + \|\dot{\lambda}_{c-\delta,+} - \dot{\lambda}_{c,+}\| \\
\leq& \|f(x_{c-\delta,+}) - f(x_{c,+})\| + \|\tilde{f}(\xi_{c-\delta,+}) - \tilde{f}(\xi_{c,+})\| \\
&+ \|g(x_{c-\delta,+})f_u^c(\xi_{c-\delta,+}, t) - g(x_{c,+})f_u^c(\xi_{c,+}, t)\| \\
&+ \|\tilde{g}(\xi_{c-\delta,+})f_u^c(\xi_{c-\delta,+}, t) - \tilde{g}(\xi_{c,+})f_u^c(\xi_{c,+}, t)\| \\
\leq& \alpha_1\|x_{c-\delta,+} - x_{c,+}\| + \alpha_2\|\xi_{c-\delta,+} - \xi_{c,+}\| \\
&+ \sum_{i=1}^{m}\left(\|g_i(x_{c-\delta,+})\| + \|g_i(x_{c,+})\|\right. \\
&\left.+\|\tilde{g}_i(\xi_{c-\delta,+})\| + \|\tilde{g}_i(\xi_{c-\delta,+})\|\right) u_{\mathrm{b},i} \\
\leq& \alpha_1\|x_{c-\delta,+} - x_{c,+}\| + \alpha_2\|\xi_{c-\delta,+} - \xi_{c,+}\| + 2\sum_{i=1}^{m}(\beta_{1,i} + \beta_{2,i})u_{b,i} \\
\leq& (\alpha_1 + \alpha_2)\|x_{c-\delta,+} - x_{c,+}\| + \alpha_2\|\lambda_{c-\delta,+} - \lambda_{c,+}\| \\
&+ 2\sum_{i=1}^{m}(\beta_{1,i} + \beta_{2,i})u_{b,i} \\
\leq& (\alpha_1 + \alpha_2)\|x_{c-\delta,+} - x_{c,+}\| + (\alpha_1 + \alpha_2)\|\lambda_{c-\delta,+} - \lambda_{c,+}\| \\
&+ 2\sum_{i=1}^{m}(\beta_{1,i} + \beta_{2,i})u_{b,i}.
\end{aligned}$$

Hence the following relation

$$\begin{aligned}
&\frac{\mathrm{d}}{\mathrm{d}t}\|x_{c-\delta,+} - x_{c,+}\| - (\alpha_1 + \alpha_2)\|x_{c-\delta,+} - x_{c,+}\| \\
&\quad + \frac{\mathrm{d}}{\mathrm{d}t}\|\lambda_{c-\delta,+} - \lambda_{c,+}\| - (\alpha_1 + \alpha_2)\|\lambda_{c-\delta,+} - \lambda_{c,+}\| \\
\leq& 2\sum(\beta_{1,i} + \beta_{2,i})u_{b,i},
\end{aligned} \tag{2.3.33}$$

holds. By multiplying the integrating factor $e^{-(\alpha_1+\alpha_2)t}$ to (2.3.33), we have

$$\begin{aligned}
&\frac{\mathrm{d}}{\mathrm{d}t}\left(e^{-(\alpha_1+\alpha_2)t}(\|x_{c-\delta,+} - x_{c,+}\| + \|\lambda_{c-\delta,+} - \lambda_{c,+}\|)\right) \\
&\quad \leq 2e^{-(\alpha_1+\alpha_2)t}\sum(\beta_{1,i} + \beta_{2,i})u_{b,i}.
\end{aligned} \tag{2.3.34}$$

From Lemma 2.3.2, the initial error is gained by integrating $\dot{\xi}_{c-\delta,+} - \dot{\xi}_{c,+}$ with (2.3.26) and (2.3.27) from $c - \delta$ to $c + h$. The integration of (2.3.34) from $c - \delta$ to $c + h$ leads to

$$
\begin{aligned}
& e^{-\alpha(c+h)}\|x_{c-\delta,+}(c+h) - x_{c,+}(c+h)\| \\
& + e^{-\alpha(c+h)}\|\lambda_{c-\delta,+}(c+h) - \lambda_{c,+}(c+h)\| \\
& - e^{-\alpha(c-\delta)}\|x_{c-\delta,+}(c-\delta) - x_{c,+}(c-\delta)\| \\
& - e^{-\alpha(c-\delta)}\|\lambda_{c-\delta,+}(c-\delta) - \lambda_{c,+}(c-\delta)\| \\
& \leq \frac{2\sum(\beta_{1,i}+\beta_{2,i})u_{b,i}}{\alpha}\left(e^{-\alpha(c-\delta)} - e^{-\alpha(c+h)}\right).
\end{aligned}
\tag{2.3.35}
$$

Since $x_{c-\delta,+}(c-\delta) = x_{c,+}(c-\delta)$ and $\lambda_{c-\delta,+}(c-\delta) = \lambda_{c,+}(c-\delta)$ hold from (2.3.22), it follows from (2.3.35) that

$$
\begin{aligned}
& \|x_{c-\delta,+}(c+h) - x_{c,+}(c+h)\| + \|\lambda_{c-\delta,+}(c+h) - \lambda_{c,+}(c+h)\| \\
& \leq \frac{2\sum(\beta_{1,i}+\beta_{2,i})u_{b,i}}{\alpha}\left(e^{\alpha(h+\delta)} - 1\right),
\end{aligned}
$$

and the relation

$$
\begin{aligned}
& \|\xi_{c-\delta,+}(c+h) - \xi_{c,+}(c+h)\| \\
& \leq \|x_{c-\delta,+}(c+h) - x_{c,+}(c+h)\| + \|\lambda_{c-\delta,+}(c+h) - \lambda_{c,+}(c+h)\|,
\end{aligned}
$$

yields

$$
\|\epsilon^{\mathrm{I}}_{J_{c-\delta}}(c+h)\| \leq \frac{2\sum(\beta_{1,i}+\beta_{2,i})u_{b,i}}{\alpha}\left(e^{\alpha(h+\delta)} - 1\right).
$$

Here the relation $\xi_{c,+}(c+h) = \xi_{c,-}(c+h) = \xi_{c-\delta,-}(c+h)$ is used. In the same way, for the case $t_{\mathrm{f}} - h \leq c \leq t_{\mathrm{f}}$, it follows from Lemma 2.3.1 that

$$
\begin{aligned}
\|\epsilon^{\mathrm{I}}_{J_{c-\delta}}(c+h)\| &\leq \frac{2\sum(\beta_{1,i}+\beta_{2,i})u_{b,i}}{\alpha}\left(e^{\alpha(t_{\mathrm{f}}-(c-\delta))} - 1\right) \\
&\leq \frac{2\sum(\beta_{1,i}+\beta_{2,i})u_{b,i}}{\alpha}\left(e^{\alpha(h+\delta)} - 1\right),
\end{aligned}
$$

holds since $t_{\mathrm{f}} - (c-\delta) \leq h+\delta$, and for the case $-h \leq c < \delta$, it follows from Lemma 2.3.3 that

$$
\begin{aligned}
\|\epsilon^{\mathrm{I}}_{J_{c-\delta}}(c+h)\| &\leq \frac{2\sum(\beta_{1,i}+\beta_{2,i})u_{b,i}}{\alpha}\left(e^{\alpha(c+h)} - 1\right) \\
&\leq \frac{2\sum(\beta_{1,i}+\beta_{2,i})u_{b,i}}{\alpha}\left(e^{\alpha(h+\delta)} - 1\right),
\end{aligned}
$$

holds since $c+h \leq h+\delta$. This completes the proof. □

Remark 2.3.1. *Theorem 2.3.1 provides a clear guideline for adjusting the parameters δ and h in solving problems with the locally deforming continuation method. For* *example, the theorem shows that both h and δ should be decreased for reducing the initial error, that is, reducing $h+\delta$ brings the guess of the solution in each iteration closer to the solution and thus makes the algorithm more likely to succeed. Hence, h should be chosen so that it is as large as δ, and vice versa. In addition, if $h+\delta$ is sufficiently small, the upper bound of the initial error $\epsilon^{\mathrm{I}}_{J_{c-\delta}}(f_{t_{\mathrm{mid}}}(c))$ varies linearly with respect to $h+\delta$ and $\epsilon^{\mathrm{I}}_{J_{c-\delta}}(f_{t_{\mathrm{mid}}}(c))$ is also expected to change linearly.*

The next section shows the effectiveness of the proposed method through numerical examples.

2.4 Numerical example

In this example, an L^1/L^2-optimal control [44] is applied to a two-wheeled rover depicted in Fig. 2.4, where the horizontal axis is X, the vertical axis is Y, x_1 is the angle of the rover, and x_2 and x_3 are x-position and y-position of the rover, respectively. The system of the rover is denoted by

$$\frac{\mathrm{d}x(t)}{\mathrm{d}t} = g(x)u = \begin{pmatrix} 1 & 0 \\ 0 & \cos(x_1(t)) \\ 0 & \sin(x_1(t)) \end{pmatrix} \begin{pmatrix} u_1(t) \\ u_2(t) \end{pmatrix}, \tag{2.4.1}$$

and the input is restricted by $u_{\mathrm{b},1} = u_{\mathrm{b},2} = 5$. Define an optimal control problem with the cost function

$$J_{\mathrm{O}} = \int_0^2 \frac{1}{2}\sum_{i=1}^{2}\left(u_i(t)^2\right) + 2|u_1(t)|\mathrm{d}t \tag{2.4.2}$$

and a boundary condition

$$x(0) = (0,0,0)^\top,\ x(2) = \left(\frac{\pi}{5}, 1, 1\right)^\top \in \mathbb{R}^3. \tag{2.4.3}$$

The resultant trajectory of this optimal control problem is known as a hands-off trajectory [5], where the input $u_1(t)$ takes zero in large part of the control sequence. The details of the L^1/L^2-optimal control technique are explained in Chapter 4. The next subsection first shows that the L^1/L^2-optimal control problem is difficult to solve without the continuation method.

2.4.1 Solve the problem without the continuation method

In this example, we solve the problem with the shooting method in Section 2.2 without using the continuation method. Since the shooting method requires an initial guess

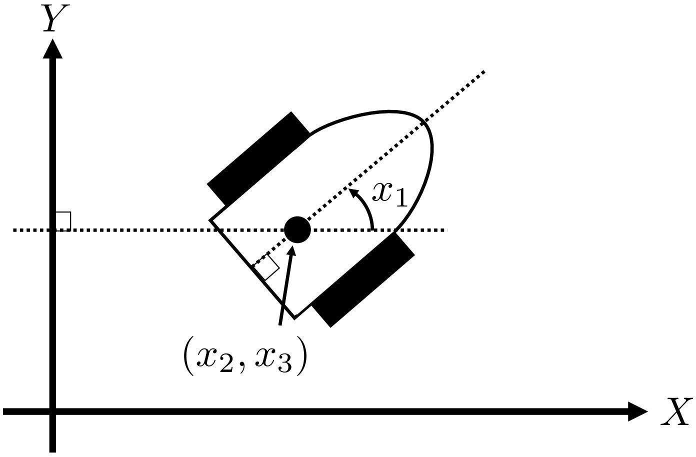

Figure 2.4: Two-wheeled rover

of the solution, we first solve an L^2-optimal control problem with the cost function

$$J_{\mathrm{E}} = \int_0^2 \frac{1}{2} \sum_{i=1}^{2} \left(u_i(t)^2\right) \mathrm{d}t, \tag{2.4.4}$$

and set its solution as an initial guess for solving the L^1/L^2-optimal control problem. Figures 2.5-2.7 show the responses of the states, the generated trajectory, and the responses of the inputs, respectively. In Fig. 2.5, the first row shows $x_1(t)$, the second row shows $x_2(t)$, and the third row shows $x_3(t)$. The horizontal axis is time and the vertical axis is the state. The plus sign markers show the boundary conditions of each state. Figure 2.6 shows the generated trajectory, where the horizontal axis is X, the vertical axis is Y, the black asterisk and plus signs show the start and goal point, and the red solid line is the generated trajectory. In Fig. 2.7, the blue dash-dotted line is $u_1(t)$ and the blue dashed line is $u_2(t)$, where the horizontal axis is time and the vertical axis is the input. As these figures show, the generated trajectories do not satisfy the boundary conditions, that is, the shooting method fails to solve the L^1/L^2-optimal control problem.

In the next example, the locally deforming continuation method is used for solving the L^1/L^2-optimal control problem.

2.4.2 Solve the problem with the locally deforming continuation method

In this example, we use the locally deforming continuation method for solving the L^1/L^2-optimal control problem. In the method, J_{O} and J_{E} are defined as (2.4.2) and

Table 2.1: Combinations of h and δ

Case	1	2	3	4
h	$\frac{h_0}{4}$	$\frac{h_0}{5}$	$\frac{h_0}{10}$	$\frac{h_0}{20}$
δ	$\frac{\delta_0}{4}$	$\frac{\delta_0}{5}$	$\frac{\delta_0}{10}$	$\frac{\delta_0}{20}$

(2.4.4), and J_c is defined by (2.3.4) and (2.3.5) with

$$l^{\mathrm{C}}(x(t), u(t), t) = \frac{1}{2}\sum_{i=1}^{2}\left(u_i(t)^2\right) + f_w(t)|u_1(t)|, \tag{2.4.5}$$

$$f_w(t) = \cos\left(\frac{\pi(c+h-t)}{h}\right) + 1. \tag{2.4.6}$$

To confirm the effectiveness of our method, we performed Algorithm 1 under several combinations of h and δ listed in Table 2.1. Here we define $h_0 = 0.500$ and $\delta_0 = 0.125$. Figure 2.8 shows the log-log plot of the relation between the mean of the initial errors of each case and $h+\delta$. The horizontal axis is $h+\delta$, and the vertical axis is the mean of the Euclidean norm of the initial errors of the shooting method during the Algorithm 1. The green line shows the line of $y = 0.2x$, where y is the mean of the initial errors and x is $h+\delta$. From Fig. 2.8, we can see that the error decreases linearly with respect to $h+\delta$ if $h+\delta$ is small enough. Figures 2.9-2.11 show the responses of the states, the generated trajectory, and the responses of the inputs in Case 4 in the same way as Figs. 2.5-2.7. As can be seen from Figs. 2.9-2.11, the proposed method successfully generates trajectories satisfying the boundary conditions and the generated input $u_1(t)$ takes zero in large part. These results show that the locally deforming continuation method is effective for solving a relatively difficult optimal control problem like an L^1/L^2-optimal control problem.

2.4.3 Comparison between the proposed method and the conventional method

In the example, we compare the initial errors of the conventional method and the proposed method in 5 cases, in which the number of iterations of each continuation method is the same in each case. Here the boundary condition at $t_{\mathrm{f}} = 2$ is set to $x(2) = (1,1,1)^\top$. The conventional method with the cost function (2.3.3) is solved by the shooting method introduced in Section 2.2, and the initial error in this method is defined as follows.

Table 2.2: Iteration number of each case

Case	1	2	3	4	5
Iteration	2	3	4	5	9

Definition 2.4.1. *Define the initial guess of $\lambda^*(0)$ as λ_0^{g}. The corresponding initial error ϵ_x^{I} is defined as*

$$\epsilon_x^{\mathrm{I}} := x(t_{\mathrm{f}}) - x^{\mathrm{f}} \textit{ with } \xi(0) = \begin{pmatrix} x^0 \\ \lambda_0^{\mathrm{g}} \end{pmatrix} \textit{ s.t. (2.2.6)} \tag{2.4.7}$$

In addition, the continuation parameter c in (2.3.3) is changed in each iteration as $c \leftarrow c - \bar{\delta}$ with $\bar{\delta} > 0$, from 0 towards 1.

In Fig. 2.12, the upper figure shows the means of the initial errors of the conventional method, and the lower figure shows those of the proposed one, where the cases that succeeded to find the solutions are marked in blue and the failed cases are colored in red. In each case, $\bar{\delta}$ and $h + \delta$ take the values as in horizontal axes, where $\bar{\delta}_0 = 1/2$, $h_0 = 2$, $\delta_0 = 2$ and $h = \delta$. The vertical axes are the mean of the Euclidean norm of the initial errors. The iteration number of each case is listed in Table 2.2. In the conventional method, if the iteration number is increased, the estimate of the solution is expected to become close to the solution. However, as shown in the upper figure of Fig. 2.12, the means of the initial errors in Cases 1 and 2 are almost the same in the conventional methods. On the other hand, the means of the initial errors of the proposed method decrease as in the lower figure of Fig. 2.12, as mentioned in Remark 2.3.1. Although there is no difference in the success or failure of searching the solution, this example shows that the proposed method is superior to the conventional method in terms that it provides a guideline on how to change the continuation parameter for successfully obtaining the solution.

2.5 Conclusion

In this chapter, we proposed a new continuation method based on the modified shooting method for optimal control problems. We clarify the relationship between the continuation parameter and the proximity of the solutions before and after a deformation in terms of the error in the shooting method, which has been unclear in the conventional continuation methods. This relation is useful in solving the optimal control problem in the sense that it provides a guideline on how to change the continuation parameter so that an initial guess falls within the convergence region at each iteration. In the next chapter, a new numerical solution method is proposed for a sparse optimal control problem, in the framework of the direct method.

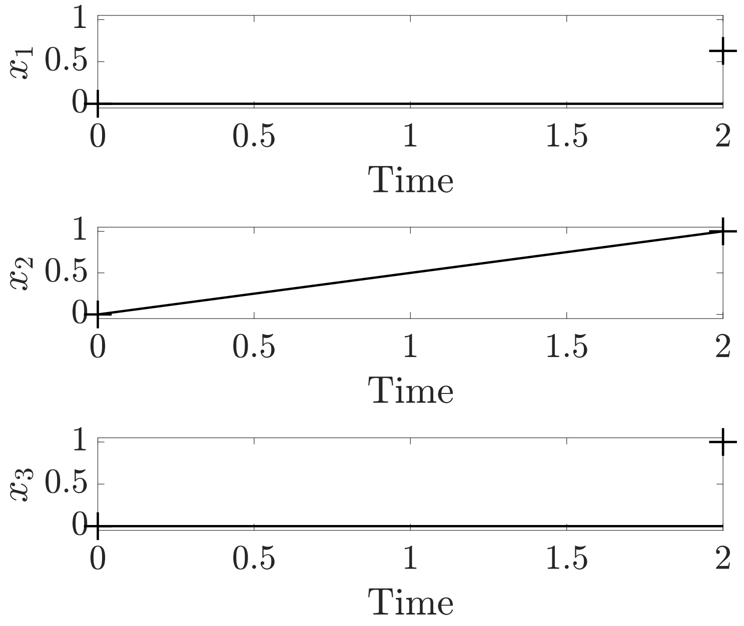

Figure 2.5: States of the trajectory generated without continuation method

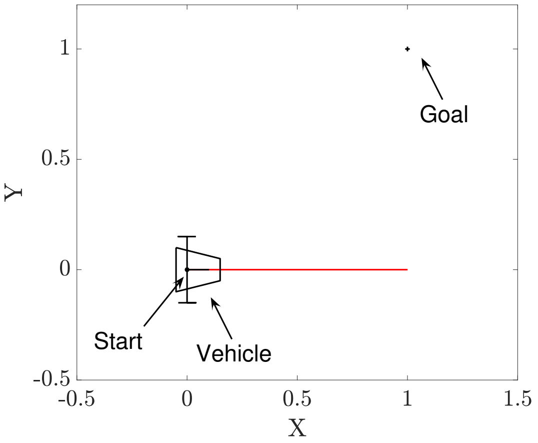

Figure 2.6: Trajectory generated without continuation method

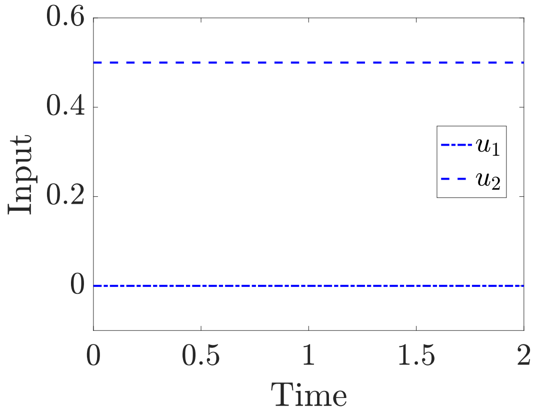

Figure 2.7: Inputs of the trajectory generated without continuation method

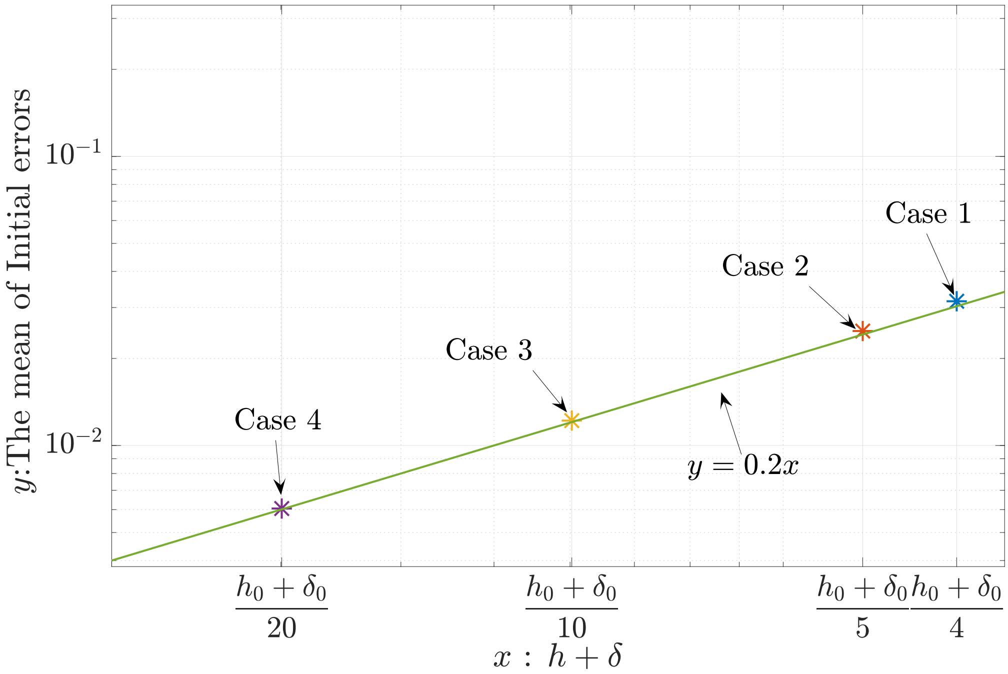

Figure 2.8: The log-log plot of the mean of the errors in each case listed in Table 2.1

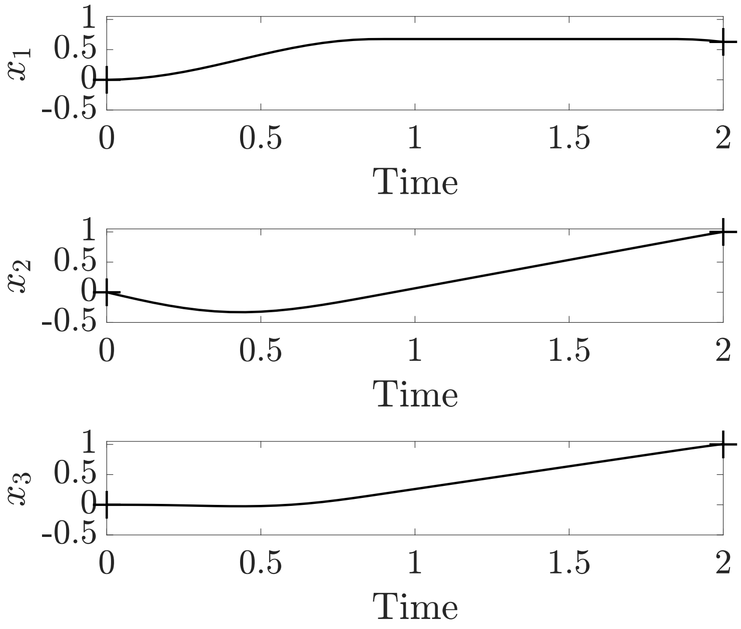

Figure 2.9: States of the trajectory generated by the proposed method

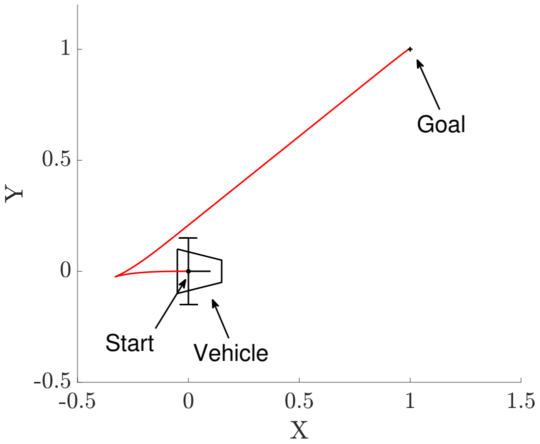

Figure 2.10: The trajectory generated by the proposed method

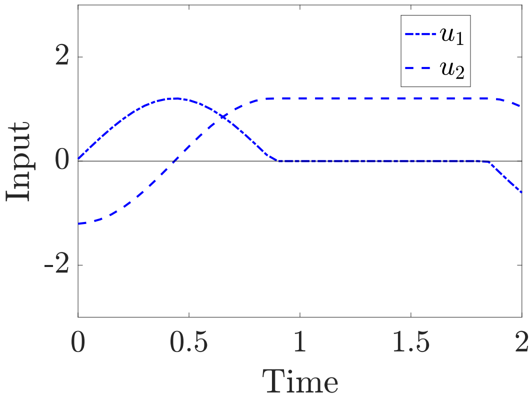

Figure 2.11: Inputs of the trajectory generated by the proposed method

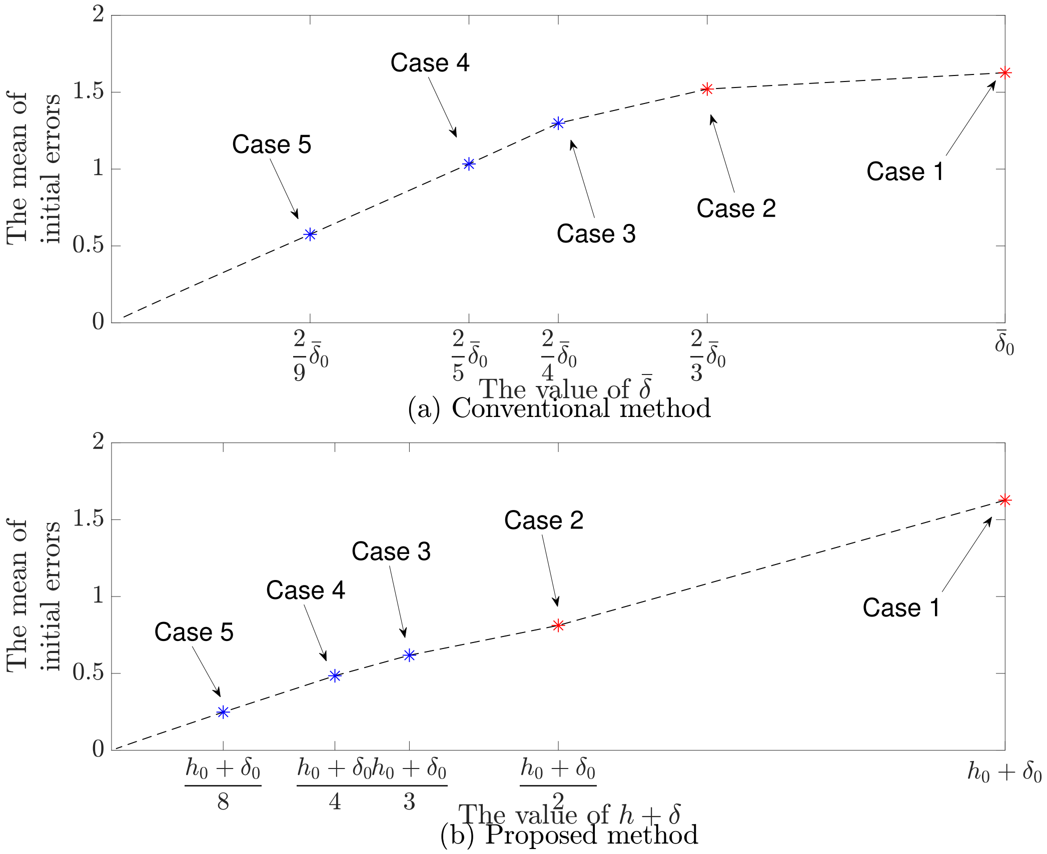

(a) Conventional method

(b) Proposed method

Figure 2.12: Comparison of the means of the initial errors

Chapter 3

Modified Sparse Newton Method

This chapter proposes a new direct method for solving ℓ^1-optimal control problems. Sparse optimal control is a control method whose inputs take zero in large part, i.e., they are sparse. The sparse optimal control problem is formulated as an ℓ^0-optimal control problem, which can only be solved by brute-force search in most cases, and is therefore often replaced by a relatively easy problem, an ℓ^1-optimal control problem that is a good approximation of the ℓ^0-optimal control problem [49, 44]. Due to the sparsity of the inputs, ℓ^1-optimal control has been applied to a variety of problems, such as minimum fuel problems and vehicle trajectory generation problems [5, 6, 7].

There are two main types of methods for solving optimal control problems such as ℓ^1-optimal control problems: indirect methods and direct methods [8]. In recent years, several methods for solving nonlinear ℓ^1-optimal control problems are studied in both approaches [6, 11, 7, 12]. In [6, 11], the problem is solved by collocation methods. In the collocation method, if the system is linear, the ℓ^1-optimal control problem is equal to the linear programming problem and is solved easily. However, when the system is nonlinear, the problem is reduced to a nonlinear programming problem that is difficult to solve. Especially in the case of the ℓ^1-optimal control problem, the nonlinear programming problem is more difficult to solve since ℓ^1-optimal solutions are often non-differentiable. Hence, in those existing methods, the convergence and the convergence rate of the algorithm have not been discussed much.

Recently, Polyak et al. have proposed a sparse Newton method that guarantees convergence in the framework of the direct method [26, 50]. In this method, the boundary conditions are regarded as a nonlinear function of the input sequence. In the algorithm, the inputs are updated according to the Newton method so that the boundary conditions are satisfied. In the Newton method, the update direction of the inputs is obtained as a solution to linear equations determined by the boundary conditions and their gradients with respect to the inputs. If the number of equations and the dimension of the direction are the same, the update direction is uniquely determined. However, in the case of discretized optimal control problems, this direction is not uniquely determined because the dimension of the direction is significantly larger than the number of equations. The method of Polyak et al. takes advantage of the fact that there is a choice of update directions; that is, the method expects the solution to be sparse by choosing the sparsest update direction. This method is good because it has quadratic convergence, but it does not guarantee the ℓ^1-optimality of the input.

We propose a modified sparse Newton method ensuring that the obtained solution is ℓ^1-optimal. In our method, we choose the update direction so that the updated inputs are ℓ^1-optimal instead of the update direction being sparsest. By choosing the update direction in this way, we can guarantee the ℓ^1-optimality of the inputs, which cannot be guaranteed by the sparse Newton method. In addition, the direction is chosen so that its magnitude is restricted by the residual of the boundary condition for ensuring the convergence. This restriction on the choice of the direction is an analogy to the Newton method for a scalar case. As a result, quadratic convergence is also guaranteed in the proposed method. This chapter also proposes a practical algorithm for solving ℓ^1-optimal control problems under input restrictions.

The rest of this chapter is organized as follows. In Section 3.1, we set up the problem and introduce the existing methods. In Section 3.2, we explain the proposed method. In Section 3.3, we apply the proposed method to a trajectory generation problem to confirm that an ℓ^1-optimal solution is obtained. Section 3.4 concludes this chapter.

3.1 Problem setting and preliminaries

In this section, we formulate an ℓ^1-optimal control problem to be solved and introduce a previous approach for this problem.

3.1.1 Problem setting

Consider the following discretized nonlinear system

$$x[j+1] = f(x[j], u[j]),\ j = 0, \cdots, N-1, \tag{3.1.1}$$

where $x[j] \in \mathbb{R}^n$ is the state vector, $u[j] \in \mathbb{R}^m$ is the input vector, $f : \mathbb{R}^n \times \mathbb{R}^m \to \mathbb{R}^n$ is a nonlinear map that is differentiable for $x[j]$ and $u[j]$. Note that the value of $N \in \mathbb{Z}_+$ is selected to be sufficiently large.

Our objective is to find ℓ^1-optimal inputs by solving the following optimal control problem.

$$
\begin{aligned}
\text{minimize} \;\; & \|\mathbf{u}\|_1 = \sum_{j=0}^{N-1} \|u[j]\|_1, && (3.1.2)\\
\text{s.t.} \;\; & (3.1.1), \\
& x[0] = x^0, \; x[N] = x^{\mathrm{f}}, && (3.1.3)\\
& |u_i[j]| \leq \bar{u}_i, \; (i = 1, \cdots, m), && (3.1.4)
\end{aligned}
$$

where $\mathbf{u} := (u[0]^\top, \cdots, u[N-1]^\top)^\top \in \mathbb{R}^{mN}$ represents the control sequence, $\bar{u}_i \in \mathbb{R}_+$ is the upper bound of the magnitude of u_i, and x^0, $x^{\mathrm{f}} \in \mathbb{R}^n$ are given initial and terminal conditions, respectively. Note that (3.1.3) denotes the boundary condition of the state and (3.1.4) denotes the input restrictions of the system.

Polyak have proposed a sparse Newton method for solving the defined problem witout input restrictions [26]. Before introducing the sparse Newton method, the standard Newton method is introduced in the next subsection.

3.1.2 Standard Newton method

Consider the problem of finding a root of the following nonlinear equation.

$$P(a) = 0, \tag{3.1.5}$$

with $a \in \mathbb{R}$ and $P : \mathbb{R} \to \mathbb{R}$. In the standard Newton method, the root is found by starting from a certain initial value a^0 and updating it according to the following update rule.

$$
\begin{aligned}
a^{k+1} &= a^k - w^k, \\
w^k &= \frac{P(a^k)}{P'(a^k)}.
\end{aligned} \tag{3.1.6}
$$

Here $P'(a)$ denotes the derivative of $P(a)$ with respect to a, k is the iteration number that starts from 0, and $w^k \in \mathbb{R}$. The important features of the Newton method are that the update direction w^k satisfies the relation $P'(a^k)w^k = P(a^k)$ and w^k becomes 0 when $P(a^k) = 0$. The standard Newton method is known to have quadratic convergence [51]. The sparse Newton method proposed by Polyak is based on this Newton method.

3.1.3 Sparse Newton method

Noting that $x[N]$ can be regarded as a function of $\mathbf{u}$, rewrite the boundary condition (3.1.3) as

$$P(\mathbf{u}) \coloneqq x[N](\mathbf{u}) - x^{\mathrm{f}} = 0_{n\times 1} \in \mathbb{R}^n, \mathbf{u} \in \mathbb{R}^q, \tag{3.1.7}$$

with $q \coloneqq mN$, $q \gg n$. In the sparse Newton method, the inputs are updated as

$$\begin{aligned} w^k &= \operatorname*{argmin}_{w \in \mathcal{W}^k} \|w\|_1, \\ \mathcal{W}^k &\coloneqq \{w \mid P'(\mathbf{u}^k)w = P(\mathbf{u}^k)\}, \\ \mathbf{u}^{k+1} &= \mathbf{u}^k - w^k, \end{aligned} \tag{3.1.8}$$

where k is the iteration number that starts from 0, $P'(\mathbf{u}) \in \mathbb{R}^{n\times q}$ denotes the Jacobian matrix of $P(\mathbf{u})$ with respect to $\mathbf{u}$, $\mathbf{u}^k$ is the value of $\mathbf{u}$ at the k-step in the algorithm, and $w^k \in \mathbb{R}^q$ is an update direction at that step. Since the direction w^k is determined to satisfy

$$P'(\mathbf{u}^k)w^k = P(\mathbf{u}^k), \tag{3.1.9}$$

and $w^k = 0_{q\times 1}$ when $P(\mathbf{u}^k) = 0_{n\times 1}$, this algorithm is a Newton method and is proved to converge to the solution quadratically under certain conditions. If $P'(\mathbf{u}^k)$ is a square and non-singular matrix, w^k is determined uniquely. However, in the case of our problem, (3.1.9) is strongly underdetermined since $q \gg n$. Thus, there are a lot of candidates of w^k that satisfies (3.1.9). The key idea of the sparse Newton method is to choose w^k among those candidates so that the ℓ^1-norm of w^k is minimized. Since the minimization of the ℓ^1-norm makes w^k sparse at each iteration, the obtained solution is expected to be sparse providing that the algorithm starts from zero initial solution $\mathbf{u}^0 = 0_{q\times 1}$ and can find the solution in a few steps. However, ℓ^1-optimality is not guaranteed in this algorithm. Motivated by this problem, we propose another type of Newton method that ensures ℓ^1-optimality of the solution.

3.2 Proposed method

The basic idea of our method is to modify the update law (3.1.8) so that $\|\mathbf{u}^{k+1}\|_1$ is optimized instead of $\|w^k\|_1$. The input sequence is updated according to the following equations.

$$\begin{aligned} w^k &= \operatorname*{argmin}_{w \in \mathcal{W}^k} \|\mathbf{u}^k - w\|_1, \\ \mathcal{W}^k &\coloneqq \left\{w \,\middle|\, P'(\mathbf{u}^k)w = P(\mathbf{u}^k)\right\}, \\ \mathbf{u}^{k+1} &= \mathbf{u}^k - w^k, \end{aligned} \tag{3.2.1}$$

A similar idea was used in [12]. However, no analysis on convergence was made in that paper. We combine (3.1.8) and (3.2.1) to ensure the convergence.

3.2.1 Modified sparse Newton method

Similar to the sparse Newton method, consider the case that there are no input restrictions. In our method, we update $\mathbf{u}$ according to the following equation.

$$\begin{aligned} \mathbf{u}^{k+1} &= \mathbf{u}^k - w^k, \\ w^k &:= w^k_{\text{min}} + w^k_{\text{null}}, \end{aligned} \tag{3.2.2}$$

where w^k_{min} is determined first by

$$\begin{aligned} w^k_{\text{min}} &= \underset{w\in\mathcal{W}^k}{\text{argmin}}\ \|w\|_1, \\ \mathcal{W}^k &:= \left\{ w \,\middle|\, P'(\mathbf{u}^k)w = P(\mathbf{u}^k) \right\}, \end{aligned} \tag{3.2.3}$$

and then, w^k_{null} is determined as

$$\begin{aligned} w^k_{\text{null}} &= \underset{w\in\mathcal{W}^k_{\text{null}}}{\text{argmin}}\ \|\mathbf{u}^k - (w^k_{\text{min}} + w)\|_1, \\ \mathcal{W}^k_{\text{null}} &:= \left\{ w \,\middle|\, \begin{matrix} P'(\mathbf{u}^k)w = 0_{m\times 1}, \\ \|w\|_1 \le \alpha\|P(\mathbf{u}^k)\|_1 \end{matrix} \right\}, \end{aligned} \tag{3.2.4}$$

with a scalar $\alpha > 0$. Note that w^k_{min} is a solution of $P'(\mathbf{u}^k)w^k = P(\mathbf{u}^k)$. Since $w^k_{\text{null}} \in \text{null}(P'(\mathbf{u}^k))$,

$$P'(\mathbf{u}^k)w^k = P'(\mathbf{u}^k)w^k_{\text{min}} = P(\mathbf{u}^k), \tag{3.2.5}$$

always holds and w^k is actually an Newton direction. In addition, $w^k = 0_{q\times 1}$ holds when $P(\mathbf{u}^k) = 0_{n\times 1}$ because of the restriction $\|w\|_1 \le \alpha\|P(\mathbf{u}^k)\|_1$. Therefore, this method also has the characteristics of the standard Newton method. The next theorem shows the condition for the convergence of this algorithm.

Theorem 3.2.1. *Define $S = \{\mathbf{u} \mid \|\mathbf{u} - \mathbf{u}^0\|_1 \le \rho\}$. Consider the case that the input vector $\mathbf{u}^k$ is updated according to (3.2.2)-(3.2.4). Assume that the following conditions are satisfied on S:*

1. *$P(\mathbf{u})$ is differentiable with respect to $\mathbf{u} \in S$.*

2. *$\exists \mu_0 \in \mathbb{R}_+$, $\|P'(\mathbf{u})^\top h\|_\infty \ge \mu_0\|h\|_\infty$, $\mu_0 > 0$, $\forall h \in \mathbb{R}^n$, $\mathbf{u} \in S$,*

3. *$\exists L \in \mathbb{R}_+$, $\|P'(\mathbf{x}) - P'(\mathbf{y})\|_1 \le L\|\mathbf{x} - \mathbf{y}\|_1$, $\forall \mathbf{x}, \mathbf{y} \in S$,*

4. $\delta^0 := L\lambda^2\|P(\mathbf{u}^0)\|_1/2 < 1,$
$\lambda := (1/\mu_0) + \alpha.$

Then, if $r_1 := \lambda\|P(\mathbf{u}^0)\|_1/(1-\delta^0) \le \rho$ *holds,* $\mathbf{u}^k$ *converges to* $\mathbf{u}^*$ *in* S *that satisfies* $P(\mathbf{u}^*) = 0_{m\times 1}$ *and* $\|\mathbf{u}^0 - \mathbf{u}^*\|_1 \le r_1$. *In addition, the convergence rate is quadratic, that is, for large* $k > 0$, $\exists M \in \mathbb{R}_+$, s.t. $\|P(\mathbf{u}^{k+1})\|_1 \le M\|P(\mathbf{u}^k)\|_1^2$.

Proof. This proof refers to [52]. It follows from (3.2.3) and Assumption 2 that there exists a solution $P'(\mathbf{u}^k)w^k = P(\mathbf{u}^k)$, and

$$\|w^k_{\min}\|_1 \le \frac{1}{\mu_0}\|P(\mathbf{u}^k)\|_1, \tag{3.2.6}$$

holds (See Lemma 3.1 in [53] for details). Hence, w^k satisfies

$$\begin{aligned}\|w^k\|_1 &= \|w^k_{\min} + w^k_{\text{null}}\|_1\\ &\le \|w^k_{\min}\|_1 + \|w^k_{\text{null}}\|_1\\ &\le \left(\frac{1}{\mu_0} + \alpha\right)\|P(\mathbf{u}^k)\|_1\\ &\le \lambda\|P(\mathbf{u}^k)\|_1. \end{aligned}\tag{3.2.7}$$

The third line of (3.2.7) follows from the relation $\|w^k_{\text{null}}\|_1 \le \alpha\|P(\mathbf{u}^k)\|_1$ in (3.2.4). Since

$$\begin{aligned}&P(\mathbf{u}^{k+1}) = P(\mathbf{u}^k)\\ &+\int_0^1 P'(\mathbf{u}^k + t(\mathbf{u}^{k+1} - \mathbf{u}^k))(\mathbf{u}^{k+1} - \mathbf{u}^k)\mathrm{d}t,\end{aligned}$$

always holds, by calculating the Euclidean norm of $P(\mathbf{u}^{k+1})$, we have

$$\begin{aligned}&\|P(\mathbf{u}^{k+1})\|_1 = \big\|P(\mathbf{u}^k) - P'(\mathbf{u}^k)w^k\\ &+\int_0^1 \left\{P'(\mathbf{u}^k)w^k - P'(\mathbf{u}^k - tw^k)w^k\right\}\mathrm{d}t\big\|_1\\ &\le \int_0^1 \left\{\|(P'(\mathbf{u}^k) - P'(\mathbf{u}^k - tw^k))w^k\|_1\right\}\mathrm{d}t.\end{aligned}$$

The last line of the relation follows from $P'(\mathbf{u}^k)w^k = P(\mathbf{u}^k)$. It follows from Assumption 3 and the consistency of the induced norm that

$$\begin{aligned}\|P(\mathbf{u}^{k+1})\|_1 &\le \int_0^1 L\|tw^k\|_1\|w^k\|_1\mathrm{d}t\\ &\le L\|w^k\|_1^2\int_0^1 \|t\|_1\mathrm{d}t\\ &= \frac{L}{2}\|w^k\|_1^2.\end{aligned}$$

Hence, by using (3.2.7), we have

$$\|P(\mathbf{u}^{k+1})\|_1 \leq \frac{L\lambda^2}{2}\|P(\mathbf{u}^k)\|_1^2, \tag{3.2.8}$$

and this proves the quadratic convergence of the algorithm. Define δ^k as $\delta^k = L\lambda^2\|P(\mathbf{u}^k)\|_1/2$, then

$$\|P(\mathbf{u}^{k+1})\|_1 \leq \delta^k\|P(\mathbf{u}^k)\|_1, \tag{3.2.9}$$

and the relation $\|P(\mathbf{u}^1)\|_1 \leq \delta^0\|P(\mathbf{u}^0)\|_1 < \|P(\mathbf{u}^0)\|_1$ follows from Assumption 4. Thus,

$$\begin{aligned}\|P(\mathbf{u}^2)\|_1 &\leq \frac{L\lambda^2}{2}\|P(\mathbf{u}^1)\|_1^2 \\ &< \frac{L\lambda^2}{2}\|P(\mathbf{u}^0)\|_1^2 \\ &\leq \delta^0\|P(\mathbf{u}^0)\|_1 \\ &< \|P(\mathbf{u}^0)\|_1,\end{aligned}$$

and, by using induction, we have $\|P(\mathbf{u}^k)\|_1 < \|P(\mathbf{u}^0)\|_1$. In addition, the following relation holds for δ_k.

$$\begin{aligned}\delta^k &= \frac{L\lambda^2}{2}\|P(\mathbf{u}^k)\|_1 \\ &< \frac{L\lambda^2}{2}\|P(\mathbf{u}^0)\|_1 \\ &= \delta^0.\end{aligned}$$

Hence, for $\|P(\mathbf{u}^k)\|_1$,

$$\|P(\mathbf{u}^k)\|_1 \leq \|P(\mathbf{u}^0)\|_1\prod_{i=0}^{k-1}\delta^i < (\delta^0)^k\|P(\mathbf{u}^0)\|_1, \tag{3.2.10}$$

holds, and this leads to $\|P(\mathbf{u}^k)\|_1 \to 0$ as $k \to \infty$.

On the other hand, the relation

$$\begin{aligned}\|\mathbf{u}^{k+1} - \mathbf{u}^k\|_1 &= \|w^k\|_1 \\ &\leq \lambda\|P(\mathbf{u}^k)\|_1 \\ &< \lambda(\delta^0)^k\|P(\mathbf{u}^0)\|_1,\end{aligned}$$

leads to

$$\begin{aligned}
\|\mathbf{u}^{k+\ell} - \mathbf{u}^k\|_1 &\leq \sum_{i=k}^{k+\ell-1} \|\mathbf{u}^{i+1} - \mathbf{u}^i\|_1 \\
&< \lambda \|P(\mathbf{u}^0)\|_1 \sum_{i=k}^{k+\ell-1} (\delta^0)^i \\
&= \frac{\lambda}{1-\delta^0} \|P(\mathbf{u}^0)\|_1 ((\delta^0)^k - (\delta^0)^{k+\ell}) \\
&= r_1((\delta^0)^k - (\delta^0)^{k+\ell}).
\end{aligned}$$

Thus, $\mathbf{u}^k$ is a Cauchy sequence from the fact that $(\delta^0)^k \to 0$ as $k \to \infty$, and there exists $\mathbf{u}^*$ that satisfies

$$\mathbf{u}^* = \lim_{k\to\infty} \mathbf{u}^k, \quad P(\mathbf{u}^*) = 0. \tag{3.2.11}$$

Note that $\|\mathbf{u}^k - \mathbf{u}^0\|_1 \leq r_1(1-(\delta^0)^k) \leq \rho$ holds, and all $\mathbf{u}^k$ remain in S. This completes the proof. □

Remark 3.2.1. *The assumptions in Theorem 3.2.1 are reasonable. Assumption 2 is a condition that $P'(\mathbf{u})$ has full row rank equal to m and $P'(\mathbf{u})w = P(\mathbf{u})$ has some solutions. Assumption 3 mentions that $P'(\mathbf{u})$ is Lipschitz continuous on S. Assumption 4 shows a condition for convergence, and from the condition, one can know how to choose $\mathbf{u}^0$. Note that Assumption 4 is satisfied easily by choosing the value of $\|P(\mathbf{u}^0)\|_1$ small.*

Remark 3.2.2. *Since w^k_{null} is chosen so that $\|\mathbf{u}^{k+1}\|_1$ is minimized, the obtained solution with this algorithm is an ℓ^1-optimal solution.*

Although the modified sparse Newton method is ensured to converge quadratically, the obtained solution is local optimal because of the limitation on the search area $\|w^k_{\text{null}}\|_1 \leq \alpha\|P(\mathbf{u}^k)\|_1$. In the next subsection, we propose a more practical algorithm for the modified sparse Newton method, where the limitation is relaxed and the input restrictions are considered.

3.2.2 Practical algorithm for the modified sparse Newton method

In order to relax the limitation on the search area, we propose an algorithm that combines (3.2.1) and (3.2.2)-(3.2.4). Before describing the details of the algorithm, we explain how to perform the computation of the proposed update rule, including the case that input constraints exist.

Corollary 3.2.1. *Direction $w^k_{\min}$ is obtained as the solution of the following problem.*

$$\begin{aligned} w^k_{\min} &= \underset{w}{\operatorname{argmin}}\ \|w\|_1, \\ \text{s.t. } & P'(\mathbf{u}^k)w = P(\mathbf{u}^k), \\ & |\mathbf{u}_i - w_i| \le \bar{\mathbf{u}}_i, \end{aligned} \tag{3.2.12}$$

with a vector $\bar{\mathbf{u}} := (\bar{u}^\top, \cdots, \bar{u}^\top)^\top \in \mathbb{R}^q_+$. Similarly, w^k_{null} is obtained by solving

$$\begin{aligned} w^k_{\mathrm{null}} &= \underset{w}{\operatorname{argmin}}\ \|\mathbf{u} - w - w^k_{\min}\|_1, \\ \text{s.t. } & P'(\mathbf{u}^k)w = 0_{m\times 1}, \\ & \|w\|_1 \le \alpha\|P(\mathbf{u}^k)\|_1, \\ & |\mathbf{u}^k_i - w_i - w^k_{\min,i}| \le \bar{\mathbf{u}}_i. \end{aligned} \tag{3.2.13}$$

As in Corollary 3.2.1, update directions $w^k_{\min}$ and w^k_{null} defined as (3.2.3) and (3.2.4) under the input restrictions are obtained easily by solving linear programming problems. Note that w^k in (3.2.1) under the input restrictions is also obtained by solving the following linear programming problem.

$$\begin{aligned} w^k &= \underset{w\in\mathcal{W}^k}{\operatorname{argmin}}\ \|\mathbf{u}^k - w\|_1, \\ \text{s.t. } & P'(\mathbf{u}^k)w = P(\mathbf{u}^k), \\ & \left|\mathbf{u}^k_i - w_i\right| \le \bar{\mathbf{u}}_i. \end{aligned} \tag{3.2.14}$$

When solving (3.2.12)-(3.2.14), it is necessary to calculate $P'(\mathbf{u}^k)$ and $P(\mathbf{u}^k)$. As in [26], the following result immediately follows.

$$\begin{aligned} P(\mathbf{u}) &= x[N](\mathbf{u}) - x^{\mathrm{f}} = f(x[N-1], u[N-1]) - x^{\mathrm{f}} \\ &= f(f(\cdots f(x[0], u[0]), \cdots), u[N-1]) - b. \end{aligned} \tag{3.2.15}$$

In addition, the chain rule leads to the following equation for $P'(\mathbf{u})$.

$$\frac{\partial P(\mathbf{u})}{\partial \mathbf{u}} = \left(\tfrac{\partial P(\mathbf{u})}{\partial u[0]},\ \tfrac{\partial P(\mathbf{u})}{\partial u[1]},\ \cdots,\ \tfrac{\partial P(\mathbf{u})}{\partial u[N-1]}\right), \tag{3.2.16}$$

where

$$\begin{aligned} \frac{\partial P(\mathbf{u})}{\partial u[N-1]} &= \frac{\partial f}{\partial u}(x[N-1], u[N-1]), \\ \frac{\partial P(\mathbf{u})}{\partial u[i]} &= \prod_{j=N-1}^{i+1} \frac{\partial f}{\partial x}(x[j], u[j]) \frac{\partial f}{\partial u}(x[i], u[i]), \\ & 0 \le i \le N-2. \end{aligned}$$

Our method is summarized in Algorithm 2. In the algorithm, we first try to update $\mathbf{u}^k$ with (3.2.1). If the error $\|P(\mathbf{u}^k - w^k)\|_1$ calculated with w^k obtained from (3.2.14) is less than the prior error, the input is updated by using the obtained direction. If the error increases with the update law (3.2.1), then we update the input by using (3.2.2) with w^k obtained from (3.2.12) and (3.2.13). If there are no input restrictions, these steps ease the limitation on the search area of the proposed method while ensuring convergence. Under the input constraints, the algorithm can often find an ℓ^1-optimal solution, although convergence cannot always be guaranteed. Before performing this algorithm, N, x^0, x^{f}, $\bar{u}$, $\mathbf{u}^0$, α and ε have to be given, where α is a design parameter for the algorithm and ε is the user-defined acceptable error.

Algorithm 2 Modified sparse Newton method

```
Input: $N, x^0, x^{\mathrm{f}}, \bar{u}, \mathbf{u}^0, \alpha, \varepsilon$
Output: $\mathbf{u}^{k+1}$
$k \leftarrow 0$
while $\|P(\mathbf{u}^k)\|_1 > \varepsilon$ do
    $P(\mathbf{u}^k) \leftarrow$(3.2.15)
    $P'(\mathbf{u}^k) \leftarrow$(3.2.16)
    $w^k \leftarrow$ the solution of (3.2.14)
    $P(\mathbf{u}^k - w^k) \leftarrow$ (3.2.15)
    if $\|P(\mathbf{u}^k - w^k)\|_1 \geq \|P(\mathbf{u}^k)\|_1$ then
        $w^k_{\mathrm{min}} \leftarrow$ the solution of (3.2.12)
        $w^k_{\mathrm{null}} \leftarrow$ the solution of (3.2.13)
        $w^k \leftarrow w^k_{\mathrm{min}} + w^k_{\mathrm{null}}$
    end if
    $\mathbf{u}^{k+1} \leftarrow \mathbf{u}^k - w^k$
    $k \leftarrow k + 1$
end while
```

To show the effectiveness of our approach, we apply this algorithm to an ℓ^1-optimal trajectory generation problem in the next section.

3.3 Numerical example

In this example, we use CVX, a package for solving convex problems [54, 55], to solve (3.2.12)-(3.2.14). Consider the following continuous nonlinear system

$$\frac{\mathrm{d}x}{\mathrm{d}t} = F(x, u) := \begin{pmatrix} (x_1 - \sin(x_2/10))/10 \\ 1 - \cos((x_1 - x_2)/10) + u \end{pmatrix}, \tag{3.3.1}$$

and discretize this system by using the Heun method as follows.

$$\begin{aligned} f(x[j],u[j]) &= \frac{F_1(x[j],u[j]) + F_2(x[j],u[j])}{2}, \\ F_1(x[j],u[j]) &= F(x[j],u[j])\Delta t + x[j], \\ F_2(x[j],u[j]) &= F(F_1(x[j],u[j]),u[j])\Delta t + x[j], \end{aligned} \tag{3.3.2}$$

where $x \in \mathbb{R}^2$, $u \in \mathbb{R}$, Δt is the sampling time. In this simulation, we solve an ℓ^1-optimal control problem given as (3.1.2)-(3.1.4) with the sparse Newton method and the proposed method. We set parameters as $\Delta t = 0.05$, $N = 800$, $x^0 = (0.2, 0.2)^\top$, $x^{\mathrm{f}} = (0,0)^\top$, $\bar{\mathbf{u}} = (0.8, \cdots, 0.8)^\top \in \mathbb{R}^q$, $\mathbf{u}^0 = 0_{q\times 1}$, $\alpha = 1$, $\varepsilon = 10^{-3}$.

Figures 3.1 and 3.2 show the responses of x in the existing method and the proposed method, respectively. The horizontal axes are time, the vertical axes are the values of the states, the red solid lines with asterisks show x_1, and the yellow solid lines with plus signs show x_2. In both cases, the boundary conditions are satisfied. In terms of the number of steps, the existing method converges in 9 steps as in Fig. 3.3 and the proposed method converges in 5 steps as in Fig. 3.4, where the horizontal axes show the number of the Newton steps and the vertical axes show the values of $\|P(\mathbf{u}^k)\|_1$. These figures show that both methods converge rapidly. However, there is a significant difference in the response of u as in Figs. 3.5 and 3.6, where the horizontal axes show the time step, the vertical axes show the values of the input, the red solid lines with asterisks show u_1. Regarding the value of the cost, as listed in Table 3.1, $\|\mathbf{u}\|_1$ in the case of the existing method is 1.057×10^2, while the cost in the proposed method is 0.997×10^2, that is, the proposed method successfully obtains an ℓ^1-optimal solution while the existing method cannot. These results show that the proposed method is effective for solving ℓ^1-optimal control problems.

3.4 Conclusion

In this chapter, we have proposed a method to solve ℓ^1-optimal control problems for nonlinear systems. Our method is superior in that the convergence is ensured while the method successfully obtains ℓ^1-optimal inputs. We have also shown a practical algorithm that makes it possible to expand the search area and obtain a more optimal solution under the input restrictions. The next chapter shows an application of a sparse optimal control technique to a nonlinear system.

Table 3.1: The cost of the obtained solutions.

Existing method	Proposed method
1.057×10^2	0.997×10^2

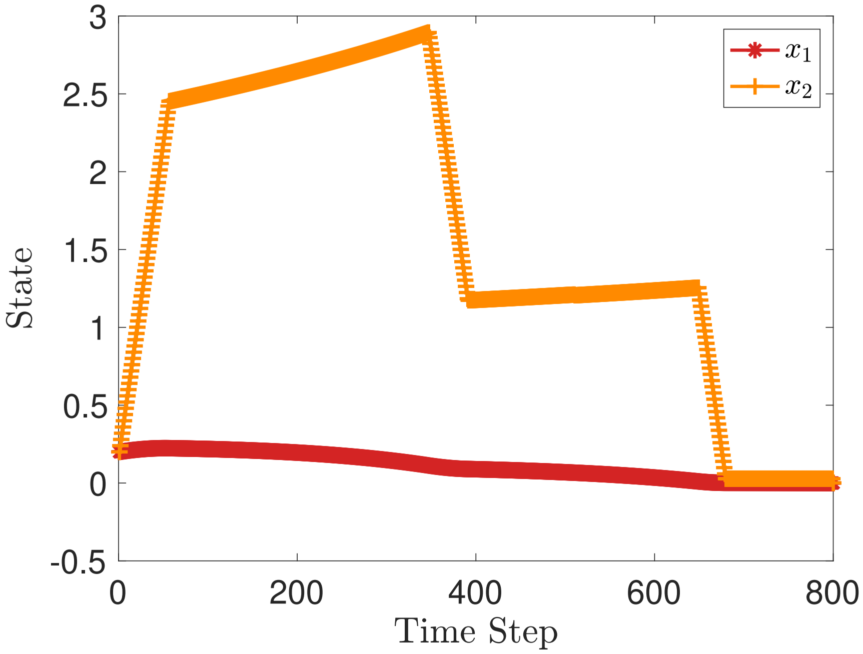

Figure 3.1: The responses of x in the existing method.

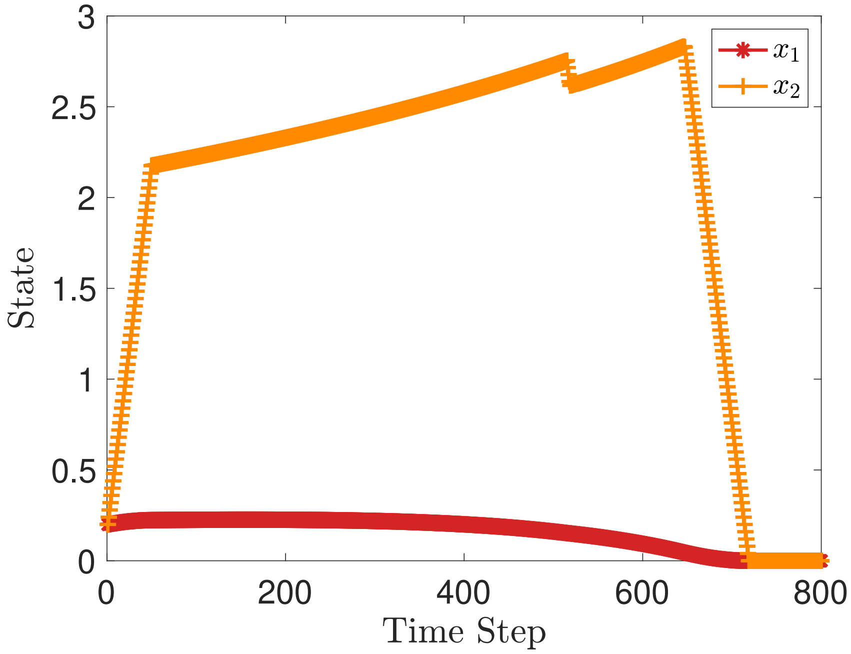

Figure 3.2: The responses of x in the proposed method.

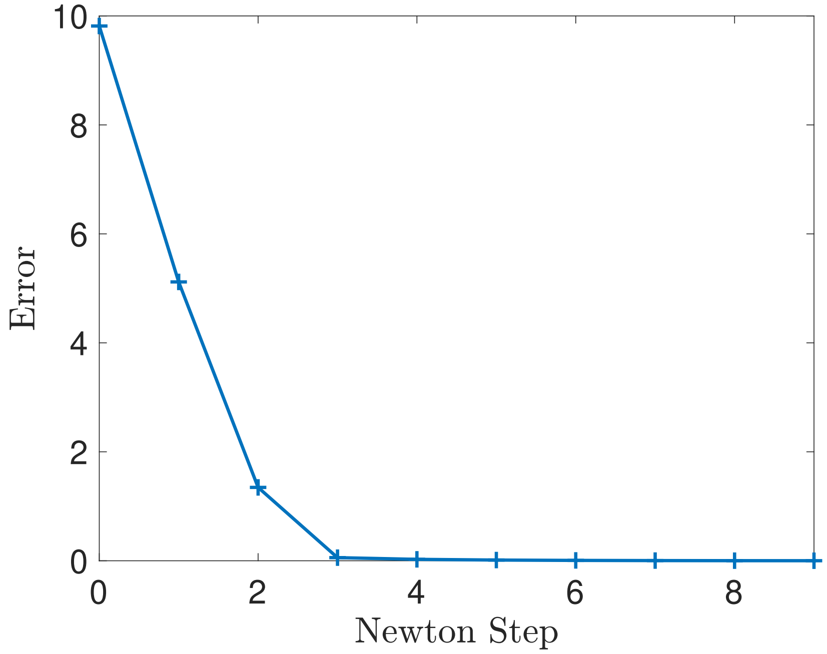

Figure 3.3: The value of $\|P(\mathbf{u}^k)\|_1$ (the error) at each Newton step k in the existing method.

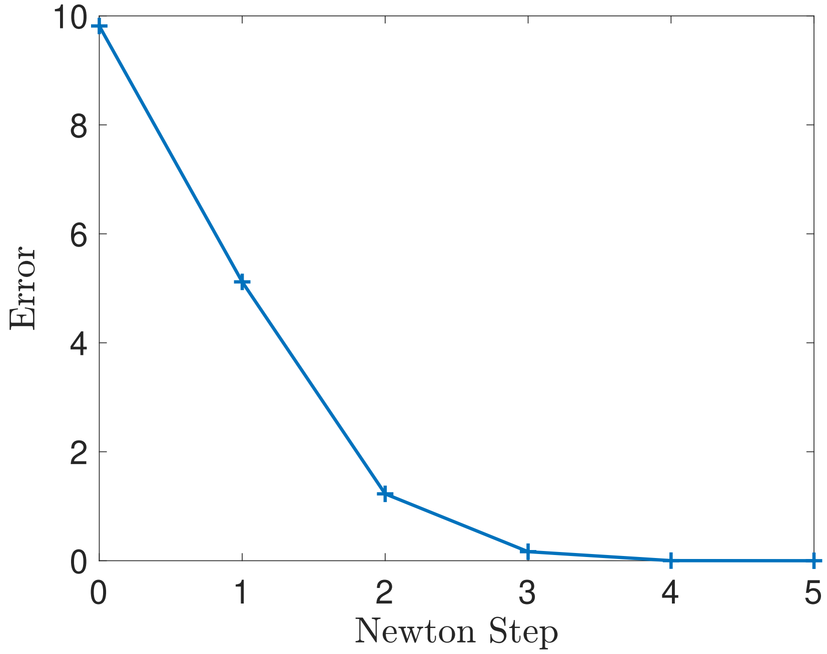

Figure 3.4: The value of $\|P(\mathbf{u}^k)\|_1$ (the error) at each Newton step k in the proposed method.

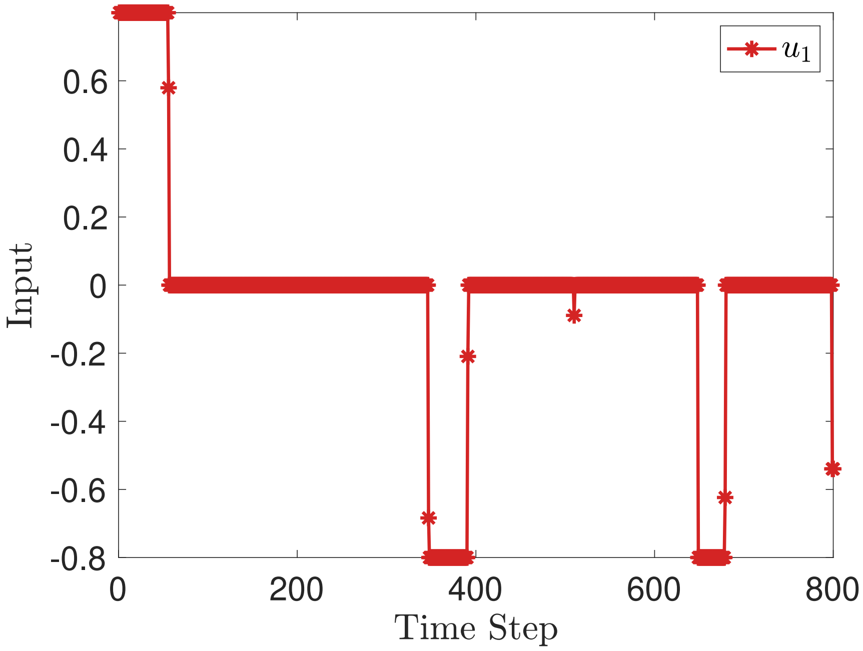

Figure 3.5: The response of u in the existing method.

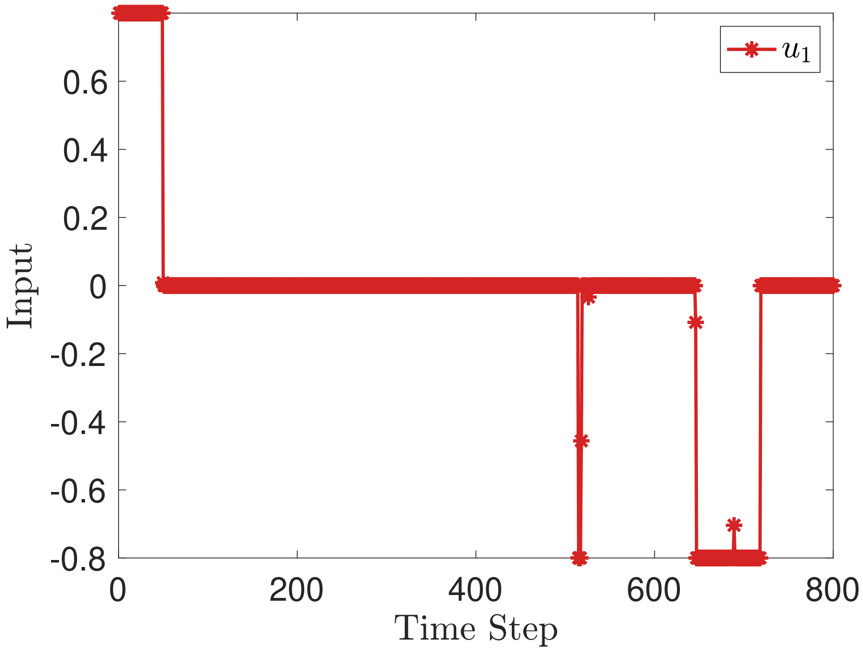

Figure 3.6: The response of u in the proposed method.

Chapter 4

Circular-Clothoid Trajectory Generation Based on L^1/L^2-Optimal Control

This chapter introduces an application of a sparse optimal control technique, that is useful for developing an autonomous driving system. Autonomous driving systems become essential in various areas in recent years. For example, the aging population causes skilled workers shortage at the construction site in Japan. Therefore, there is a need to develop unmanned construction systems in which the construction vehicles move autonomously [56]. Such systems are also useful for works under severe environments as the Moon [57].

In such a system, a vehicle moves autonomously by tracking a trajectory generated beforehand. A lot of trajectory generation (or path planning) methods have been proposed [58, 59, 60, 61, 62]. A circular-clothoid trajectory is one of the trajectories that are easy to track. In this trajectory, circular curves are connected by clothoid curves so that the curvature of the trajectory changes continuously. Since vehicles do not have to steer in a circular curve, such trajectories are easy to track. Besides, these trajectories are useful to avoid the abrupt change of the curvature that causes trouble like a slip. Because of these reasons, such trajectories are often used in trajectory planning [27, 28, 29]. D. H. Shin et al. proposed a method of generating a path using clothoid segments [30]. In that paper, a path composed of clothoid segments is shown to be easier to track than a path consisting of circular curves and straight lines. The method proposed by Kelly et al. focuses on generating a smooth trajectory, for example, clothoid curves [31], in which the proposed method generates a trajectory by using polynomial spirals with the assumption that the longitudinal velocity is constant. In some of those conventional methods, a designer first has to specify waypoints appropriately, and then the trajectory is generated so that it passes through the defined waypoints. Besides, even though the continuous change of the velocity is desirable for tracking, the velocity of the generated trajectory changes discontinuously at the turning points where the vehicle changes the direction of travel. Some conventional methods are able to generate a trajectory whose velocity is continuous. Howard et al. presented a method for trajectory generation, in which they consider energy consumption and obstacle avoidance [63]. Tocker et al. also proposed a trajectory planning method [64], where a path is generated first, and then its velocity profile is optimized. In these methods, although the velocity is continuous, the generated trajectories have a property that the curvature of the trajectory changes discontinuously. The abrupt change of the curvature causes the steep change of the centrifugal force, and vehicles following such trajectories will slip. Hence such a trajectory is not always easy to track.

This chapter presents a method to generate a trajectory whose curvature and velocity are continuous while they are constant in large part by using an L^1/L^2-optimal control technique, which is one of the sparse optimal control techniques. The generated trajectory becomes circular or clothoid in the part where the longitudinal velocity is constant. Since the trajectory becomes circular or clothoid almost everywhere, we call the generated trajectory as a circular-clothoid trajectory. In this trajectory, the velocity and curvature change continuously even at the turning point where the vehicle switches the direction of travel. Hence the vehicle can track the generated trajectory with smooth steering and accelerator operation.

The specific procedure for generating a circular-clothoid trajectory is as follows. First, a vehicle system is transformed into a system whose inputs are the longitudinal velocity and the time derivative of the curvature. A circular-clothoid trajectory generation problem for the system is then interpreted as a problem of finding the inputs such that the longitudinal velocity input and the input of the time derivative of the curvature is piecewise constant in large part. This problem is solved as an L^1/L^2-optimal control problem. The desired trajectory is obtained numerically by applying the locally deforming continuation method proposed in Chapter 2.

This chapter is organized as follows. Section 4.1 gives the problem setting. Section 4.2 describes some existing mathematical results. In Section 4.3, we propose a circular-clothoid trajectory generation method based on L^1/L^2-optimal control. Section 4.4 shows the effectiveness of the proposed method by a numerical simulation. Section 4.5 concludes this chapter.

4.1 Problem setting

The objective of the proposed method is to generate a trajectory whose curvature and longitudinal velocity are continuous while they are constant in large part. The generated trajectory is classified into a circular-clothoid trajectory. Here we define the circular-clothoid trajectory as follows.

Definition 4.1.1. *If the time derivative of the curvature and the longitudinal velocity are piecewise constant in a trajectory, the trajectory is a circular-clothoid trajectory.*

The target of the method is a front steering vehicle. The physical parameters of the vehicle are defined as in Fig. 4.1. The symbol $x_{1,\mathrm{c}}$ denotes the attitude angle, v denotes the longitudinal velocity, and $x_{4,\mathrm{c}}$ denotes the steering angle. The coordinate of the center of the axle of the front wheel and the rear wheel are $(x_{2,\mathrm{a}}, x_{3,\mathrm{a}})$ and $(x_{2,\mathrm{c}}, x_{3,\mathrm{c}})$, respectively. The distance between $(x_{2,\mathrm{a}}, x_{3,\mathrm{a}})$ and $(x_{2,\mathrm{c}}, x_{3,\mathrm{c}})$ is defined as L. Defining $\dot{x}_{1,\mathrm{c}}$ and v as inputs u_1, u_2, respectively, the state space model of the vehicle is denoted by

$$\frac{\mathrm{d}}{\mathrm{d}t}\begin{pmatrix} x_{1,\mathrm{c}} \\ x_{2,\mathrm{c}} \\ x_{3,\mathrm{c}} \\ x_{4,\mathrm{c}} \end{pmatrix} = \begin{pmatrix} 0 & \frac{\tan x_{4,\mathrm{c}}}{L} \\ 0 & \cos x_{1,\mathrm{c}} \\ 0 & \sin x_{1,\mathrm{c}} \\ 1 & 0 \end{pmatrix} \begin{pmatrix} u_1 \\ u_2 \end{pmatrix}. \tag{4.1.1}$$

For simplicity, we use the following notation

$$\dot{x} = G(x)u \tag{4.1.2}$$

instead of (4.1.1), where

$$G(x) := \begin{pmatrix} 0 & \frac{\tan x_{4,\mathrm{c}}}{L} \\ 0 & \cos x_{1,\mathrm{c}} \\ 0 & \sin x_{1,\mathrm{c}} \\ 1 & 0 \end{pmatrix}. \tag{4.1.3}$$

In (4.1.2), $x := (x_{1,\mathrm{c}}, x_{2,\mathrm{c}}, x_{3,\mathrm{c}}, x_{4,\mathrm{c}})^{\mathrm{T}}$ and $u := (u_1, u_2)^{\mathrm{T}}$ are the states and the inputs of the system, respectively. The input vector $u(t)$ is constrained in magnitude by

$$|u_i(t)| \leq m_i, \tag{4.1.4}$$

where $m_i \in \mathbb{R}$, $m_i > 0$ $(i = 1, 2)$. The value of m_i is determined by the performance of the vehicle.

The problem setting is shown in Fig. 4.2. The axis X and Y denote the Cartesian coordinates of the horizontal plane. The time interval of the trajectory is set to

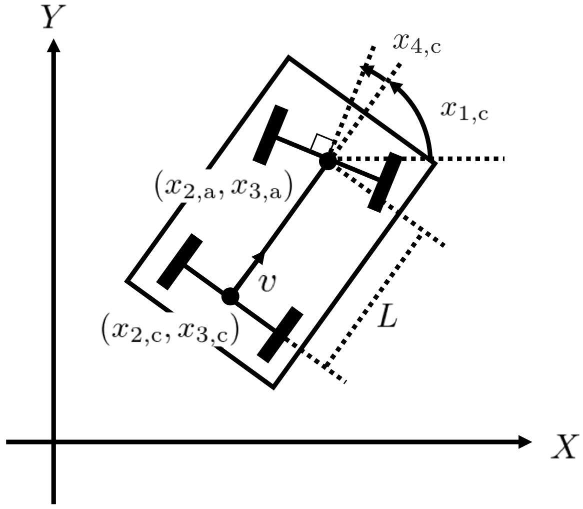
Y
$x_{4,\mathrm{c}}$
$x_{1,\mathrm{c}}$
$(x_{2,\mathrm{a}}, x_{3,\mathrm{a}})$
v
L
$(x_{2,\mathrm{c}}, x_{3,\mathrm{c}})$
X

Figure 4.1: A front steering vehicle model.

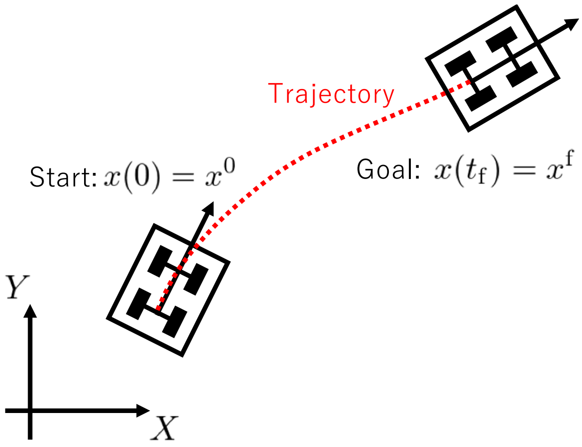

Figure 4.2: Problem setting.

$[0, t_\mathrm{f}]$, where $t_\mathrm{f} > 0$ is the terminal time. The objective of the proposed method is to generate a circular-clothoid trajectory from the initial state $x^0 \in \mathbb{R}^4$ to the terminal state $x^\mathrm{f} \in \mathbb{R}^4$ for the front steering vehicle, illustrated as the dotted curve in Fig. 4.2.

4.2 Preliminaries

The mathematical results used in the proposed method are reviewed in this section. The following discussion is based on the system (4.1.2) and the problem explained in Section 4.1.

4.2.1 L^1/L^2-optimal control theory

The objective of an L^1/L^2-optimal control problem is to find an optimal input vector $u^*(t), t \in [0, t_\mathrm{f}]$ which is a solution of the following problem.

$$\begin{aligned} \underset{u}{\text{minimize}}\ J_{12} := \int_0^{t_\mathrm{f}} \sum_{i=1}^{2} \left(w_i |u_i(t)| + r_i |u_i(t)|^2 \right) \mathrm{d}t \\ \text{s.t. } x(0) = x^0,\ x(t_\mathrm{f}) = x^\mathrm{f}, \end{aligned} \tag{4.2.1}$$

where $w_i > 0, r_i > 0$ $(i = 1, 2)$ are the weights of the norm. The time t_f has to be larger enough than the minimum time t_f^* that is obtained by solving a minimum time optimal control problem [65].

The optimal input is obtained analytically as a function of $x(t)$ and $p(t)$ by analyzing a Hamiltonian function with respect to the L^1/L^2-optimal control problem, where $p(t) \in \mathbb{R}^4$ is a costate vector of $x(t)$, $p(t) \in \mathbb{R}^4$. The Hamiltonian function is defined as

$$\begin{aligned} &H(x(t), p(t), u(t)) \\ &:= \sum_{i=1}^{2} \left(w_i |u_i(t)| + \frac{r_i}{2} u_i(t)^2 \right) + p(t)^\mathrm{T} G(x(t)) u(t). \end{aligned} \tag{4.2.2}$$

According to the Pontryagin's minimum principle [45, 46, 47], the optimal state $x^*(t)$, the optimal costate $p^*(t)$, and the optimal input $u^*(t)$ minimizing the Hamiltonian function (4.2.2) also minimize the cost function (4.2.1).

Assume that $x^*(t)$ and $p^*(t)$ are given. By completing the square, the Hamiltonian function is written by

$$\begin{aligned} &H(x^*(t), p^*(t), u(t)) \\ &= \sum_{i=1}^{2} \left(w_i |u_i(t)| + p^*(t)^\mathrm{T} g_i(x^*(t)) u_i(t) + \frac{r_i}{2} u_i(t)^2 \right) \\ &= \sum_{i=1}^{2} \begin{cases} \frac{r_i}{2} \left(u_i + \frac{(w_i + p^{*\mathrm{T}} g_i(x^*))}{r_i} \right)^2 + C_i & \text{if } u_i \geq 0, \\ \frac{r_i}{2} \left(u_i - \frac{(w_i - p^{*\mathrm{T}} g_i(x^*))}{r_i} \right)^2 + \tilde{C}_i & \text{if } u_i < 0 \end{cases} \end{aligned} \tag{4.2.3}$$

with $x^*(t)$ and $p^*(t)$. In the last line of (4.2.3), we omit t for simplicity. The symbols g_i $(i = 1, 2)$ denote the column vectors of G, and they are in the relation $G(x(t)) = (g_1(x(t)), g_2(x(t)))$. In (4.2.3), C_i and $\tilde{C}_i$ $(i = 1, 2)$ are functions of $x^*(t)$ and $p^*(t)$, and they are independent of $u(t)$. Hence, from (4.2.3), the optimal input $u^*(t) = (u_1^*(t), u_2^*(t))^\mathrm{T}$ minimizing the Hamiltonian function (4.2.2) is denoted by

$$u_i^*(t) = -\mathrm{sat}_{m_i} \left(S_{\alpha_i} \left(\frac{p^*(t)^\mathrm{T} g_i(x^*(t))}{r_i} \right) \right) \tag{4.2.4}$$

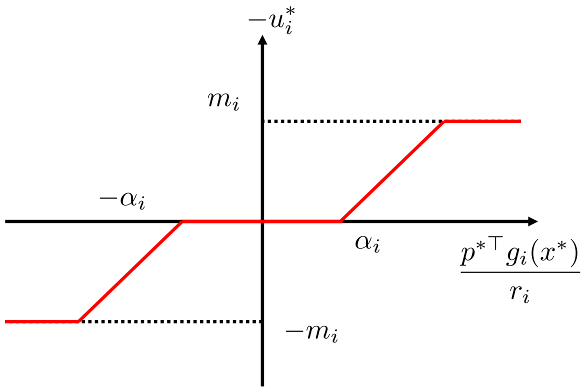

Figure 4.3: Shape of the L^1/L^2-optimal input $u^*(x^*, p^*)$.

with $x^*(t)$ and $p^*(t)$, where α_i is the ratio of w_i to r_i, defined as $\alpha_i = w_i/r_i$. The symbol $S_\alpha(\cdot)$ denotes the shrinkage function represented by

$$S_\alpha(v) := \begin{cases} v + \alpha & \text{if } v < -\alpha, \\ 0 & \text{if } -\alpha \leq v \leq \alpha, \\ v - \alpha & \text{if } \alpha < v, \end{cases} \tag{4.2.5}$$

and $\mathrm{sat}_m(\cdot)$ denotes the saturation function

$$\mathrm{sat}_m(v) := \begin{cases} -m & \text{if } v < -m, \\ v & \text{if } -m \leq v \leq m, \\ m & \text{if } m < v. \end{cases} \tag{4.2.6}$$

Figure 4.3 shows the optimal input (4.2.4) as a red solid line. As the figure shows, the optimal input is more likely to become zero. The L^1/L^2-optimal input becomes like a bang-off-bang form when the weight of the L^1 norm becomes greater enough than the weight of the L^2 norm. This property is explained in the next subsection.

4.2.2 Bang-off-bang property of L^1/L^2-optimal control

To show that the L^1/L^2-optimal control input has a form like bang-off-bang, we explain the limiting property of L^1/L^2-optimal control. The L^1/L^2-optimal control is a mixture of L^1-optimal control and L^2-optimal control. A cost function of an L^1-optimal control problem is defined as

$$\begin{aligned} J_1 &:= \int_0^{t_\mathrm{f}} \sum_{i=1}^{2} \left(w_i |u_i(t)| \right) \mathrm{d}t \\ &\text{s.t. } x(0) = x^0, \ x(t_\mathrm{f}) = x^\mathrm{f}. \end{aligned} \tag{4.2.7}$$

The L^1-optimal input u^* minimizing (4.2.7) is given by

$$u_i^*(t) = -D_{m_i,w_i}\left(p^*(t)^{\mathrm{T}} g_i(x^*(t))\right), \tag{4.2.8}$$

where D_{m_i,w_i} is a dead-zone function defined as

$$\begin{aligned} D_{m,w}(v) &= \begin{cases} -m & \text{if } v < -w, \\ 0 & \text{if } -w < v < w, \\ m & \text{if } w < v, \end{cases} \\ D_{m,w}(v) &\in [-m, 0] \ \text{ if } v = -w, \\ D_{m,w}(v) &\in [0, m] \quad \text{if } v = w. \end{aligned} \tag{4.2.9}$$

Note that the value of the dead-zone function $D_{m,w}$ is not uniquely determined when the argument is equal to $\pm w$. The problem is called normal if the L^1-optimal control input is uniquely determined at almost all $t \in [0, t_{\mathrm{f}}]$ [66].

On the other hand, the cost function of an L^2-optimal control problem is defined as

$$\begin{aligned} J_2 &:= \int_0^{t_{\mathrm{f}}} \sum_{i=1}^{2} \left(\frac{r_i}{2} \cdot |u_i(t)|^2\right) \mathrm{d}t \\ &\text{s.t. } x(0) = x^0,\ x(t_{\mathrm{f}}) = x^{\mathrm{f}}. \end{aligned} \tag{4.2.10}$$

The L^2-optimal input $u^*(t)$ minimizing (4.2.10) is given by

$$u_i^*(t) = -\mathrm{sat}_{m_i}\left(\frac{p^*(t)^{\mathrm{T}} g_i(x^*(t))}{r_i}\right). \tag{4.2.11}$$

The L^1/L^2-optimal input has the following limiting property with respect to the L^1-optimal input and the L^2-optimal input [66].

Proposotion 4.2.1. *Assume the L^1-optimal control problem is normal. Let $u^{L^1}(w)$, $u^{L^2}(r)$, and $u^{L^1/L^2}(w, r)$ be the L^1-optimal input, the L^{L^2}-optimal input, and the L^1/L^2-optimal input with weight parameters $w := (w_1, w_2)$, $r := (r_1, r_2)$, respectively. For any fixed $w > 0$,*

$$\lim_{r \to 0_{2\times 1}} u^{L^1/L^2}(w, r) = u^{L^1}(w) \tag{4.2.12}$$

holds. In addition, for any fixed $r > 0$,

$$\lim_{w \to 0_{2\times 1}} u^{L^1/L^2}(w, r) = u^{L^2}(r) \tag{4.2.13}$$

holds.

Hence, if the weight of the L^1 norm becomes greater enough than the weight of the L^2 norm, the L^1/L^2-optimal input becomes like a bang-off-bang form. Note that the L^1/L^2-optimal input is continuous though the L^1-optimal input is discontinuous. The proposed method generates a circular-clothoid trajectory by using this property.

4.3 Proposed method

The objective of the proposed method is to generate a trajectory whose curvature and longitudinal velocity are continuous while they are piecewise constant in large part. The proposed method is based on two new ideas. One is to transform the original plant system into another system that has two inputs, the longitudinal velocity and the time derivative of the curvature. The other is to formulate the trajectory generation problem with the transformed system as an L^1/L^2-optimal control problem. The optimal control problem is transformed into a TPBVP, and the solution is obtained numerically by the shooting method with the locally deforming continuation method.

4.3.1 Transformation of the vehicle system

From the definition, the curvature κ_c of the trajectory of the vehicle is denoted as

$$\kappa_\mathrm{c} = \frac{\mathrm{d}x_{1,\mathrm{c}}}{\mathrm{d}s} = \frac{\mathrm{d}x_{1,\mathrm{c}}}{\mathrm{d}t}\frac{\mathrm{d}t}{\mathrm{d}s}, \tag{4.3.1}$$

where s is the arc length of the trajectory. Since the time derivative of s is equal to u_2 in the problem,

$$\frac{\mathrm{d}x_{1,\mathrm{c}}}{\mathrm{d}t} = \kappa_\mathrm{c} u_2 = \frac{\tan x_{4,\mathrm{c}}}{L} u_2 \tag{4.3.2}$$

holds from (4.3.1). Define a new input vector $\tilde{u} = [\tilde{u}_1, \tilde{u_2}]^\mathrm{T}$ as

$$\tilde{u}_1 = \dot{\kappa}, \tag{4.3.3}$$

$$\tilde{u}_2 = u_2, \tag{4.3.4}$$

and use κ_c instead of $x_{4,\mathrm{c}}$, (4.1.1) is transformed to

$$\frac{\mathrm{d}}{\mathrm{d}t}\begin{pmatrix} x_{1,\mathrm{c}} \\ x_{2,\mathrm{c}} \\ x_{3,\mathrm{c}} \\ \kappa_\mathrm{c} \end{pmatrix} = \begin{pmatrix} 0 & \kappa_\mathrm{c} \\ 0 & \cos x_{1,\mathrm{c}} \\ 0 & \sin x_{1,\mathrm{c}} \\ 1 & 0 \end{pmatrix} \begin{pmatrix} \tilde{u}_1 \\ \tilde{u}_2 \end{pmatrix}. \tag{4.3.5}$$

For simplicity, we use the following notation

$$\dot{\tilde{x}} = \tilde{G}(\tilde{x})\tilde{u} \tag{4.3.6}$$

instead of (4.3.5), where

$$\tilde{G}(\tilde{x}) := \begin{pmatrix} 0 & \kappa_\mathrm{c} \\ 0 & \cos x_{1,\mathrm{c}} \\ 0 & \sin x_{1,\mathrm{c}} \\ 1 & 0 \end{pmatrix}. \tag{4.3.7}$$

In (4.3.6), $\tilde{x} := (x_{1,\mathrm{c}}, x_{2,\mathrm{c}}, x_{3,\mathrm{c}}, \kappa_{\mathrm{c}})^{\mathrm{T}}$ is the state of the system. In the proposed method, $\tilde{u}(t)$ is constrained in magnitude by the new relation

$$|\tilde{u}_i(t)| \leq \tilde{m}_i, \tag{4.3.8}$$

where $\tilde{m}_i \in \mathbb{R}$, $\tilde{m}_i > 0$ $(i = 1, 2)$. The value of $\tilde{m}_i$ is determined by the performance of the vehicle.

4.3.2 Design of the optimal control problem

Next, the trajectory generation problem is formulated as an L^1/L^2-optimal control problem in the proposed method. The cost function of the optimal control problem is defined as follows.

$$\begin{aligned} J &:= \int_0^{t_{\mathrm{f}}} w_1 \left|\tilde{u}_1(t)\right| + w_2 \left|\tilde{u}_2(t)\right| + \frac{r_1}{2}|\tilde{u}_1(t)|^2 + \frac{r_2}{2}|\tilde{u}_2(t)|^2 \mathrm{d}t \\ &\text{s.t. } \tilde{x}(0) = \tilde{x}^0,\ \tilde{x}(t_{\mathrm{f}}) = \tilde{x}^{\mathrm{f}}. \end{aligned} \tag{4.3.9}$$

The weights satisfy $w_i > 0$ and $r_i > 0$ $(i = 1, 2)$. The boundary conditions are defined as

$$\tilde{x}^0 = \Phi(x^0),\ \tilde{x}^{\mathrm{f}} = \Phi(x^{\mathrm{f}}), \tag{4.3.10}$$

where

$$\Phi : \begin{pmatrix} x_{1,\mathrm{c}} & x_{2,\mathrm{c}} & x_{3,\mathrm{c}} & x_{4,\mathrm{c}} \end{pmatrix}^{\mathrm{T}} \to \begin{pmatrix} x_{1,\mathrm{c}} & x_{2,\mathrm{c}} & x_{3,\mathrm{c}} & \tan\left(x_{4,\mathrm{c}}\right)/L \end{pmatrix}^{\mathrm{T}}. \tag{4.3.11}$$

It follows from (4.2.4) that the optimal input $\tilde{u}^*(t)$ minimizing the cost function (4.3.9) is denoted by the following equation :

$$\tilde{u}_i^*(t) = -\mathrm{sat}_{m_i}\left(S_{\frac{w_i}{r_i}} \left(\frac{\tilde{p}^*(t)^{\mathrm{T}} \tilde{g}_i(\tilde{x}^*(t))}{r_i} \right) \right) \ (i = 1, 2), \tag{4.3.12}$$

where $\tilde{G}(\tilde{x}(t)) = (\tilde{g}_1(\tilde{x}(t)), \tilde{g}_2(\tilde{x}(t)))$, and $\tilde{p}^*(t)$ is the optimal costate of the optimal state $\tilde{x}^*(t)$. Note that a circular trajectory and a clothoid trajectory are characterized in terms of the time derivative of the curvature with the constant longitudinal velocity, as $\dot{\kappa}_{\mathrm{c}} = 0$ and $\dot{\kappa}_{\mathrm{c}} = \text{const.}$, respectively. Since the L^1/L^2-optimal input is more likely to become zero, the curvature becomes constant in the large part of the trajectory. Besides, because of the bang-off-bang property of L^1/L^2-optimal control, the optimal inputs $\tilde{u}_1^*(t) = \dot{\kappa}_{\mathrm{c}}(t)$ and $\tilde{u}_2^*(t)$ become like bang-off-bang if the weight w_i is set to be larger enough than r_i. Hence, the trajectory generated with the L1/L2-optimal inputs is classified into the circular-clothoid trajectory.

4.4 Numerical example

This section shows several examples of generating a circular-clothoid trajectory. In these examples, given L^1/L^2-optimal control problems are solved with the locally deforming continuation method proposed in Chapter 2, where J_{E} and J_{O} are set to

$$J_{\mathrm{E}} = \int_0^{t_{\mathrm{f}}} \sum_{i=1}^{2} \frac{1}{2}\tilde{u}_i(t)^2 \mathrm{d}t, \tag{4.4.1}$$

$$J_{\mathrm{O}} = \int_0^{t_{\mathrm{f}}} \sum_{i=1}^{2} \frac{1}{2}\tilde{u}_i(t)^2 + 2|\tilde{u}_i| \mathrm{d}t, \tag{4.4.2}$$

and $l^{\mathrm{C}}(\tilde{x}(t), \tilde{u}(t), t)$ is given as

$$l^{\mathrm{C}}(\tilde{x}(t), \tilde{u}(t), t) = \sum_{i=1}^{2} \frac{1}{2}\tilde{u}_i(t)^2 + f_w(t)|\tilde{u}_i|, \tag{4.4.3}$$

$$f_w(t) = 2(t-c)/h, \tag{4.4.4}$$

with $h = \delta = 0.2$.

4.4.1 Example 1 : reduction of the steering operation

The parameters are defined as $x^0 = (0,0,0,0)^{\mathrm{T}}, x^{\mathrm{f}} = (0,4,0.5,0)^{\mathrm{T}}, t_{\mathrm{f}} = 4, r_1 = r_2 = 1, w_1 = w_2 = 2, \tilde{m}_1 = 0.3, \tilde{m}_2 = 0.8$, in this example.

Figure 4.4 shows the generated trajectory. The horizontal and vertical axes are X and Y, respectively. The solid line illustrates the generated trajectory. Figure 4.5 shows the responses of the inputs, where the horizontal axis is time and the vertical axis is the input. In the figure, the thick solid line denotes the input of the time derivative of the curvature $\tilde{u}_1^*(t)$ while the thin solid line is the longitudinal velocity input $\tilde{u}_2^*(t)$ of the vehicle. The dashed lines illustrate the upper and lower bounds of $\tilde{u}_1^*(t)$ and $\tilde{u}_2^*(t)$. As Fig. 4.5 shows, the time derivative of the curvature is zero in large part, that is, the curvature is constant in large part. Since the time derivative of the curvature and the longitudinal velocity are piecewise constant in large part, the generated trajectory is classified into the circular-clothoid trajectory.

To make clear the advantage of the proposed method, Fig. 4.6 shows the trajectory generated by the conventional method, and Fig. 4.7 shows the responses of the inputs of the generated trajectory. The trajectory is generated by solving the L^2-optimal control problem whose cost function is given as (4.3.9) with the parameters $r_1 = r_2 = 1, w_1 = w_2 = 0, t_{\mathrm{f}} = 4$, where the boundary conditions are given as $x^0 = (0,0,0,0)^{\mathrm{T}}, x^{\mathrm{f}} = (0,4,0.5,0)^{\mathrm{T}}$. The inputs are restricted by $\tilde{m}_1 = 0.3, \tilde{m}_2 = 1.1$. In

Fig. 4.6, the horizontal and vertical axes are X and Y, respectively. The solid line illustrates the generated trajectory. In Fig. 4.7, the horizontal axis is time, and the vertical axis is the input. In the figure, the thick solid line denotes the input of the time derivative of the curvature $\tilde{u}_1^*(t)$ while the thin solid line is the longitudinal velocity input $\tilde{u}_2^*(t)$ of the vehicle. The dashed lines illustrate the upper and lower bounds of $\tilde{u}_1^*(t)$ and $\tilde{u}_2^*(t)$. As Fig. 4.7 shows, both the time derivative of the curvature and the longitudinal velocity are not piecewise constant. Hence the trajectory generated by the conventional method requires much steering operation.

4.4.2 Example 2 : automatic generation of the turning point

The parameters are defined as $x^0 = (\pi/4, 0, 0, 0)^{\mathrm{T}}, x^{\mathrm{f}} = (0, 1, 0.5, 0)^{\mathrm{T}}, t_{\mathrm{f}} = 4, r_1 = r_2 = 1, w_1 = w_2 = 2, \tilde{m}_1 = 0.3, \tilde{m}_2 = 1.1$, in this example.

Figure 4.8 shows the generated circular-clothoid trajectory, in which the vehicle goes forward first and then goes backward. Note that any waypoint is not specified. The horizontal and vertical axes are X and Y, respectively. The solid line illustrates the generated trajectory. Figure 4.9 shows the responses of the inputs, where the horizontal axis is time and the vertical axis is the input. In the figure, the thick solid line denotes the input of the time derivative of the curvature $\tilde{u}_1^*(t)$, while the thin solid line is the longitudinal velocity input $\tilde{u}_2^*(t)$ of the vehicle. The dashed lines illustrate the upper and lower bounds of $\tilde{u}_1^*(t)$ and $\tilde{u}_2^*(t)$. As Fig. 4.9 shows, though the curvature is not constant in large part because of the boundary conditions, the generated trajectory is a circular-clothoid trajectory. Besides, the longitudinal velocity changes continuously, even at the turning point.

4.5 Conclusion

In this chapter, we have proposed the method for generating a trajectory whose curvature and longitudinal velocity are continuous while they are piecewise constant in large part. The method is based on L^1/L^2-optimal control. In the proposed method, the vehicle system is transformed to the system whose inputs are the time derivative of the curvature and the longitudinal velocity. The trajectory generation problem is then formulated as the specific L^1/L^2-optimal control problem. This problem is successfully solved by the locally deforming continuation method propose in Chapter 2. The trajectory generated by the proposed method is confirmed to be classified into the circular-clothoid trajectory through numerical simulations.

In the previous chapters, we have focused on sparse optimal control, one of the feedforward control techniques, and have made some proposals on its applications and how to obtain such inputs. Those proposals will make it possible to use feedforward control based on sparse optimal control techniques in practical applications. The next chapter focuses on feedback control and proposes several control methods.

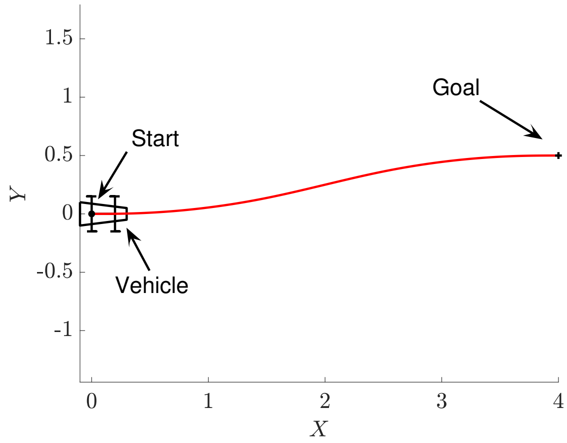

Figure 4.4: The generated circular-clothoid trajectory.

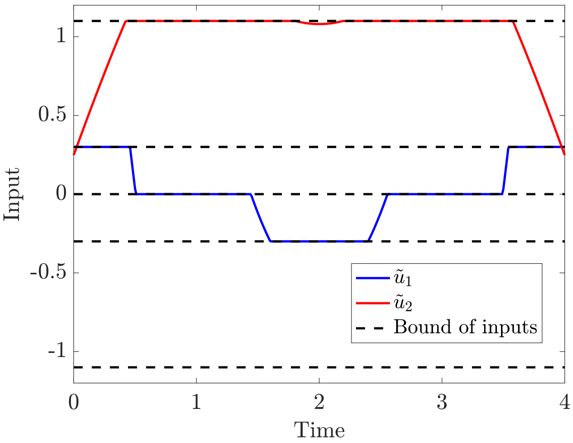

Figure 4.5: The response of the inputs.

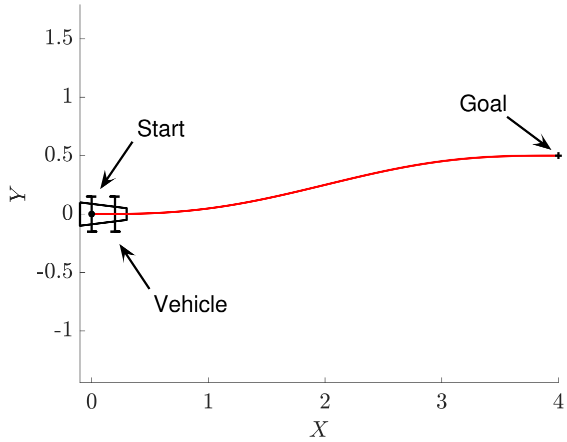

Figure 4.6: The generated trajectory with the conventional method.

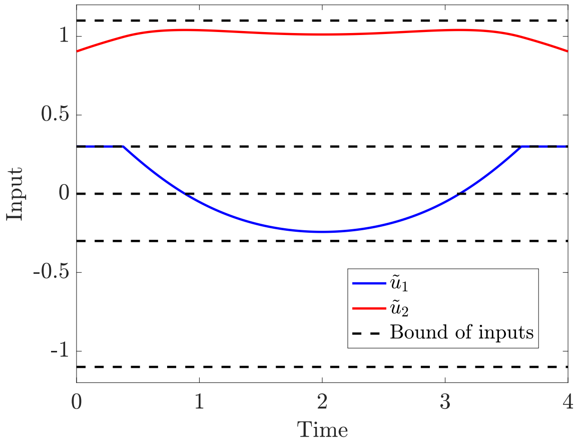

Figure 4.7: The responses of the inputs of the generated trajectory with the conventional method.

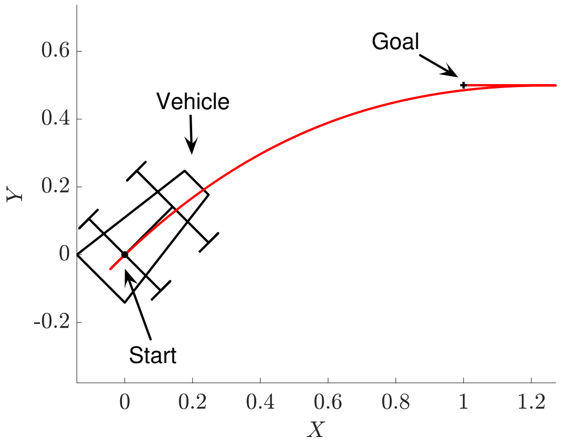

Figure 4.8: The generated circular-clothoid trajectory.

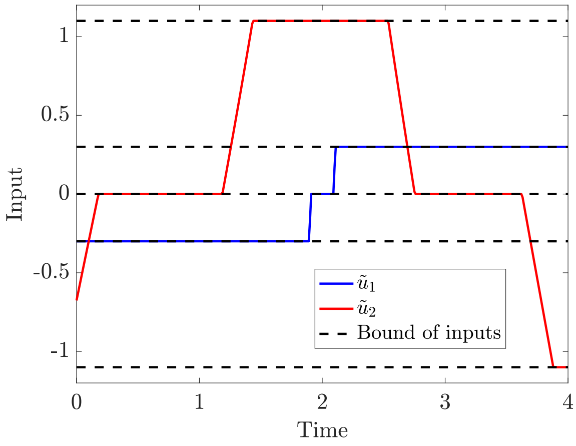

Figure 4.9: The responses of the inputs.

Chapter 5

Passivity-Based Lag Compensator

This chapter and the next chapter focus on feedback control techniques for nonlinear mechanical systems represented in the pH framework and propose feedback controllers with which the output response can be easily tuned. The pH framework has proven to be suitable to represent a broad class of mechanical systems [32, 33]. An advantage of the pH approach is the explicit representation of physical phenomena and concepts such as energy, interconnection patterns, and dissipation, which may provide some intuition to ease the analysis of the system and the control design process. Due to the energy-based nature of the pH models, passivity-based control (PBC) techniques arise as a natural option to devise controllers to stabilize these systems [34], where the control design process consists of two steps: energy-shaping and damping injection.

Concerning the stabilization of mechanical systems via PBC techniques, the literature is vast, e.g., [35, 36, 37, 38, 39, 40, 41]. However, most of PBC methods focus only on stabilizing the system under study. Therefore, there are no clear guidelines on how to tune the controller gains to ensure desired responses of the closed-loop system. To address this issue, several recent studies have focused on the tuning method of the control gains as in [67, 68, 69, 70]. For example, in [67, 68], the authors presented a tuning policy for PBC techniques to suppress overshoots and oscillations. Especially in [68], the authors introduce a passivity-based dynamic feedback controller and propose to tune it using a transfer function representation. In this approach, the obtained controller admits a lead compensator interpretation, and the control gains can be chosen based on frequency analysis. It is noteworthy that, while this control approach can improve the responsiveness of the closed-loop system, it cannot reduce the steady-state error since these compensators cannot change the characteristics of low-frequency signals. An alternative to overcome this issue is given by the so-called lag-compensators, which amplify the input signals at low frequencies. This property makes it possible to reduce the steady-state error without changing the responsiveness property [71].

In this work, we propose a PBC approach to stabilize nonlinear mechanical systems, where the controllers can be interpreted as lag compensators. Therefore, the resulting controllers can effectively reduce the steady-state error while mitigating the windup phenomenon often exhibited by integral control [72]. To this end, we propose a dynamic extension such that the pH structure is preserved for the closed-loop system, which eases the stability proof. Moreover, the proposed control method does not require velocity measurements and can deal with input constraints by naturally saturating the control signals.

The rest of this chapter is organized as follows. In Section 5.1, we introduce the pH representation of mechanical systems, the problem formulation, and briefly revisit some previous results regarding PBC techniques with dynamic extension. Next, in Section 5.2 we propose a passivity-based lag compensator and a modified passivity-based lag compensator where the controller is saturated. In Section 5.3, we illustrate experimental results of the implementation of the lag compensators in a two degrees-of-freedom (DoF) planar manipulator with flexible joints. We summarize this chapter in Section 5.4.

5.1 Problem setting and previous results

Let us consider mechanical systems whose behavior is represented by

$$\begin{pmatrix} \dot{q} \\ \dot{p} \end{pmatrix} = \begin{pmatrix} 0_{n\times n} & I_n \\ -I_n & -D(q,p) \end{pmatrix} \begin{pmatrix} \nabla_q H(q,p) \\ \nabla_p H(q,p) \end{pmatrix} + \begin{pmatrix} 0_{n\times m} \\ G \end{pmatrix} u, \tag{5.1.1}$$

$$H(q,p) = \frac{1}{2} p^\top M(q)^{-1} p + V(q), \tag{5.1.2}$$

where $q, p \in \mathbb{R}^n$ are the generalized positions and momenta, respectively, $u \in \mathbb{R}^m$ is the input vector, with $n, m \in \mathbb{Z}_+$, $n < m$, $D : \mathbb{R}^n \times \mathbb{R}^n \to \mathbb{R}^{n\times n}$ is the positive definite symmetric damping matrix, $H : \mathbb{R}^n \times \mathbb{R}^n \to \mathbb{R}_+$ is the Hamiltonian function of the system, where $V : \mathbb{R}^n \to \mathbb{R}_+$ is the potential energy of the system and $M : \mathbb{R}^n \to \mathbb{R}^{n\times n}$ is the positive definite inertia matrix, and the input gain matrix G is defined as

$$G := \begin{pmatrix} 0_{k\times m} \\ I_m \end{pmatrix}; \quad k := n - m. \tag{5.1.3}$$

Hence, we can split the state vector as follows

$$q = \begin{pmatrix} q_{\mathrm{u}} \\ q_{\mathrm{a}} \end{pmatrix}, \quad p = \begin{pmatrix} p_{\mathrm{u}} \\ p_{\mathrm{a}} \end{pmatrix}, \tag{5.1.4}$$

where

$$q_{\mathrm{u}} := G^{\perp} q,\ q_{\mathrm{a}} := G^{\top} q,\ p_{\mathrm{u}} := G^{\perp} p,\ p_{\mathrm{a}} := G^{\top} p, \tag{5.1.5}$$

with $G^{\perp} = \begin{pmatrix} I_k & 0_{k\times m} \end{pmatrix}$. To formulate the problem under study, we first define the set of assignable equilibria for (5.1.1), which is given by

$$\mathcal{E} = \{q \in \mathbb{R}^n \mid \nabla_{q_u} V(q) = 0_{k\times 1}\}, \tag{5.1.6}$$

and we define the error $q^{\mathrm{e}} = q - q^*$ and $q^{\mathrm{e}}_{\mathrm{a}} = G^{\top} q^{\mathrm{e}}$, where $q^* \in \mathcal{E}$. Then, the problem under study can be formulated as follows

Problem Setting 5.1.1. *Given the mechanical system* (5.1.1) *and the desired equilibrium point* $(q^*, 0_n)$*, find a controller* u *that renders asymptotically stable* $(q^*, 0_n)$ *while ensuring that:*

- *No velocity measurements are required to achieve the control task.*
- *There is a systematic method to select the control gains to reduce the steady-state error caused by modeling errors of nonlinear friction.*

5.1.1 Some previous results on PBC with dynamic extension

In this section, we briefly revisit the results reported in [68]-[73], where the reported controllers are suitable to suppress oscillations or reject disturbances. The main idea of these methods is to propose a dynamic extension $x_{\mathrm{c}} \in \mathbb{R}^m$ and a dynamic control law of the form

$$u = f^{u}(q, p, x_{\mathrm{c}}), \tag{5.1.7}$$

$$\dot{x}_{\mathrm{c}} = f^{x_{\mathrm{c}}}(q, p, x_{\mathrm{c}}), \tag{5.1.8}$$

such that the closed-loop system takes the form

$$\dot{\xi} = \begin{pmatrix} 0_{n\times n} & I_n & F_{13} \\ -I_n & -D(q,p) & F_{23} \\ -F_{13}^{\top} & -F_{23}^{\top} & F_{33} \end{pmatrix} \nabla_{\xi} H_{\mathrm{d}}(\xi), \tag{5.1.9}$$

$$H_{\mathrm{d}}(\xi) = H(q,p) + \bar{H}(\xi), \tag{5.1.10}$$

where $\xi = (q^{\top}, p^{\top}, x_{\mathrm{c}}^{\top})^{\top}$, $F_{13} \in \mathbb{R}^{n\times m}$, $F_{23} \in \mathbb{R}^{n\times m}$, $F_{33} \in \mathbb{R}^{m\times m}$. Following this approach, passivity-based controllers that can be interpreted as lead-compensators are reported in [68], while in [74], a kind of integrator is proposed for removing matched disturbances. Additionally, in [68, 75, 73], the dynamic extension removes the necessity of velocity measurements to inject damping into the closed-loop system and ensure the asymptotic convergence towards the desired equilibrium. Inspired by these results, in the following section, we propose a new PBC method where the controller can be interpreted as a lag-compensator.

5.2 Proposed method

The lead-compensator in [68] is effective for removing oscillations without measuring velocities, but cannot deal with steady-state errors. On the other hand, the integrator in [74] ensures that the steady-state error equals zero and is suitable to reject some disturbances. Alas, this controller requires velocity measurements. To address these issues, in this section, we present the main contribution of this chapter, namely, a passivity-based lag compensator that can reduce the steady-state error without measuring velocities. To this end, we implement a dynamic extension that leads to a pH system different from (5.1.9).

5.2.1 Passivity-based lag compensator

The following theorem introduces a dynamic extension and a control law such that the closed-loop system admits a pH representation. Additionally, it provides conditions to ensure the stability of the desired equilibrium.

Theorem 5.2.1. *Consider system* (5.1.1)*, the virtual state* $x_{\mathrm{c}} \in \mathbb{R}^m$ *with nonlinear dynamics*

$$\dot{x}_{\mathrm{c}} = -\tilde{D}\nabla_{x_{\mathrm{c}}}\bar{H}(q_{\mathrm{a}}, x_{\mathrm{c}}), \tag{5.2.1}$$

and the nonlinear control law

$$u = -\nabla_{q_{\mathrm{a}}}\bar{H}(q_{\mathrm{a}}, x_{\mathrm{c}}) - 2\nabla_{x_{\mathrm{c}}}\bar{H}(q_{\mathrm{a}}, x_{\mathrm{c}}). \tag{5.2.2}$$

Then, the closed-loop system takes the form of a pH system

$$\dot{\xi} = (\mathcal{J} - \mathcal{D})\nabla_{\xi}H_{\mathrm{d}}(\xi), \tag{5.2.3}$$

$$\mathcal{J} = \begin{pmatrix} 0_{n\times n} & I_n & 0_{n\times m} \\ -I_n & 0_{n\times n} & -G \\ 0_{m\times n} & G^{\top} & 0_{m\times m} \end{pmatrix}, \tag{5.2.4}$$

$$\mathcal{D} = \begin{pmatrix} 0_{n\times n} & 0_{n\times n} & 0_{n\times m} \\ 0_{n\times n} & D & G \\ 0_{m\times n} & G^{\top} & \tilde{D} \end{pmatrix}, \tag{5.2.5}$$

if the following condition holds.

$$\begin{pmatrix} D(q,p) & G \\ G^\top & \tilde{D} \end{pmatrix} \succeq 0, \tag{5.2.6}$$

where $\tilde{D} \in \mathbb{R}^{m\times m}$ is a positive definite symmetric matrix, and $H_\mathrm{d}(\xi) := H(q,p) + \bar{H}(\xi)$, with $\bar{H}(\xi)$ to be defined. Furthermore, the desired equilibrium point $\xi^* = (q^{*\top}, 0_{n\times 1}^\top, 0_{m\times 1}^\top)^\top$ is asymptotically stable if the following conditions hold.

C1. $$\begin{pmatrix} D(q,p) & G \\ G^\top & \tilde{D} \end{pmatrix} \succ 0. \tag{5.2.7}$$

C2. *$H_\mathrm{d}(\xi)$ has an isolated minimum at $\xi = \xi^*$.*

C3. $\nabla_p H_\mathrm{d}(\xi) = 0_{n\times 1}, \nabla_{x_\mathrm{c}} H_\mathrm{d}(\xi) = 0_{m\times 1} \Rightarrow q = q^*, x_\mathrm{c} = 0_{m\times 1}$.

Proof. Note that

$$\nabla_q H_\mathrm{d}(\xi) = \nabla_q H(q,p) + \nabla_q \bar{H}(q_\mathrm{a}, x_\mathrm{c}), \tag{5.2.8}$$

$$\nabla_p H_\mathrm{d}(\xi) = \nabla_p H(q,p), \nabla_{x_\mathrm{c}} H_\mathrm{d}(\xi) = \nabla_{x_\mathrm{c}} \bar{H}(q_\mathrm{a}, x_\mathrm{c}). \tag{5.2.9}$$

By substituting (5.2.2) in (5.1.1), we have

$$\dot{q} = \nabla_p H(q,p) = \nabla_p H_\mathrm{d}(\xi), \tag{5.2.10}$$

$$\begin{aligned} \dot{p} =& - \nabla_q H(q,p) - D(q,p)\nabla_p H(q,p) + Gu \\ =& - \nabla_q H(q,p) - D(q,p)\nabla_p H(q,p) \\ &+ G\left(-\nabla_{q_\mathrm{a}} \bar{H}(q_\mathrm{a}, x_\mathrm{c}) - 2\nabla_{x_\mathrm{c}} \bar{H}(q_\mathrm{a}, x_\mathrm{c})\right) \\ =& - \nabla_q H_\mathrm{d}(\xi) - D(q,p)\nabla_p H_\mathrm{d}(\xi) - 2G\nabla_{x_\mathrm{c}} H_\mathrm{d}(\xi), \end{aligned} \tag{5.2.11}$$

and (5.2.1) leads to

$$\dot{x}_\mathrm{c} = -\tilde{D}\nabla_{x_\mathrm{c}} \bar{H}(q_\mathrm{a}, x_\mathrm{c}) = -\tilde{D}\nabla_{x_\mathrm{c}} H_\mathrm{d}(\xi). \tag{5.2.12}$$

Hence, the dynamic extension (5.2.2) and (5.2.1) transforms (5.1.1) into (5.2.3), and if (5.2.6) holds, $\mathcal{D} \succeq 0$ holds and this shows that (5.2.3) is a pH system from the fact that $\mathcal{J}^\top = -\mathcal{J}$. Hereafter, we omit the arguments q, p in D in this proof for simplicity. It follows from (5.2.4) and (5.2.5) that

$$\dot{H}_\mathrm{d} = -(\nabla_\zeta H_\mathrm{d}(\xi))^\top \begin{pmatrix} D & G \\ G^\top & \tilde{D} \end{pmatrix} \nabla_\zeta H_\mathrm{d}(\xi) \leq 0$$

and $\dot{H}_\mathrm{d} = 0$ holds if and only if $\nabla_p H_\mathrm{d}(\xi) = 0_{n\times 1}$, $\nabla_{x_\mathrm{c}} H_\mathrm{d}(\xi) = 0_{m\times 1}$, holds, where $\zeta = (p^\top, x_\mathrm{c}^\top)^\top$. Hence it follows from the assumptions that Krasovskii-Barbashin theorem [76] proves asymptotic stability. □

The following theorem establishes a linear relationship between the control input and the error in positions such that the controller (5.2.2) with (5.2.1) admits a lag compensator interpretation.

Theorem 5.2.2. *Design the function* $\bar{H}(q_{\rm a}, x_{\rm c})$ *as*

$$\bar{H}(q_{\rm a}, x_{\rm c}) = \frac{1}{2}\|q_{\rm a}^{\rm e}\|_{K_{\rm P}}^2 + \frac{1}{2}\|x_{\rm c} - q_{\rm a}^{\rm e}\|_{K_{\rm I}}^2, \tag{5.2.13}$$

and $\tilde{D}$ *as* $\tilde{D} = R_{\rm c}$, *where* $K_{\rm P}, K_{\rm I}, R_{\rm c} \in \mathbb{R}^{m\times m}$ *are diagonal positive definite matrices. When* $K_{{\rm P},i} - K_{{\rm I},i} > 0$ $(i = 1, 2, \cdots, m)$ *holds, the controller (5.2.2) with (5.2.1) represents a lag compensator, where the relation between* $q_{\rm a}^{\rm e}$ *and* u

$$\mathscr{U}(s) = \mathrm{diag}\,(G_i(s))_{i=1}^m\, \mathscr{Q}_{\rm a}^{\rm e}(s), \tag{5.2.14}$$

is given by

$$G_i(s) = K_i \frac{T_i s + 1}{\alpha_i T_i s + 1}, \tag{5.2.15}$$

$$K_i = K_{{\rm P},i},\ T_i = \frac{K_{{\rm P},i} - K_{{\rm I},i}}{K_{{\rm P},i}K_{{\rm I},i}R_{{\rm c},i}},\ \alpha_i = \frac{K_{{\rm P},i}}{K_{{\rm P},i} - K_{{\rm I},i}},$$

where $\mathscr{Q}_{\rm a}^{\rm e}(s) = \mathcal{L}[q_{\rm a}^{\rm e}(t)]$, $\mathscr{U}(s) = \mathcal{L}[u(t)]$.

Proof. The dynamic extension (5.2.2) and (5.2.1) with (5.2.13) is calculated as

$$\begin{aligned} u &= -K_{\rm P} q_{\rm a}^{\rm e} - K_{\rm I}(x_{\rm c} - q_{\rm a}^{\rm e}), \\ \dot{x}_{\rm c} &= -R_{\rm c} K_{\rm I}(x_{\rm c} - q_{\rm a}^{\rm e}). \end{aligned} \tag{5.2.16}$$

Since the matrices $K_{\rm P}$, $K_{\rm I}$, $R_{\rm c}$ are diagonal, for each element,

$$\mathscr{U}_i = -K_{{\rm P},i}\mathscr{Q}_{{\rm a},i}^{\rm e} - K_{{\rm I},i}(\mathscr{X}_{{\rm c},i} - \mathscr{Q}_{{\rm a},i}^{\rm e}), \tag{5.2.17}$$

$$s\mathscr{X}_{{\rm c},i} = -R_{{\rm c},i}K_{{\rm I},i}(\mathscr{X}_{{\rm c},i} - \mathscr{Q}_{{\rm a},i}^{\rm e}), \tag{5.2.18}$$

hold, where $\mathscr{U}_i(s) = \mathcal{L}[u_i(t)]$, $\mathscr{X}_{{\rm c},i}(s) = \mathcal{L}[x_{{\rm c},i}(t)]$, $\mathscr{Q}_{{\rm a},i}^{\rm e}(s) = \mathcal{L}[q_{{\rm a},i}^{\rm e}(t)]$. Hence we have the following relation

$$\begin{aligned} \mathscr{U}_i &= -K_{{\rm P},i}\mathscr{Q}_{{\rm a},i}^{\rm e} - K_{{\rm I},i}\left(\frac{R_{{\rm c},i}K_{{\rm I},i}}{s + R_{{\rm c},i}K_{{\rm I},i}}\mathscr{Q}_{{\rm a},i}^{\rm e} - \mathscr{Q}_{{\rm a},i}^{\rm e}\right) \\ &= -\frac{(K_{{\rm P},i} - K_{{\rm I},i})s + K_{{\rm P},i}R_{{\rm c},i}K_{{\rm I},i}}{s + R_{{\rm c},i}K_{{\rm I},i}}\mathscr{Q}_{{\rm a},i}^{\rm e}. \end{aligned} \tag{5.2.19}$$

It follows from (5.2.19) that (5.2.14) with (5.2.15) holds. □

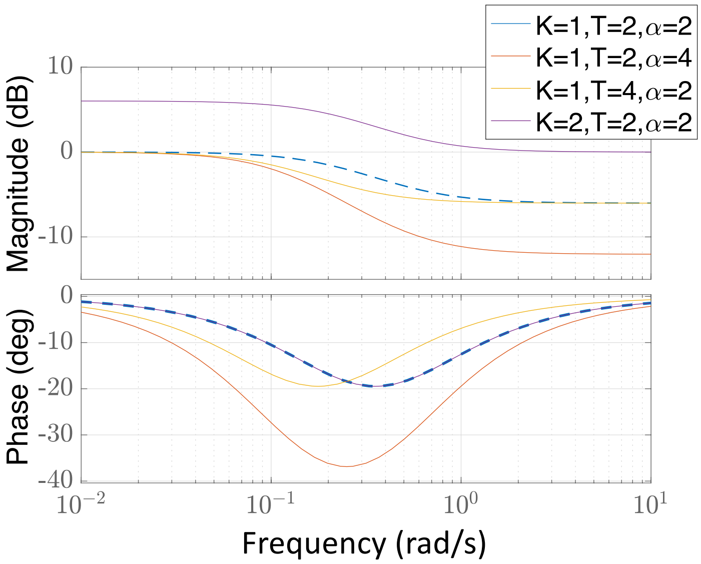

Figure 5.1: Bode plot of the lag compensator (5.2.15) (©2020 IEEE)

As Theorem 5.2.2 claims, the value of α_i in (5.2.15) takes more than one if $K_{\mathrm{P},i} - K_{\mathrm{I},i} > 0$ $(i = 1, 2, \cdots, m)$ holds, which implies that the controller (5.2.2) with (5.2.1) works as a lag-compensation. Figure 5.1 shows the Bode plot of the transfer function (5.2.15), where the values of K_i, T_i, α_i are varied as in the legends of the figure. As in the figure, the lag compensator keeps the gain high at low frequencies and low at high frequencies. Hence, this compensator can improve the steady-state characteristics. The tuning of the controller can also be done intuitively. It follows from (5.2.19) that

$$K_{\mathrm{P},i} = K_i, K_{\mathrm{I},i} = \frac{\alpha_i - 1}{\alpha_i} K_i, R_{\mathrm{c},i} = \frac{1}{(\alpha_i - 1) T_i K_i}, \tag{5.2.20}$$

hold, so the parameters in (5.2.13) and R_{c} are decided by specifying K, α, T. When tuning the gains, one can choose K, α, T appropriately, referring the Bode plot of the lag compensator. In practical applications, inputs are often restricted. In the next subsection, we propose another passivity-based controller that represents a passivity-based lag compensator dealing with input saturation.

5.2.2 Passivity-based lag compensator with input saturation

In [75], Wesselink et al. propose a lead-compensator considering input saturation. Inspired by this method, we propose a passivity-based lag compensator that takes into account input saturation.

Theorem 5.2.3. *Select the function* $\bar{H}(q_{\mathrm{a}}, x_{\mathrm{c}})$ *as*

$$\bar{H}(q_{\mathrm{a}}, x_{\mathrm{c}}) = \phi^1_{(K_{\mathrm{P}})}(q^{\mathrm{e}}_{\mathrm{a}}) + \phi^2_{(K_{\mathrm{I}})}(x_{\mathrm{c}} - q^{\mathrm{e}}_{\mathrm{a}}), \tag{5.2.21}$$

and $\tilde{D}$ as $\tilde{D} = R_{\rm c}$, where $K_{\rm P}, K_{\rm I}, R_{\rm c} \in \mathbb{R}^{m\times m}$ are diagonal positive definite matrices and $\phi^{l}_{(\cdot)}(\cdot)$ $(l = 1, 2)$ are given as

$$\phi^{l}_{(C)}(z) = \sum_{i}^{m} C_i \frac{\alpha_{l,i}}{\beta_{l,i}} \log(\cosh(\beta_{l,i} z_i)), \tag{5.2.22}$$

with design parameters $\alpha_{l,i} > 0$, and $\beta_{l,i} > 0$. Then, the input (5.2.2) always satisfies

$$|u_i| \leq K_{{\rm P},i}\alpha_{1,i} + K_{{\rm I},i}\alpha_{2,i}. \tag{5.2.23}$$

In addition, the linear approximation of the controller (5.2.2) with (5.2.1) represents a lag compensator under the condition

$$K_{{\rm P},i}\alpha_{1,i}\beta_{1,i} - K_{{\rm I},i}\alpha_{2,i}\beta_{2,i} > 0.$$

Proof. The input (5.2.2) is calculated as

$$\begin{aligned} u_i =& -\nabla_{q_{{\rm a},i}}\phi^{1}_{(K_{\rm P})}(q^{\rm e}_{\rm a}) - \nabla_{q_{{\rm a},i}}\phi^{2}_{(K_{\rm I})}(x_{\rm c} - q^{\rm e}_{\rm a}) \\ & - 2\nabla_{x_{\rm c}}\phi^{2}_{(K_{\rm I})}(x_{\rm c} - q^{\rm e}_{\rm a}) \\ =& - K_{{\rm P},i}\alpha_{1,i}\tanh(\beta_{1,i} q^{\rm e}_{{\rm a},i}) \\ & - K_{{\rm I},i}\alpha_{2,i}\tanh(\beta_{2,i}(x_{{\rm c},i} - q^{\rm e}_{{\rm a},i})). \end{aligned} \tag{5.2.24}$$

Since $|\tanh(\cdot)| \leq 1$, it follows from (5.2.24) that

$$|u_i| \leq K_{{\rm P},i}\alpha_{1,i} + K_{{\rm I},i}\alpha_{2,i}.$$

Maclaurin series of $\tanh(z)$ is $\tanh(z) = z + o(\|z\|)$ as $z \to 0$, hence, if $\beta_{1,i} q^{\rm e}_{\rm a}$ and $\beta_{2,i}(x_{{\rm c},i} - q^{\rm e}_{{\rm a},i})$ are small enough that $\tanh(\cdot)$ can be linearly approximated, the input (5.2.2) and the dynamics (5.2.1) are given as

$$\begin{aligned} u_i &= -K_{{\rm P},i}\alpha_{1,i}\beta_{1,i} q^{\rm e}_{{\rm a},i} - K_{{\rm I},i}\alpha_{2,i}\beta_{2,i}(x_{{\rm c},i} - q^{\rm e}_{{\rm a},i}), \\ \dot{x}_{{\rm c},i} &= -R_{{\rm c},i}K_{{\rm I},i}\alpha_{2,i}\beta_{2,i}(x_{{\rm c},i} - q^{\rm e}_{{\rm a},i}). \end{aligned} \tag{5.2.25}$$

Replacing $K_{{\rm P},i}\alpha_{1,i}\beta_{1,i}$ and $K_{{\rm I},i}\alpha_{2,i}\beta_{2,i}$ with $\tilde{K}_{{\rm P},i}$ and $\tilde{K}_{{\rm I},i}$ immediately confirms that (5.2.25) represents a lag compensator, and this completes the proof. □

The parameters of the controller (5.2.2)-(5.2.1) with (5.2.21) are designed in the same way as the proposed lag compensator by specifying K, T, and α of (5.2.15). If the input is saturated as $|u_i| \leq \mathcal{U}_{\tt max_i}$, the parameters $\alpha_{1,i}$ and $\alpha_{2,i}$ are chosen so that $(K_{{\rm P},i}\alpha_{1,i} + K_{{\rm I},i}\alpha_{2,i}) \leq \mathcal{U}_{\tt max_i}$ is satisfied. The parameters $\beta_{1,i}$ and $\beta_{2,i}$, that affect the region where the controller can be linearly approximated, can be freely chosen.

5.3 Practical implementation of the passivity-based lag compensator

To confirm the effectiveness of the proposed controllers in Section 5.2, this section shows experimental results of the implementation of the controllers in the 2 DoF manipulator by Quanser depicted in Fig. 5.2. The first experiment consists in applying the passivity-based lag compensator to the manipulator and corroborate its suitability to deal with steady-state errors by choosing appropriate gains. The second experiment compares the performance of a PID controller and the passivity-based lag compensator, where the inputs are saturated.

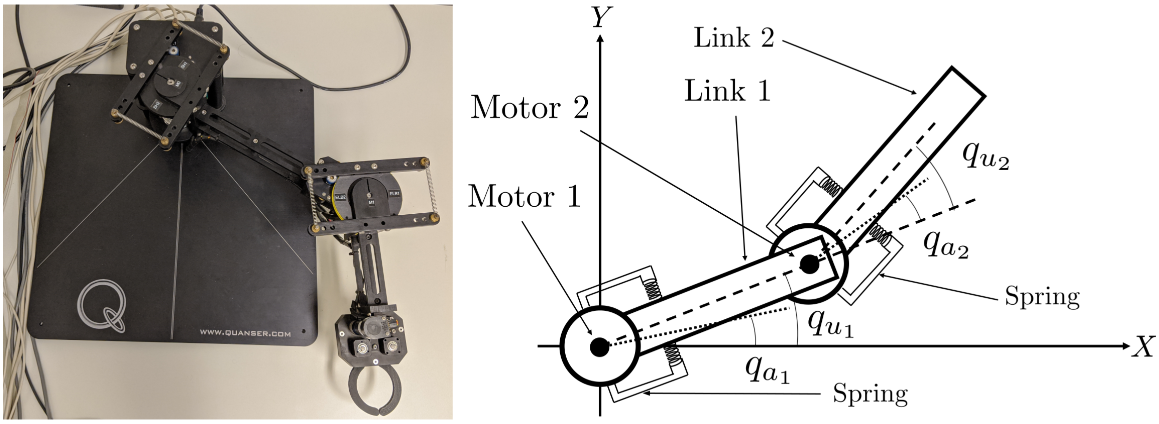

Figure 5.2: 2 DoF serial flexible joint by Quanser and its corresponding schematic (©2020 IEEE)

In these experiments, only the positions q are measured, and the inputs are the currents supplied to the motors. Note that, strictly speaking, the control inputs we analytically devise should be torques. However, there exists a static relationship between the torque of each motor and the corresponding current. Such relationships are considered during the practical implementation of the controllers. We refer the reader to [77] for further details.

5.3.1 Control design

The 2 DoF planar robot with flexible joints in Fig. 5.2 admits a pH representation of the form (5.1.1) where

$$
\begin{aligned}
&D = \begin{pmatrix} D_{\mathrm{u}} & 0_{2\times 2} \\ 0_{2\times 2} & D_{\mathrm{a}} \end{pmatrix}, \\
&D_{\mathrm{u}} = \operatorname{diag}\left(d_{\mathrm{u}_1}, d_{\mathrm{u}_2}\right), D_{\mathrm{a}} = \operatorname{diag}\left(d_{\mathrm{a}_1}, d_{\mathrm{a}_2}\right), \\
&M(q) = \begin{pmatrix} M_{\mathrm{u}}(q) & 0_{2\times 2} \\ 0_{2\times 2} & M_{\mathrm{a}} \end{pmatrix}, M_{\mathrm{a}} = \operatorname{diag}\left(\mathcal{I}_1, \mathcal{I}_2\right), \\
&M_{\mathrm{u}}(q) = \begin{pmatrix} a_1 + a_2 + 2b\cos\left(q_{\mathrm{u}_2}\right) & a_2 + b\cos\left(q_{\mathrm{u}_2}\right) \\ a_2 + b\cos\left(q_{\mathrm{u}_2}\right) & a_2 \end{pmatrix}, \\
&V(q) = \frac{1}{2}\|q_{\mathrm{u}} - q_{\mathrm{a}}\|^2_{K_{\mathrm{s}}}, K_{\mathrm{s}} = \operatorname{diag}\left(K_{\mathrm{s}_1}, K_{\mathrm{s}_2}\right).
\end{aligned}
$$

For this system, $n = 4$ and $m = 2$. Furthemore, q_{a_1} and q_{a_2} denote the angle of the first and second motor, q_{u_1} and q_{u_2} denote the angle of the first and second link, respectively, where each link is connected to a motor through springs. The parameters of this system are provided in Table 5.1.

Note that the assignable equilibria for this system are characterized by the constraint $q_{\mathrm{a}} = q_{\mathrm{u}}$. Accordingly, the control objective is to stabilize the manipulator at the desired configuration

$$
q_{\mathrm{a}} = q_{\mathrm{u}} = q_{\mathrm{a}}^*, \tag{5.3.1}
$$

where $q_{\mathrm{a}}^* \in \mathbb{R}^2$. To this end, the following corollary proves that the passivity-lag compensator proposed in Section 5.2 solves the control problem.

Corollary 5.3.1. *The desired equilibrium positions of the system defined in (5.3.1) are asymptotically stabilized by the controller (5.2.2)-(5.2.1) with (5.2.13) or (5.2.21) if $R_{\mathrm{c},i} > 1/D_{\mathrm{a},i}$ holds.*

Proof. We only prove the case of (5.2.13) due to space constraints. Since the pH system (5.1.1) is transformed into the new pH system (5.2.3) by the controller, if an isolated minimum of $H_{\mathrm{d}}(\xi)$ is the equilibrium point $q^* := (q_{\mathrm{a}}^*, q_{\mathrm{a}}^*)^\top$ and if (5.2.7) holds, the desired positions (5.3.1) are asymptotically stable. We first check whether (5.2.7) holds. Define

$$
\hat{D} = \begin{pmatrix} D_{\mathrm{u}} & 0_{\times 2} & 0_{2\times 2} \\ 0_{2\times 2} & D_{\mathrm{a}} & I_2 \\ 0_{2\times 2} & I_2 & R_{\mathrm{c}} \end{pmatrix}. \tag{5.3.2}
$$

Since $D_{\mathrm{u}} \succ 0$ hold, the condition (5.2.7), that can be written as $\hat{D} \succ 0$, holds if and only if

$$\begin{pmatrix} D_{\mathrm{a}} & I_2 \\ I_2 & R_{\mathrm{c}} \end{pmatrix} \succ 0. \tag{5.3.3}$$

From the Schur complement condition, (5.3.3) holds if and only if $D_{\mathrm{a}} \succ 0$ and $R_{\mathrm{c}} - I_2^\top D_{\mathrm{a}}^{-1} I_2 \succ 0$ hold. Noting that R_{c}, D_{a}, I_2 are all positive diagonal matrices, this condition can be rewritten as $R_{\mathrm{c},i} > 1/D_{\mathrm{a},i}$, hence (5.2.7) holds.

Since the time derivative of $H_{\mathrm{d}}(\xi)$ is

$$\dot{H}_{\mathrm{d}}(\xi) = -(\nabla_\zeta H_{\mathrm{d}}(\xi))^\top \hat{D} \nabla_\zeta H_{\mathrm{d}}(\xi) \leq 0, \tag{5.3.4}$$

the equilibrium point q^* is asymptotically stabilized if both

$$\nabla_p H_{\mathrm{d}}(\xi) = 0_{4\times 1},\ \nabla_{x_{\mathrm{c}}} H_{\mathrm{d}}(\xi) = 0_{2\times 1}, \tag{5.3.5}$$

hold only at the desired point. It follows from (5.3.5) that $p = 0_{4\times 1}$ hold since $M(q)$ has full rank. In addition, since $\dot{p}$ is also zero at the equilibrium point, we have

$$\begin{aligned} \dot{p} =& 0_{4\times 1} = -\nabla_q H_{\mathrm{d}}(\xi) - D\nabla_p H_{\mathrm{d}}(\xi) \\ =& -\nabla_q H_{\mathrm{d}}(\xi) - 0_{4\times 1} \\ =& -\frac{\partial}{\partial q}\left(\frac{1}{2} p^\top M(q)^{-1} p\right) + \begin{pmatrix} 0_{2\times 1} \\ K_{\mathrm{I}}(x_{\mathrm{c}} - q_{\mathrm{a}}^{\mathrm{e}}) \end{pmatrix} \\ & - \begin{pmatrix} K_{\mathrm{s}}(q_{\mathrm{u}} - q_{\mathrm{a}}) \\ -K_{\mathrm{s}}(q_{\mathrm{u}} - q_{\mathrm{a}}) + K_{\mathrm{P}}(q_{\mathrm{a}} - q_{\mathrm{a}}^*) \end{pmatrix}. \end{aligned} \tag{5.3.6}$$

It follows from (5.3.5) that the first term and the second term of the bottom row of (5.3.6) become zero. Hence, $q_{\mathrm{u}} - q_{\mathrm{a}} = 0_{2\times 1},\ q_{\mathrm{a}} - q_{\mathrm{a}}^* = q_{\mathrm{a}}^{\mathrm{e}} = 0_{2\times 1}, x_{\mathrm{c}} = 0_{2\times 1}$ always hold under the condition (5.3.5) and this completes the proof. The proof of the case (5.2.21) is the same as above. □

The following subsections are devoted to the experimental results.

5.3.2 Experiment 1: reduction of the steady-state error

The objective of this experiment is to confirm that the proposed passivity-based lag compensator (5.2.2)-(5.2.1) with (5.2.13) is effective for reducing steady-state errors. Towards this end, we perform two experiments with different gains. In the first case, the response of the closed-loop system exhibits steady-state errors, which are probably the result of non-modeled phenomena, e.g., dry friction. In the second experiment, we successfully reduce these errors by modifying the control gains. For the experiments,

Table 5.1: System parameters

d_{u_1}	0.38 $[N \cdot m \cdot s/\mathrm{rad}]$	d_{u_2}	0.30 $[N \cdot m \cdot s/\mathrm{rad}]$
d_{a_1}	0.30 $[N \cdot m \cdot s/\mathrm{rad}]$	d_{a_2}	0.14 $[N \cdot m \cdot s/\mathrm{rad}]$
a_1	0.068 $[kg \cdot m^2]$	a_2	0.013 $[kg \cdot m^2]$
b	0.018 $[kg \cdot m^2]$		
$\mathcal{I}_1$	0.042 $[kg \cdot m^2]$	$\mathcal{I}_2$	0.0070 $[kg \cdot m^2]$
K_{s_1}	9.4 $[N \cdot m/\mathrm{rad}]$	K_{s_2}	4.2 $[N \cdot m/\mathrm{rad}]$

we consider $q_{\mathrm{a}}^* = (1, -1)^\top$. Figs. 5.3 and 5.4 show the response of q and u respectively, where the blue lines are the results of applying the controller designed with $K = \mathrm{diag}(0.2, 0.4)$, and the red lines are the case that $K = \mathrm{diag}(0.4, 0.6)$. For both cases, we select $T = \mathrm{diag}(0.4, 0.2)$, $\alpha = \mathrm{diag}(1.7, 1.01)$. As mentioned before, the steady-state error present in the first experiment–the blue case–may be caused by nonlinear friction that is neglected in the model. On the other hand, in the red case with a greater gain K, the steady-state error is zero. This result shows that the proposed controller actually works as a lag compensator, where the deviations are reduced by amplifying the low frequency signals. Note that the removal of oscillations is outside the scope of our control objectives.

5.3.3 Experiment 2: suppressing the wind-up phenomenon

The objective of this experiment is to confirm that the proposed passivity-based lag compensator mitigates the windup phenomenon under input restrictions. Consider the case that the system is physically constrained for a certain amount of time such that the state cannot reach the desired values (5.3.1) during this interval. Consequently, applying a PID will cause that the internal variables of the integrator to continue increasing while constrained, producing an overshoot in the response after the constraints are removed if the inputs are saturated. Such a problem does not occur when the lag compensator is applied. In the experiment, first we just applied the lag compensator and a PID controller to the system and verify that the control objective is achieved by both approaches under normal operation conditions. Next, we fix the links so that all the angles remain 0 while $t \leq 2$ [s]. Then, we release the links. The desired values are set to $q_{\mathrm{a}}^* = (1, -1)^\top$. The saturated lag compensator (5.2.2)-(5.2.1) with (5.2.21) is designed by specifying the parameters as $K = \mathrm{diag}(0.15, 1.2), T = \mathrm{diag}(2, 1), \alpha = \mathrm{diag}(1.7, 1.01), \alpha_1 = (1.7, 0.29), \alpha_2 =$

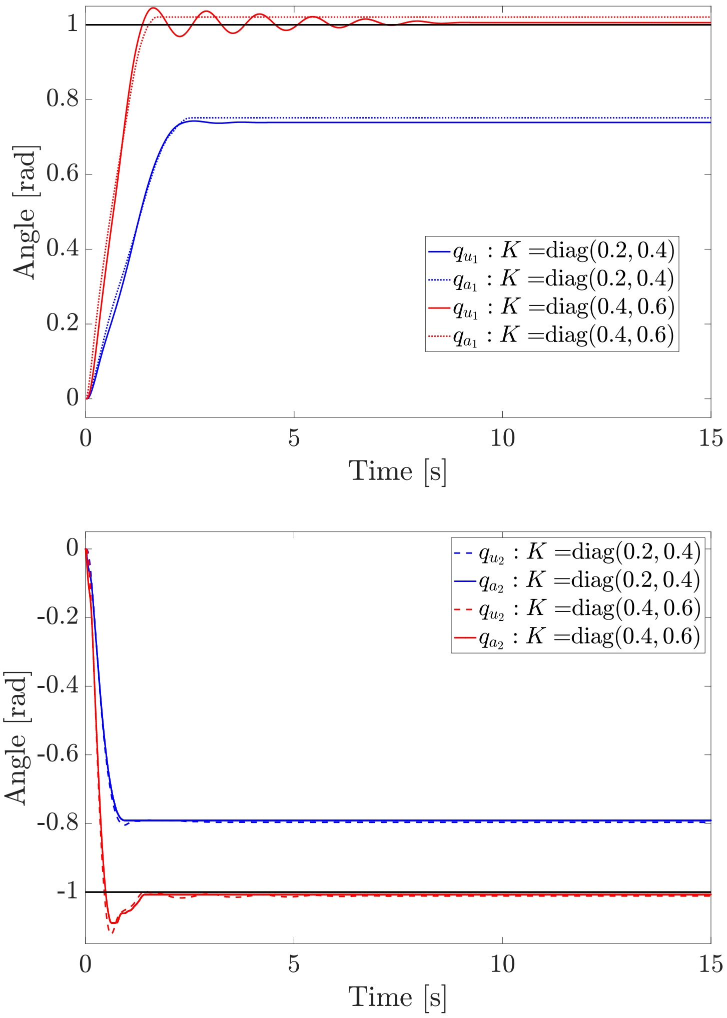

Figure 5.3: The resulting responses of $q(t)$ with the proposed compensator

$(4, 0.7), \beta_1 = (0.8, 2.8), \beta_2 = (0.8, 2.8)$, and the PID controller is designed as

$$u(t) = -G_{\mathrm{P}} q_{\mathrm{a}}^{\mathrm{e}}(t) - G_{\mathrm{D}} \dot{q}_{\mathrm{a}}^{\mathrm{e}}(t) - G_{\mathrm{I}} \int_0^t q_{\mathrm{a}}^{\mathrm{e}}(t) \mathrm{d}t,$$

with $G_{\mathrm{P}} = \mathrm{diag}(1.5, 4)$, $G_{\mathrm{D}} = \mathrm{diag}(1, 2)$, and $G_{\mathrm{I}} = \mathrm{diag}(0.4, 1)$, where the magnitude of each input is restricted as $|u_1(t)| \leq 0.5$, $|u_2(t)| \leq 0.35$. The velocities $\dot{q}_{\mathrm{a}}^{\mathrm{e}}$ are estimated from $q_{\mathrm{a}}^{\mathrm{e}}$ by using a derivative filter provided by Quanser. Note that such a filter is not necessary for the lag compensator since we use a dynamic extension. Figs. 5.5 and 5.6 show the result of the experiments. Fig. 5.5 shows the case when the system is not constrained, and Fig. 5.6 depicts the case when the system is constrained for 2 seconds, where the first row figures show the response of the angle $q(t)$, the second row figures show the response of $u_1(t)$, and the third row figures show

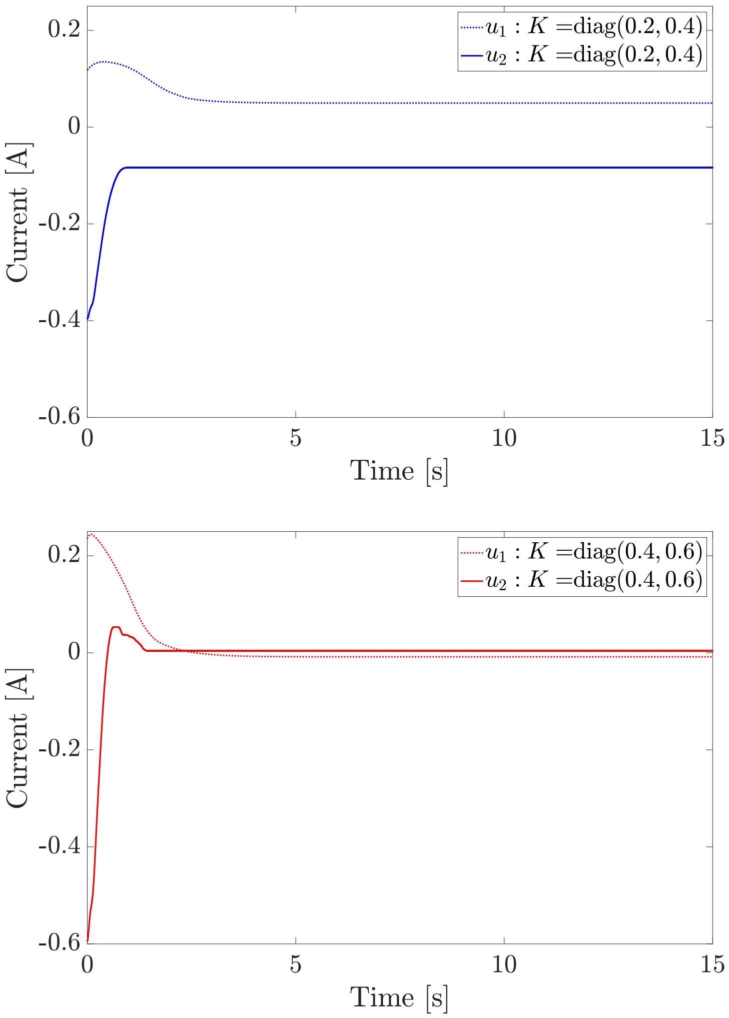

Figure 5.4: The resulting responses of $u(t)$ with the proposed compensator

the response of $u_2(t)$, the blue lines are the result of the PID controller and the red lines are the result of the lag compensator. In the right figures, the dashed black line and the black solid line show the saturation values of u_1 and u_2, respectively. Figs. 5.5 and 5.6 show that, although the steady-state error is almost zero in both cases, there is overshoot in the PID case, while the lag compensator does not evoke such an overshoot. This result proves that the passivity-based lag compensator is also effective for mitigating the windup phenomena.

5.4 Conclusion

In this chapter, we have proposed a PBC method suitable to stabilize a class of nonlinear mechanical systems, where the control law admits a lag compensator interpretation. Some additional properties of the resulting controllers are that they do not require velocity measurements and can be designed to deal with input constraints via the saturation of their signals. The proposed method has two main advantages: first, the pH preservation simplifies the stability analysis of the closed-loop system. Second, the lag compensator interpretation provides clear insight, via frequency analysis, into the performance of the closed-loop system. These advantages have been illustrated through the implementation of the proposed method to stabilize a planar robot, where the frequency analysis provided guidelines to select control gains that ensures the reduction of the steady-state error in the closed-loop system. In the next chapter, we generalize the result of this chapter.

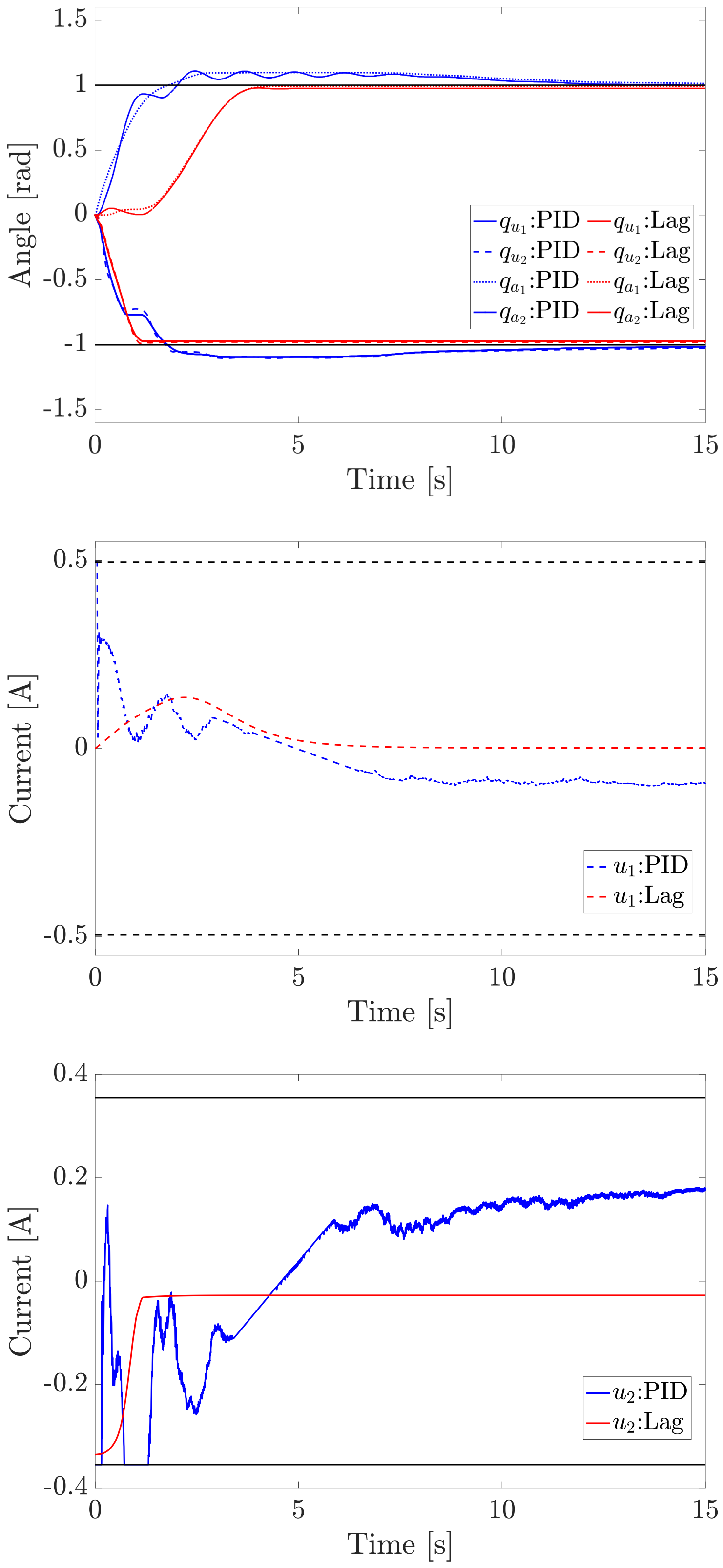

Figure 5.5: The case that the physical constraint is not imposed

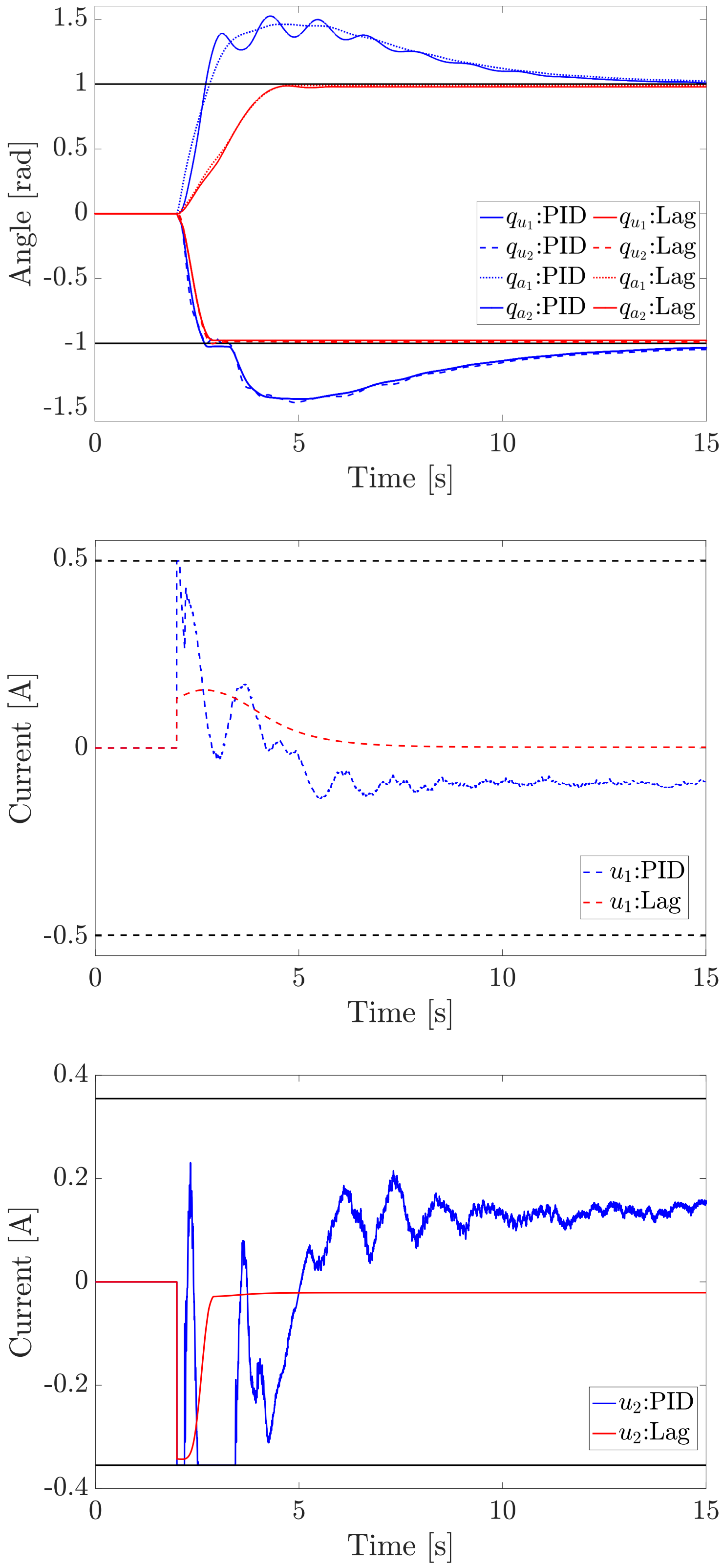

Figure 5.6: The case that the system is constrained for 2 seconds

Chapter 6

Passivity-Based High-Order Compensators

This chapter gives a generalized result of the PBC technique proposed in Chapter 5. As mentioned in Chapter 5, Dirksz has proposed a passivity-based dynamic feedback controller that can be interpreted as a lead compensator [68]. In Chapter 5, we have also proposed a passivity-based lag compensator using the dynamic extension and provided some guidelines on designing the controller for reducing steady-state errors. These passivity-based approaches are useful because they do not require velocity measurement and guarantee stability while allowing one to tune the responses in the frequency domain. However, in those methods, the transfer function of the resulting controllers is first-order, which reduces the flexibility in shaping the closed-loop responses.

The scope of this chapter is to propose passivity-based dynamic output feedback controllers with high-order transfer function representations that ensure both stability and high flexibility in tuning them. Referring to [68] and Chapter 5, we design output dynamic feedback controllers so that they preserve the pH structure and are parametrized by transfer function representations, where the outputs have only the information of positions. The resulting controllers include lead-lag compensators, so they effectively suppress oscillations and reduce steady-state errors while ensuring stability. In addition, it is not required to measure the velocity for these controllers.

The remainder of this chapter is organized as follows. Section 6.1 defines the problem we tackle. Next, Section 6.2 gives our main result and strategies to choose control gains. In Section 6.3, we show the effectiveness of our controller through a numerical example. Finally, we provide the conclusions in Section 6.4.

6.1 Problem setting

Let us consider a class of mechanical systems represented by (5.1.1), and define the output as $y(q,p) : \mathbb{R}^n \times \mathbb{R}^n \to \mathbb{R}^j$ with $j \in \mathbb{Z}_+$. Our goal is to solve the following problem.

Problem Setting 6.1.1. *To avoid velocity measurements, restrict the output to $y(q)$. Find an output dynamic feedback controller u such that*

- *The closed-loop system is asymptotically stable at $q = q^*$ and $p = 0_{n\times 1}$.*
- *There is a guideline to tune the gains for suppressing oscillations and steady-state errors.*

6.2 Passivity-based compensators

This section presents a passivity-based dynamic output feedback controller and a tuning method for the controller. Note that $y(q)$ is not the passive output of (5.1.1). The next subsection introduces a PBC method to find an entire class of dynamic output feedback controllers that preserve the port-Hamiltonian structure.

6.2.1 Passivity-based output feedback controller

The following theorem studies an entire class of passivity-based output feedback controllers by parameterizing the closed-loop system in the pH framework.

Theorem 6.2.1. *Consider the dynamic output feedback controller*

$$\dot{x}_{\rm c} = f^{\rm c}(x_{\rm c}, y(q)),\ u = h^{\rm c}(x_{\rm c}, y(q)), \tag{6.2.1}$$

with $x_{\rm c} \in \mathbb{R}^{m\ell}$, $f_{\rm c} : \mathbb{R}^{m\ell} \times \mathbb{R}^j \to \mathbb{R}^{m\ell}$ and $h^{\rm c} : \mathbb{R}^{m\ell} \times \mathbb{R}^j \to \mathbb{R}^m$, and parametrize a closed-loop system (5.1.1) with (6.2.1) as[1]

$$\begin{aligned}\dot{\xi} &= F(q,p,x_{\rm c},y(q))\nabla_\xi H_{\rm d}(\xi), \qquad (6.2.2)\\ F(q,p,x_{\rm c},y(q)) &:= \begin{pmatrix} F_{11}(x_{\rm c},y(q)) & F_{12}(x_{\rm c},y(q)) & F_{13}(x_{\rm c},y(q)) \\ F_{21}(x_{\rm c},y(q)) & -D(q,p)+F_{22}(x_{\rm c},y(q)) & F_{23}(x_{\rm c},y(q)) \\ F_{31}(x_{\rm c},y(q)) & F_{32}(x_{\rm c},y(q)) & F_{33}(x_{\rm c},y(q)) \end{pmatrix}.\end{aligned}$$

[1] Note that we omit the arguments of $F_{i,j}$, $i,j = 1,2,3$, and D.

Consider that $M(q)$ in (5.1.1) is not constant. Then, the closed-loop system (6.2.2) is a pH system if and only if the the following conditions hold.

$$\begin{cases} F_{11}(x_{\mathrm{c}}, y(q)) = F_{22}(x_{\mathrm{c}}, y(q)) = 0_{n\times n}, \\ F_{13}(x_{\mathrm{c}}, y(q)) = F_{31}(x_{\mathrm{c}}, y(q))^\top = 0_{n\times m\ell}, \\ F_{12}(x_{\mathrm{c}}, y(q)) = -F_{21}(x_{\mathrm{c}}, y(q))^\top = I_n, \\ F_{32}(x_{\mathrm{c}}, y(q)) = 0_{m\ell\times n}, \\ Gh^c(x_{\mathrm{c}}, y(q)) = -\nabla_q \bar{H}(x_{\mathrm{c}}, y(q)) + F_{23}(x_{\mathrm{c}}, y(q))\nabla_{x_{\mathrm{c}}}\bar{H}(x_{\mathrm{c}}, y(q)), \\ f^{\mathrm{c}}(x_{\mathrm{c}}, y(q)) = F_{33}(x_{\mathrm{c}}, y(q))\nabla_{x_{\mathrm{c}}}\bar{H}(x_{\mathrm{c}}, y(q)), \end{cases} \tag{6.2.3}$$

$$\begin{pmatrix} 2D(q,p) & -F_{23}(x_{\mathrm{c}}, y(q)) \\ -F_{23}(x_{\mathrm{c}}, y(q))^\top & -F_{33}(x_{\mathrm{c}}, y(q)) - F_{33}(x_{\mathrm{c}}, y(q))^\top \end{pmatrix} \succeq 0. \tag{6.2.4}$$

Here $\xi := (q^\top, p^\top, x_{\mathrm{c}}^\top)^\top$, $H_{\mathrm{d}}(\xi) := H(q,p) + \bar{H}(x_{\mathrm{c}}, y(q))$, $\bar{H}(x_{\mathrm{c}}, y(q)) : \mathbb{R}^{m\ell} \times \mathbb{R}^j \to \mathbb{R}_+$, and $F_{11}(x_{\mathrm{c}}, y(q))$, $F_{12}(x_{\mathrm{c}}, y(q))$, $F_{21}(x_{\mathrm{c}}, y(q))$, $F_{22}(x_{\mathrm{c}}, y(q)) \in \mathbb{R}^{n\times n}$, $F_{13}(x_{\mathrm{c}}, y(q))$, $F_{23}(x_{\mathrm{c}}, y(q)) \in \mathbb{R}^{n\times m\ell}$, $F_{31}(x_{\mathrm{c}}, y(q))$, $F_{32}(x_{\mathrm{c}}, y(q)) \in \mathbb{R}^{m\ell\times n}$, $F_{33}(x_{\mathrm{c}}, y(q)) \in \mathbb{R}^{m\ell\times m\ell}$ are the matrices for the parameterization.

See Appendix A for the proof of Theorem 6.2.1. Note that (6.2.3) and (6.2.4) are only sufficient conditions if $M(q)$ is a constant matrix. The next theorem establishes conditions that guarantee that the closed-loop system has an equilibrium point at the desired configuration.

Theorem 6.2.2. *Consider the closed-loop system (6.2.2) satisfying (6.2.3) and (6.2.4). Then, the equilibrium point $\xi^* := (q^{*\top}, 0_{1\times n}, 0_{1\times m\ell})^\top \in \mathcal{E}$ is asymptotically stable if the following conditions hold.*

C1. $\begin{pmatrix} 2D(q,p) & -F_{23}(x_{\mathrm{c}}, y(q)) \\ -F_{23}(x_{\mathrm{c}}, y(q))^\top & -F_{33}(x_{\mathrm{c}}, y(q)) - F_{33}(x_{\mathrm{c}}, y(q))^\top \end{pmatrix} \succ 0,$

C2. *$H_{\mathrm{d}}(\xi)$ has an isolated minimum at $\xi = \xi^*$,*

C3. $\nabla_p H_{\mathrm{d}}(\xi) = 0_{n\times 1},\ \nabla_{x_{\mathrm{c}}} H_{\mathrm{d}}(\xi) = 0_{m\ell\times 1}$
$\Rightarrow q = q^*,\ x_{\mathrm{c}} = 0_{m\ell\times 1}.$

Proof. Hereafter, we omit the argument of the functions for the sake of readability. It follows from (6.2.3) that

$$\dot{H}_{\mathrm{d}} = -(\nabla_\zeta H_{\mathrm{d}})^\top \begin{pmatrix} 2D & -F_{23} \\ -F_{23}^\top & -F_{33} - F_{33}^\top \end{pmatrix} \nabla_\zeta H_{\mathrm{d}} \le 0, \tag{6.2.5}$$

with $\zeta = (p^\top, x_{\mathrm{c}}^\top)^\top$, and from condition **C1**, $\dot{H}_{\mathrm{d}} = 0$ holds if and only if $\nabla_p H_d = 0_{n\times 1}$ and $\nabla_{x_{\mathrm{c}}} H_{\mathrm{d}} = 0_{m\ell\times 1}$ hold. Therefore, if conditions **C2** and **C3** hold, then Krasovskii-Barbashin's theorem (see [76]) proves that ξ^* is asymptotically stable. □ □

The next subsection studies how to tune the controllers described in (6.2.1), based on the transfer function representation.

6.2.2 Tuning method

In the tuning of the controller, the transfer function representation is useful since the adjustment of the gains based on frequency analysis is possible. The following remark shows the conditions under which the linear approximation of the proposed controller has a transfer function representation. Hereafter, we design $y(q)$ so that $j = m$ and $q = q^* \to y(q) = 0_{m\times 1}$.

Remark 6.2.1. *Suppose that the Laplace transformations of the input and output signals of system (5.1.1) exist. Define* f^{c} *and* h^{c} *such that* $f^{\mathrm{c}}(0_{m\ell\times 1}, 0_{m\times 1}) = 0_{m\ell\times 1}$ *and* $h^{\mathrm{c}}(0_{m\ell\times 1}, 0_{m\times 1}) = 0_{m\times 1}$ *hold. Then, the linearization of the dynamic output feedback controller*

$$\dot{x}_{\mathrm{c}} = A_{\mathrm{c}} x_{\mathrm{c}} + B_{\mathrm{c}} y,\ u = C_{\mathrm{c}} x_{\mathrm{c}} + D_{\mathrm{c}} y, \tag{6.2.6}$$

has a transfer function representation

$$\begin{aligned}\mathscr{U}_i(s) &= k_i \frac{s^l + b_{l-1,i}s^{l-1} + \cdots + b_{1,i}s + b_{0,i}}{s^l + a_{l-1,i}s^{l-1} + \cdots + a_{1,i}s + a_{0,i}} \mathscr{Y}_i(s) \\ &= \Psi_i(s)\mathscr{Y}_i(s),\end{aligned} \tag{6.2.7}$$

if and only if the following relation holds for a nonsingular matrix T*.*

$$A_{\mathrm{c}} = T^{-1}\mathcal{A}T,\ B_{\mathrm{c}} = T^{-1}\mathcal{B},\ C_{\mathrm{c}} = \mathcal{C}T,\ D_{\mathrm{c}} = \mathcal{D}. \tag{6.2.8}$$

Here $\mathscr{U}_i(s) = \mathcal{L}[u_i(t)]$, $\mathscr{Y}_i(s) = \mathcal{L}[y_i(q(t))]$,

$$\begin{aligned} A_{\mathrm{c}} &:= \left.\frac{\partial f^{\mathrm{c}}}{\partial x_{\mathrm{c}}}\right|_{\bar{\zeta}=0_{(m+m\ell)\times 1}},\ B_{\mathrm{c}} := \left.\frac{\partial f^{\mathrm{c}}}{\partial y}\right|_{\bar{\zeta}=0_{(m+m\ell)\times 1}}, \\ C_{\mathrm{c}} &:= \left.\frac{\partial h^{\mathrm{c}}}{\partial x_{\mathrm{c}}}\right|_{\bar{\zeta}=0_{(m+m\ell)\times 1}},\ D_{\mathrm{c}} := \left.\frac{\partial h^{\mathrm{c}}}{\partial y}\right|_{\bar{\zeta}=0_{(m+m\ell)\times 1}}, \end{aligned} \tag{6.2.9}$$

for $\bar{\zeta} := (y^\top, x_{\mathrm{c}}^\top)^\top$*, and* $\mathcal{A} \in \mathbb{R}^{m\ell\times m\ell}$*,* $\mathcal{B} \in \mathbb{R}^{m\ell\times m}$*,* $\mathcal{C} \in \mathbb{R}^{m\times m\ell}$*, and* $\mathcal{D} \in \mathbb{R}^{m\times m}$ *are* *given as*

$$\mathcal{A} := \begin{pmatrix} \mathcal{A}_1 & 0_{\ell\times\ell} & \dots & 0_{\ell\times\ell} \\ 0_{\ell\times\ell} & \mathcal{A}_2 & \ddots & \vdots \\ \vdots & \ddots & \ddots & 0_{\ell\times\ell} \\ 0_{\ell\times\ell} & \dots & 0_{\ell\times\ell} & \mathcal{A}_m \end{pmatrix}, \mathcal{A}_i := \begin{pmatrix} 0 & 1 & 0 & \dots & 0 \\ \vdots & \ddots & \ddots & \ddots & \vdots \\ 0 & \dots & \ddots & \ddots & 0 \\ 0 & \dots & \dots & 0 & 1 \\ -a_{0,i} & -a_{1.i} & \dots & \dots & -a_{l-1,i} \end{pmatrix},$$

$$\mathcal{B} := \begin{pmatrix} \mathcal{B}_1 & 0_{\ell\times 1} & \dots & 0_{\ell\times 1} \\ 0_{\ell\times 1} & \mathcal{B}_2 & \ddots & \vdots \\ \vdots & \ddots & \ddots & 0_{\ell\times 1} \\ 0_{\ell\times 1} & \dots & 0_{\ell\times 1} & \mathcal{B}_m \end{pmatrix}, \mathcal{B}_i := \begin{pmatrix} 0 \\ \vdots \\ 0 \\ 1 \end{pmatrix},$$

$$\mathcal{C} := \begin{pmatrix} \mathcal{C}_1 & 0_{1\times\ell} & \dots & 0_{1\times\ell} \\ 0_{1\times\ell} & \mathcal{C}_2 & \ddots & \vdots \\ \vdots & \ddots & \ddots & 0_{1\times\ell} \\ 0_{1\times\ell} & \dots & 0_{1\times\ell} & \mathcal{C}_m \end{pmatrix}, \ \mathcal{C}_i := k_i \begin{pmatrix} b_{0,i} - a_{0,i} \\ \vdots \\ b_{l-1,i} - a_{l-1,i} \end{pmatrix}^\top,$$

$$\mathcal{D} := \begin{pmatrix} \mathcal{D}_1 & 0 & \dots & 0 \\ 0 & \mathcal{D}_2 & \ddots & \vdots \\ \vdots & \ddots & \ddots & 0 \\ 0 & \dots & 0 & \mathcal{D}_m \end{pmatrix}, \mathcal{D}_i := k_i.$$

Now we present how to select the parameters of (6.2.7) so that the closed-loop system is asymptotically stable at ξ^*. The following theorem establishes conditions over A_c, B_c, C_c and D_c to satisfy **C1**.

Theorem 6.2.3. *Assume that the matrix $D(q,p) \succ 0$ in (5.1.1) satisfies*

$$D(q,p) = \begin{pmatrix} D_\mathrm{u}(q,p) & 0_{k\times m} \\ 0_{m\times k} & D_\mathrm{a}(q,p) \end{pmatrix}, \tag{6.2.10}$$

with $D_u \in \mathbb{R}^{k\times k}$ and $D_\mathrm{a}(q,p) \in \mathbb{R}^{m\times m}$. Consider the linearized controller (6.2.6) satisfying (6.2.3) under the conditions that $y(q)$ is selected to $y(q) = q_\mathrm{a}^\mathrm{e}$, $\bar{H}(x_\mathrm{c}, q_\mathrm{a}^\mathrm{e})$ is selected to be a strictly convex function satisfying $(\partial \bar{H}(x_\mathrm{c}, q_\mathrm{a}^\mathrm{e})/\partial\bar{\zeta})|_{\bar{\zeta}=0_{(m+m\ell)\times 1}} = 0_{(m+m\ell)\times 1}$, and both $F_{23}(x_\mathrm{c}, q_\mathrm{a}^\mathrm{e})$ and $F_{33}(x_\mathrm{c}, q_\mathrm{a}^\mathrm{e})$ are chosen to be constant so that $G^\perp F_{23}(x_\mathrm{c}, q_\mathrm{a}^\mathrm{e}) = 0_{k\times m\ell}$. Then, **C1** *holds if and only if the following condition holds.*

$$\begin{pmatrix} A_\mathrm{c} & B_\mathrm{c} \\ D_\mathrm{a}^{-1} C_\mathrm{c} & D_\mathrm{a}^{-1} D_\mathrm{c} \end{pmatrix} \text{ is a Hurwitz matrix,} \tag{6.2.11}$$

where we omit the arguments of D_a.

Proof. Parameterize $\bar{H}(x_\mathrm{c}, y(q))$ as

$$\begin{aligned} \bar{H}(x_\mathrm{c}, q_\mathrm{a}^\mathrm{e}) &= \bar{H}_0 + \begin{pmatrix} \bar{H}_1 & \bar{H}_2 \end{pmatrix} \begin{pmatrix} q_\mathrm{a}^\mathrm{e} \\ x_\mathrm{c} \end{pmatrix} \\ &+ \frac{1}{2} \begin{pmatrix} q_\mathrm{a}^{\mathrm{e}\top} & x_\mathrm{c}^\top \end{pmatrix} \begin{pmatrix} \bar{H}_{11} & \bar{H}_{12} \\ \bar{H}_{12}^\top & \bar{H}_{22} \end{pmatrix} \begin{pmatrix} q_\mathrm{a}^\mathrm{e} \\ x_\mathrm{c} \end{pmatrix} + o(\|\bar{\zeta}\|^2), \end{aligned} \tag{6.2.12}$$

where $\bar{H}_0 \in \mathbb{R}$, $\bar{H}_1 \in \mathbb{R}^{1\times m}$, $\bar{H}_2 \in \mathbb{R}^{1\times m\ell}$, $\bar{H}_{11} = \bar{H}_{11}^\top \in \mathbb{R}^{m\times m}$, $\bar{H}_{22} = \bar{H}_{22}^\top \in \mathbb{R}^{m\ell\times m\ell}$, $\bar{H}_{12} \in \mathbb{R}^{m\times m\ell}$, and $o(x)$ is a function satisfying $|o(x)|/|x| \to 0$ as $x \to 0$. It follows from conditions (6.2.3), $(\partial \bar{H}(x_\mathrm{c}, q_\mathrm{a}^\mathrm{e})/\partial\bar{\zeta})|_{\bar{\zeta}=0_{(m\ell+m)\times 1}} = 0_{(m\ell+m)\times 1}$, and (6.2.9) that

$$A_\mathrm{c} = F_{33}\left.\frac{\partial \nabla_{x_\mathrm{c}} \bar{H}(x_\mathrm{c}, q_\mathrm{a}^\mathrm{e})}{\partial x_\mathrm{c}}\right|_{\bar{\zeta}=0_{m\ell+m}} = F_{33}\bar{H}_{22}, \tag{6.2.13}$$

$$B_\mathrm{c} = F_{33}\left.\frac{\partial \nabla_{x_\mathrm{c}} \bar{H}(x_\mathrm{c}, q_\mathrm{a}^\mathrm{e})}{\partial q_\mathrm{a}^\mathrm{e}}\right|_{\bar{\zeta}=0_{m\ell+m}} = F_{33}\bar{H}_{12}^\top, \tag{6.2.14}$$

$$\begin{aligned} C_\mathrm{c} =& \left.\left(-\frac{\partial \nabla_{q_\mathrm{a}^\mathrm{e}} \bar{H}(x_\mathrm{c}, q_\mathrm{a}^\mathrm{e})}{\partial x_\mathrm{c}} + G^\top F_{23}\frac{\partial \nabla_{x_\mathrm{c}} \bar{H}(x_\mathrm{c}, q_\mathrm{a}^\mathrm{e})}{\partial x_\mathrm{c}}\right)\right|_{\bar{\zeta}=0_{m\ell+m}} \\ =& -\bar{H}_{12} + G^\top F_{23}\bar{H}_{22}, \end{aligned} \tag{6.2.15}$$

$$\begin{aligned} D_\mathrm{c} =& \left.\left(-\frac{\partial \nabla_{q_\mathrm{a}^\mathrm{e}} \bar{H}(x_\mathrm{c}, q_\mathrm{a}^\mathrm{e})}{\partial q_\mathrm{a}^\mathrm{e}} + G^\top F_{23}\frac{\partial \nabla_{x_\mathrm{c}} \bar{H}(x_\mathrm{c}, q_\mathrm{a}^\mathrm{e})}{\partial q_\mathrm{a}}\right)\right|_{\bar{\zeta}=0_{m\ell+m}} \\ =& -\bar{H}_{11} + G^\top F_{23}\bar{H}_{12}^\top, \end{aligned} \tag{6.2.16}$$

and these are summarized as follows.

$$\begin{pmatrix} A_\mathrm{c} & B_\mathrm{c} \\ C_\mathrm{c} & D_\mathrm{c} \end{pmatrix} = \begin{pmatrix} F_{33} & 0_{m\ell\times m} \\ G^\top F_{23} & -I_m \end{pmatrix}\begin{pmatrix} \bar{H}_{22} & \bar{H}_{12}^\top \\ \bar{H}_{12} & \bar{H}_{11} \end{pmatrix}. \tag{6.2.17}$$

Since $\bar{H}(x_\mathrm{c}, q_\mathrm{a}^\mathrm{e})$ is strictly convex,

$$\begin{pmatrix} \bar{H}_{22} & \bar{H}_{12}^\top \\ \bar{H}_{12} & \bar{H}_{11} \end{pmatrix} \succ 0, \tag{6.2.18}$$

and it is nonsingular. Hence, the following relation

$$XP = \begin{pmatrix} F_{33} & 0_{m\ell\times m} \\ G^\top F_{23} & -I_m \end{pmatrix}, \tag{6.2.19}$$

holds with

$$P := \begin{pmatrix} \bar{H}_{22} & \bar{H}_{12}^\top \\ \bar{H}_{12} & \bar{H}_{11} \end{pmatrix}^{-1}, \ X := \begin{pmatrix} A_\mathrm{c} & B_\mathrm{c} \\ C_\mathrm{c} & D_\mathrm{c} \end{pmatrix}. \tag{6.2.20}$$

By multiplying the following matrix

$$\tilde{T} := \begin{pmatrix} I_{m\ell\times m\ell} & 0_{m\ell\times m} \\ 0_{m\times m\ell} & D_\mathrm{a} \end{pmatrix}, \tag{6.2.21}$$

by (6.2.19) from the left, the following relation is obtained.

$$X P \tilde{T} = \begin{pmatrix} F_{33} & 0_{m\ell \times m} \\ G^\top F_{23} & -D_{\mathrm{a}} \end{pmatrix}. \tag{6.2.22}$$

Hence, noting that $\tilde{T} = \tilde{T}^\top \succ 0$ and $P = P^\top \succ 0$, the following relation

$$\tilde{X} P + P \tilde{X}^\top + \tilde{T}^{-1} Q \tilde{T}^{-\top} = 0_{(m\ell+m)\times(m\ell+m)}, \tag{6.2.23}$$

have to hold with

$$\tilde{X} := \tilde{T}^{-1} X = \begin{pmatrix} A_{\mathrm{c}} & B_{\mathrm{c}} \\ D_{\mathrm{a}}^{-1} C_{\mathrm{c}} & D_{\mathrm{a}}^{-1} D_{\mathrm{c}} \end{pmatrix}, \tag{6.2.24}$$

$$Q := \begin{pmatrix} -F_{33} - F_{33}^\top & -F_{23}^\top G \\ -G^\top F_{23} & 2D_{\mathrm{a}} \end{pmatrix}. \tag{6.2.25}$$

It follows from the standard Lyapunov theory that for any $Q \succ 0$ (this is equal to $\tilde{T}^{-1} Q \tilde{T}^{-\top} \succ 0$), $P \succ 0$ satisfying (6.2.23) exists if and only if $\tilde{X}$ is a Hurwitz matrix. Note that if $Q \succ 0$ holds, then **C1** holds, and vice versa. This means that if **C1** holds, $P \succ 0$ satisfying (6.2.23) exists if and only if $\tilde{X}$ is a Hurwitz matrix, and if $\tilde{X}$ is a Hurwitz matrix, we can choose $Q \succ 0$ (this means that **C1** holds) and $P \succ 0$ that satisfy (6.2.23). □

Remark 6.2.2. *Theorem 6.2.3 provides a guideline on how to choose poles and zeros to guarantee stability while tuning the controller (6.2.6). The controller (6.2.6) can be tuned by the following steps: firstly choose poles and zeros so that (6.2.11) is satisfied. Then check whether there exists a pair of matrices F_{23}, F_{33}, $\bar{H}_0$, $\bar{H}_1$, $\bar{H}_2$, $\bar{H}_{11}$, $\bar{H}_{12}$, and $\bar{H}_{22}$ that satisfy the conditions (6.2.17) (this is equal to condition (6.2.3)),* **C1**, **C2**, *and* **C3**. *Note that when choosing poles and zeros, T in (6.2.8) is also a free parameter.*

Since the controller (6.2.6) with the representation (6.2.7) includes lead-lag compensators, it is possible to suppress steady-state errors and oscillations while ensuring stability by using Theorem 6.2.3. In the next section, we show an example of the application of our controller.

6.3 Numerical example

To illustrate the applicability of the controllers proposed in Section 6.2, in this section, we present an example in which the objective is to stabilize the system at an equilibrium point with reducing steady-state errors and oscillations. In the example,

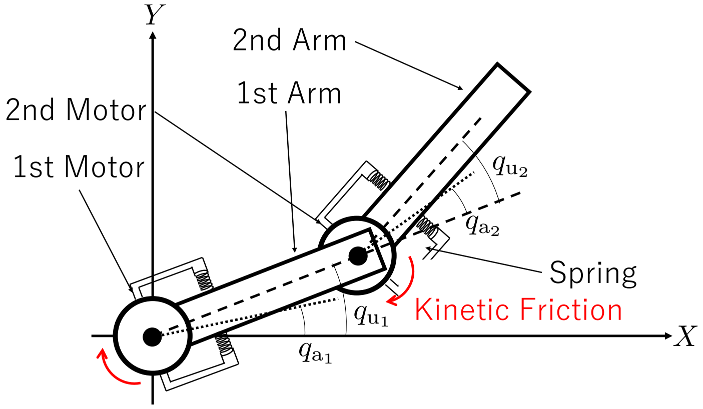

Figure 6.1: 2 DoF planar manipulator with flexible links

a lead-lag compensator is applied to a 2 DoF planar manipulator depicted in Fig. 6.1. In the figure, q_{a_1} and q_{a_2} denote the angle of the motors, and q_{u_1} and q_{u_2} denote the angle of the arms. Each arm is connected to a motor through a spring. Consequently, only q_{a_1} and q_{a_2} are actuated. In addition, unknown kinetic friction is imposed on the motors. Define the inertia of the i-th link as $\mathcal{I}_i$ and the input to the i-th motor as u_i, where the input vector is defined as $u = (u_1, u_2)^{\mathrm{T}}$. The inputs of the system are the torque of the motors. Moreover, this manipulator moves only in the horizontal plane. The next subsection analyzes stability of the closed-loop system with the controller (6.2.6).

6.3.1 Stability analysis

As described in Section 5.3.1, this system admits a pH representation of the form (5.1.1) with $n = 4$, $m = 2$, and

$$D(q,p) = \begin{pmatrix} D_{\mathrm{u}} & 0_{2\times 2} \\ 0_{2\times 2} & D_{\mathrm{a}} \end{pmatrix},$$

$$\begin{aligned} D_{\mathrm{u}} &= \mathrm{diag}\left(d_{\mathrm{u}_1}, d_{\mathrm{u}_2}\right), D_{\mathrm{a}} = \mathrm{diag}\left(d_{\mathrm{a}_1}, d_{\mathrm{a}_2}\right), \\ M(q) &= \begin{pmatrix} M_{\mathrm{u}}(q) & 0_{2\times 2} \\ 0_{2\times 2} & M_{\mathrm{a}}(q) \end{pmatrix}, M_{\mathrm{a}}(q) = \mathrm{diag}\left(\mathcal{I}_1, \mathcal{I}_2\right), \\ M_{\mathrm{u}}(q) &= \begin{pmatrix} a_1 + a_2 + 2b\cos\left(q_{\mathrm{u}_2}\right) & a_2 + b\cos\left(q_{\mathrm{u}_2}\right) \\ a_2 + b\cos\left(q_{\mathrm{u}_2}\right) & a_2 \end{pmatrix}, \\ V(q) &= \|q_{\mathrm{a}} - q_{\mathrm{u}}\|^2_{K_{\mathrm{s}}}, K_{\mathrm{s}} = \mathrm{diag}\left(K_{\mathrm{s}_1}, K_{\mathrm{s}_2}\right), \end{aligned}$$

where $d_{\mathrm{u}_1}, d_{\mathrm{u}_2}, d_{\mathrm{a}_1}, d_{\mathrm{a}_2}, a_1, a_2, b, \mathcal{I}_1, \mathcal{I}_2, K_{\mathrm{s}_1}$, and K_{s_1} are constant parameters. The desired positions are set to

$$q_{\mathrm{a}} = q_{\mathrm{u}} = q_{\mathrm{a}}^*. \tag{6.3.1}$$

Proposotion 6.3.1. *Assume that $F_{23}(x_{\mathrm{c}}, q_{\mathrm{a}}^{\mathrm{e}})$ and $F_{33}(x_{\mathrm{c}}, q_{\mathrm{a}}^{\mathrm{e}})$ are constant, and $\bar{H}(x_{\mathrm{c}}, q_{\mathrm{a}}^{\mathrm{e}})$ are chosen to be a strictly convex quadratic function parametrized as (6.2.12) with $\bar{H}_0 = 0$, $\bar{H}_1 = 0_{1\times 2}$, $\bar{H}_2 = 0_{1\times 2\ell}$. If a controller (6.2.6) satisfies (6.2.3) and* **C1***, the conditions* **C2** *and* **C3** *are satisfied, that is, the desired equilibrium point q^* of the closed-loop system is asymptotically stable.*

Proof. Since

$$\dot{H}_{\mathrm{d}}(\xi) = -(\nabla_{\zeta} H_{\mathrm{d}}(\xi))^{\top} \begin{pmatrix} 2D(q,p) & -F_{23} \\ -F_{23}^{\top} & -F_{33} - F_{33}^{\top} \end{pmatrix} \nabla_{\zeta} H_{\mathrm{d}}(\xi),$$

holds, it follows from condition **C1** that the equilibrium point q^* is asymptotically stabilized if both

$$\nabla_{p} H_{\mathrm{d}}(\xi) = 0_{4\times 1},\ \nabla_{x_{\mathrm{c}}} H_{\mathrm{d}}(\xi) = 0_{2\ell\times 1}, \tag{6.3.2}$$

hold only at $q = q^*$. Since $M(q)$ is positive definite, $p = 0_{4\times 1}$ holds, and it follows from (5.1.1), (6.2.3), (6.2.6) and (6.3.2) that

$$\begin{aligned} 0_{2\ell\times 1} =& \nabla_{x_{\mathrm{c}}} H_{\mathrm{d}}(\xi) = \bar{H}_{12}^{\top} q_{\mathrm{a}}^{\mathrm{e}} + \bar{H}_{22} x_{\mathrm{c}}, \\ \dot{p} = 0_{4\times 1} =& -\begin{pmatrix} K_{\mathrm{s}}(q_{\mathrm{u}} - q_{\mathrm{a}}) \\ -K_{\mathrm{s}}(q_{\mathrm{u}} - q_{\mathrm{a}}) \end{pmatrix} - \begin{pmatrix} 0_{2\times 1} \\ \bar{H}_{11} q_{\mathrm{a}}^{\mathrm{e}} + \bar{H}_{12} x_{\mathrm{c}} \end{pmatrix}. \end{aligned}$$

Hence, $q_{\mathrm{u}} = q_{\mathrm{a}}$ hold, which leads to the following relation.

$$0_{2\ell\times 1} = \bar{H}_{12}^{\top} q_{\mathrm{a}}^{\mathrm{e}} + \bar{H}_{22} x_{\mathrm{c}},\ 0_{2\times 1} = \bar{H}_{11} q_{\mathrm{a}}^{\mathrm{e}} + \bar{H}_{12} x_{\mathrm{c}}. \tag{6.3.3}$$

Equation (6.3.3) can be summarized as

$$0_{(2\ell+2)\times 1} = \begin{pmatrix} \bar{H}_{11} & \bar{H}_{12} \\ \bar{H}_{12}^{\top} & \bar{H}_{22} \end{pmatrix} \begin{pmatrix} q_{\mathrm{a}}^{\mathrm{e}} \\ x_{\mathrm{c}} \end{pmatrix}. \tag{6.3.4}$$

Thus, from the positive definiteness of the Hessian of $\bar{H}(x_{\mathrm{c}}, q_{\mathrm{a}}^{\mathrm{e}})$, $0_{2\times 1} = q_{\mathrm{a}}^{\mathrm{e}} = q_{\mathrm{u}}^{\mathrm{e}}$ always holds. This completes the proof. □ □

The next section shows a simulation result of applying a lead-lag compensator designed according to Theorem 6.2.3, Remark 6.2.2, and Proposition 6.3.1.

6.3.2 Simulation results

In this example, the parameters of the system are set to d_{u_1}= d_{u_2}= 0.1, d_{a_1}= $d_{\mathrm{a}_2} = 1$, $a_1 = a_2 = 5$, $b = 1$, $\mathcal{I}_1 = \mathcal{I}_2 = 1$, $K_{\mathrm{s}_1} = K_{\mathrm{s}_1} = 1$, and q^* is set as $q^* = (1, -1, 1, -1)^{\top}$. Note that this is the case satisfying the assumption in Theorem 6.2.3. To simulate the situation where kinetic friction force is imposed, the simulation is performed assuming that an external force $\tilde{h}(p) = -(\mathrm{sign}(p_{\mathrm{a},1}), \mathrm{sign}(p_{\mathrm{a},2}))^\top \times 10^{-2}$ is added to the input, where sign($\cdot$) is a sign function. Figure 6.2 shows the responses of the positions and inputs of system (5.1.1) in the case that a proportional controller

$$u = -\frac{3}{10} q_{\mathrm{a}}^{\mathrm{e}} \tag{6.3.5}$$

is applied. The horizontal axes are time, and the vertical axes show positions and inputs, respectively. In the left side of Fig. 6.2, $q_{\mathrm{u},1}$, $q_{\mathrm{u},2}$, $q_{\mathrm{a},1}$ and $q_{\mathrm{a},2}$ are depicted by the red solid line, the blue solid line, the red dashed line, and the blue dashed line, respectively. In the right side of Fig. 6.2, u_1 is colored in red and u_2 is colored in blue. As shown in Fig. 6.2, the proportional controller exhibits oscillations. To suppress the oscillations, we design a lead compensator satisfying (6.2.11), where transfer function $\Psi_i(s)$ is designed as

$$\Psi_i(s) = -2\frac{s+1}{s+10}. \tag{6.3.6}$$

In this controller, there exist matrices F_{23}, F_{33}, $\bar{H}_{11}$, $\bar{H}_{12}$, and $\bar{H}_{22}$ (to ensure the asymptotical stability, $\bar{H}(x_{\mathrm{c}}, q_{\mathrm{a}}^{\mathrm{e}})$ is selected to be a strictly convex quadratic form as in Proposition 6.3.1) that satisfy (6.2.17) and **C1**, for example,

$$F_{23} = \begin{pmatrix} 0 & 0 \\ 0 & 0 \\ -8.76 \times 10^{-2} & 0 \\ 0 & -8.76 \times 10^{-2} \end{pmatrix}, \; F_{33} = \begin{pmatrix} -6.92 \times 10^{-3} & 0 \\ 0 & -6.92 \times 10^{-3} \end{pmatrix},$$

$$\bar{H}_{11} = \begin{pmatrix} 1.47 \times 10 & 0 \\ 0 & 1.47 \times 10 \end{pmatrix}, \bar{H}_{12} = \begin{pmatrix} -1.45 \times 10^{2} & 0 \\ 0 & -1.45 \times 10^{2} \end{pmatrix},$$

$$\bar{H}_{22} = \begin{pmatrix} 1.45 \times 10^{3} & 0 \\ 0 & 1.45 \times 10^{3} \end{pmatrix}.$$

The responses of q and u are depicted in Fig. 6.3 in the same way as in Fig. 6.2. Figure 6.3 shows that the lead compensator successfully suppresses the oscillations, but the steady-state errors caused by kinetic friction remain. To reduce the steady-state errors, we add a lag compensator to controller (6.3.6) so that (6.2.11) is satisfied, where the transfer function is designed as

$$\Psi_i(s) = -\frac{2}{3}\frac{s+1}{s+10}\frac{s+1}{s+1/3}. \tag{6.3.7}$$

In this controller, as in the case of the lead compensator, there exist matrices F_{23}, F_{33}, $\bar{H}_{11}$, $\bar{H}_{12}$, and $\bar{H}_{22}$ that satisfy (6.2.17) and **C1**, for example,

$$F_{23} = \begin{pmatrix} 0 & 0 & 0 & 0 \\ 0 & 0 & 0 & 0 \\ -3.18 \times 10^{-1} & 9.87 \times 10^{-3} & 0 & 0 \\ 0 & 0 & -3.18 \times 10^{-1} & 9.87 \times 10^{-3} \end{pmatrix},$$

$$F_{33} = \begin{pmatrix} -3.03 \times 10^{-2} & 1.03 \times 10^{-2} & 0 & 0 \\ -8.69 \times 10^{-3} & -5.02 \times 10^{-3} & 0 & 0 \\ 0 & 0 & -3.03 \times 10^{-2} & 1.03 \times 10^{-2} \\ 0 & 0 & -8.69 \times 10^{-3} & -5.02 \times 10^{-3} \end{pmatrix},$$

$$\bar{H}_{11} = \begin{pmatrix} 1.29 \times 10 & 0 \\ 0 & 1.29 \times 10 \end{pmatrix},$$

$$\bar{H}_{12} = \begin{pmatrix} -4.25 \times 10 & -1.26 \times 10^2 & 0 & 0 \\ 0 & 0 & -4.25 \times 10 & -1.26 \times 10^2 \end{pmatrix},$$

$$\bar{H}_{22} = \begin{pmatrix} 1.42 \times 10^2 & 4.18 \times 10^2 & 0 & 0 \\ 4.18 \times 10^2 & 1.33 \times 10^3 & 0 & 0 \\ 0 & 0 & 1.42 \times 10^2 & 4.18 \times 10^2 \\ 0 & 0 & 4.18 \times 10^2 & 1.33 \times 10^3 \end{pmatrix}.$$

The responses of q and u are depicted in Fig. 6.4 in the same way as in Fig. 6.2. Figure 6.4 shows that the lead-lag compensator achieves a reduction of the steady-state errors and suppression of the oscillations while ensuring stability.

6.4 Conclusion

This chapter proposed a PBC technique that is suitable to stabilize a class of mechanical systems, where the resulting output feedback controller can be tuned based

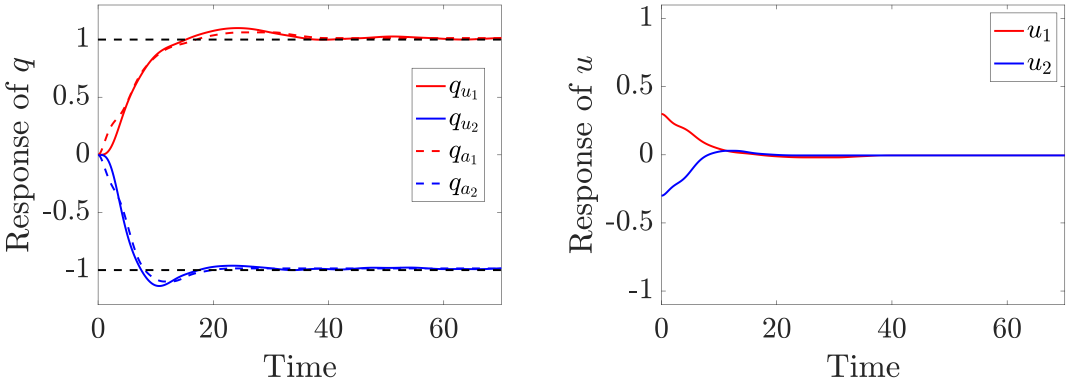

Figure 6.2: Simulation result for the proportional controller

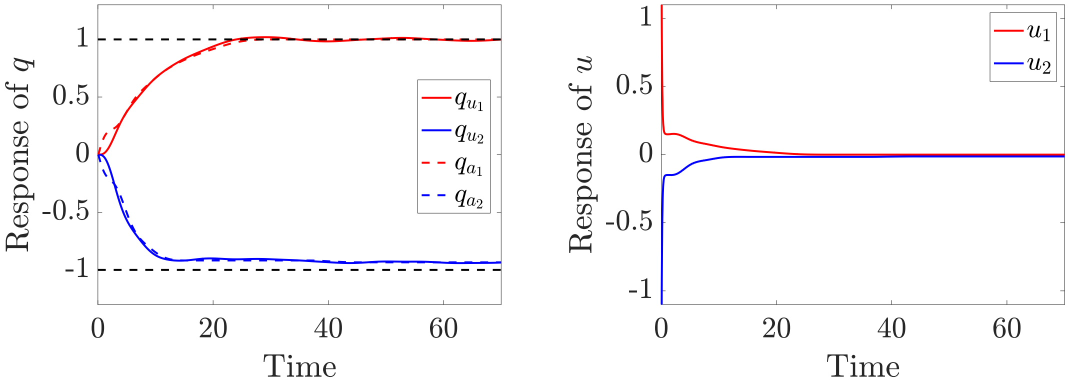

Figure 6.3: Simulation result for the lead compensator

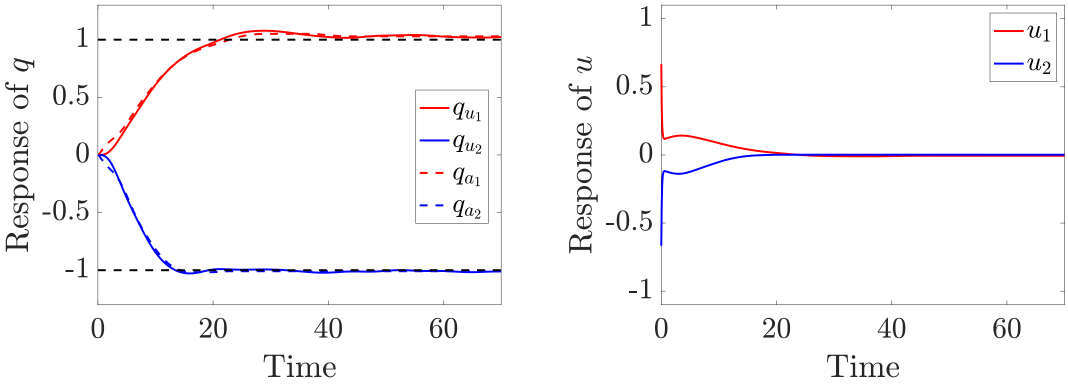

Figure 6.4: Simulation result for the lead-lag compensator

on frequency analysis. The proposed tuning method is useful for adding first-order transfer functions such as lead or lag compensators intuitively while guaranteeing stability. In addition, the controller has the advantage that the velocity measurements are not required. These advantages are shown through the numerical examples of the application of the controller to a mechanical system.

Chapter 7

Conclusions

7.1 Summary

In this thesis, we have proposed several methods to improve the performance of the feedforward and feedback control. The first part of this thesis focuses on feedforward control techniques and is devoted to proposing several numerical solution methods for finite-time sparse optimal control problems with focusing on the convergence property. In Chapter 2, we have proposed the locally deforming continuation method that gives the analytical relation between the variation of the continuation parameter and the proximity of the solutions before and after deformation. This relation tells us how to transform the continuation parameter so that the initial guess of the solution always falls within the convergence region. In Chapter 3, we have proposed the modified sparse Newton method that ensures quadratic convergence and can find an ℓ^1-optimal solution. In addition, the chapter proposed a practical algorithm that considers the input restrictions. The results obtained in these chapters will enable us to reliably calculate the input of the feedforward control and thus improve the practicality of the feedforward control techniques, including the sparse optimal control. One of the practical examples is shown in Chapter 4. In Chapter 4, we have introduced the application of the L^1/L^2-optimal control technique to the circular-clothoid trajectory generation problem. This application is useful for developing autonomous driving systems. In the application example, the locally deforming continuation method successfully obtains the desired trajectory. The second part of this thesis has focused on the feedback control techniques. Chapters 5 and 6 have proposed the passivity-based compensators that do not require velocity measurements and can be tuned in the frequency domain. The passivity-based lag compensator proposed in Chapter 5 can consider the input restrictions while ensuring stability and improving steady-state responses. In addition, the high-order compensators proposed in Chapter 6 enable us to reduce both oscillations and steady-state errors. These proposals give guidelines on how to tune the controller and contribute to improving the practicality of the feedback control techniques. The results obtained in this thesis will contribute to the development of control technology and enable the achievement of more challenging control tasks.

7.2 Discussion and future work

This section discusses future directions for research based on the results presented in this thesis.

7.2.1 Numerical solution methods for sparse optimal control problems

In Chapters 2 and 3, we focused on the convergence of algorithms and proposed the numerical solution methods in the framework of indirect and direct methods, respectively. When discussing convergence, the convergence rate and the radius of convergence become important. The convergence rate depends on how to reduce the error on the boundary conditions. Existing methods, such as the Newton method, consider the error as a function of the search parameters and use the information of the gradient of the function to achieve fast convergence. In other words, information on the gradient of the error function is necessary to discuss the convergence rate. For example, in the case of the indirect shooting method like the locally deforming continuation method, it is difficult to obtain the information of the gradient because the relationship between the search parameter and the error is given by integration. Therefore, it is difficult to improve the convergence rate for methods that cannot obtain gradient information, and for such methods, the goal should be to improve the algorithm in terms of the convergence region, as proposed in this thesis. On the other hand, if the gradient can be calculated easily, such as in the direct method or collocation method, the convergence rate can be improved by using the information on the gradient. The convergence region can also be easily studied in these methods. For example, in the modified sparse Newton method, the radius of convergence is given by using parameters such as the Lipschitz constant of the error function. However, it is difficult to estimate the radius of convergence concretely. In the modified sparse Newton method, for example, the radius of convergence is determined by the constants L and μ_0, but it is currently difficult to estimate these constants. Therefore, it is necessary to study how to estimate the radius of convergence in the future.

7.2.2 Tuning method for passivity-based controllers

In Chapters 5 and 6, we proposed methods to tune the output response while guaranteeing stability by expressing the passivity-based controllers in terms of a transfer function and organizing the relationship between the parameters of the transfer function and the stability condition. There is room for improvement in these methods. The first is the extension of the class of systems that the proposed method can handle. The systems under consideration in the proposed method do not have non-holonomic constraints and thus the proposed method cannot be applied to non-holonomic systems such as vehicles. In addition, the damping matrix of the system is assumed to have a specific structure. The first direction of improvement is to relax these constraints and expand the class of systems that can be handled. The second point to be improved is the constraint on the outputs. The proposed controllers use only the information of the actuated state variables, and therefore it cannot guarantee stability when using only the information of the unactuated variables. However, in practical use, it may be required to control using the information of unactuated variables due to the conditions of sensor installation. Therefore, we should consider extending the proposed method to use unactuated variables in control. The third point is the quantitative evaluation of the control performance. In the proposed method, it is possible to tune the responses around the desired equilibria intuitively by designing the transfer function, but no analytical result on to what extent the steady-state errors can be reduced. Therefore, in the future, it is necessary to provide some analytical evaluation of the response obtained as a result of tuning.

Appendix A

Proof of Theorem 6.2.1

Proof. Assume that (6.2.3) and (6.2.4) holds. It follows from (6.2.3) that (6.2.2) takes the form

$$\begin{aligned}
\dot{\xi} =& \begin{pmatrix} 0_{n\times n} & I_n & 0_{n\times m\ell} \\ -I_n & -D(q,p) & F_{23}(x_{\mathrm{c}}, y(q)) \\ 0_{m\ell\times n} & 0_{m\ell\times n} & F_{33}(x_{\mathrm{c}}, y(q)) \end{pmatrix} \nabla_{\xi} H_{\mathrm{d}}(\xi) \\
=&\frac{1}{2}\left\{ \begin{pmatrix} 0_{n\times n} & 2I_n & 0_{n\times m\ell} \\ -2I_n & 0_{n\times n} & F_{23} \\ 0_{m\ell\times n} & -F_{23}^{\top} & F_{33} - F_{33}^{\top} \end{pmatrix} \right. \\
& \left. - \begin{pmatrix} 0_{n\times n} & 0_{n\times n} & 0_{n\times m\ell} \\ 0_{n\times n} & 2D & -F_{23} \\ 0_{m\ell\times n} & -F_{23}^{\top} & -F_{33} - F_{33}^{\top} \end{pmatrix} \right\} \nabla_{\xi} H_{\mathrm{d}}(\xi) \\
=&\frac{1}{2}(\mathcal{J} - \mathcal{D}) \nabla_{\xi} H_{\mathrm{d}}(\xi). \qquad \text{(A.0.1)}
\end{aligned}$$

Since $\mathcal{J}^{\top} = -\mathcal{J}$ and $\mathcal{D} \succeq 0$ hold from the condition (6.2.4), closed-loop system (6.2.2) is a pH system. Note that the arguments of the matrices are omitted in the second and subsequent lines. By expanding (A.0.1), we have

$$\begin{aligned}
\dot{q} =& \nabla_p H_{\mathrm{d}}(\xi) = \nabla_p H(q,p), \\
\dot{p} =& -\nabla_q H_{\mathrm{d}}(\xi) - D(q,p) \nabla_p H_{\mathrm{d}}(\xi) \\
& + F_{23}(x_{\mathrm{c}}, y(q)) \nabla_{x_{\mathrm{c}}} H_{\mathrm{d}}(\xi) \\
=& -\nabla_q H(q,p) - D(q,p) \nabla_p H(q,p) - \nabla_q \bar{H}(x_{\mathrm{c}}, y(q)) \\
& + F_{23}(x_{\mathrm{c}}, y(q)) \nabla_{x_{\mathrm{c}}} \bar{H}(x_{\mathrm{c}}, y(q)) \\
=& -\nabla_q H(q,p) - D(q,p) \nabla_p H(q,p) + G h^{\mathrm{c}}(x_{\mathrm{c}}, y(q)), \\
\dot{x}_{\mathrm{c}} =& F_{33}(x_{\mathrm{c}}, y(q)) \nabla_{x_{\mathrm{c}}} H_{\mathrm{d}}(\xi) \\
=& F_{33}(x_{\mathrm{c}}, y(q)) \nabla_{x_{\mathrm{c}}} \bar{H}(x_{\mathrm{c}}, y(q)) \\
=& f^{\mathrm{c}}(x_{\mathrm{c}}, y(q)),
\end{aligned}$$

and thus (6.2.2) represents closed-loop system (5.1.1) with (6.2.1) under the conditions (6.2.3) and (6.2.4). This completes the proof of the sufficient condition. Next, we prove the necessity. Substituting (6.2.1) in (5.1.1) leads to

$$\dot{q} = \nabla_p H(q,p), \tag{A.0.2}$$

$$\begin{aligned}\dot{p} =& -\nabla_q H(q,p) - D(q,p)\nabla_p H(q,p)\\ &+ Gh^{\mathrm{c}}(x_{\mathrm{c}}, y(q)),\end{aligned} \tag{A.0.3}$$

$$\dot{x}_{\mathrm{c}} = f^{\mathrm{c}}(x_{\mathrm{c}}, y(q)), \tag{A.0.4}$$

and expanding (6.2.2) leads to

$$\begin{aligned}\dot{q} =& F_{11}(x_{\mathrm{c}}, y(q))\nabla_q H_{\mathrm{d}}(\xi) + F_{12}(x_{\mathrm{c}}, y(q))\nabla_p H_{\mathrm{d}}(\xi)\\ &+ F_{13}(x_{\mathrm{c}}, y(q))\nabla_{x_{\mathrm{c}}} H_{\mathrm{d}}(\xi),\end{aligned} \tag{A.0.5}$$

$$\begin{aligned}\dot{p} =& F_{21}(x_{\mathrm{c}}, y(q))\nabla_q H_{\mathrm{d}}(\xi)\\ &+ \left(F_{22}(x_{\mathrm{c}}, y(q)) - D(q,p)\right)\nabla_p H_{\mathrm{d}}(\xi)\\ &+ F_{23}(x_{\mathrm{c}}, y(q))\nabla_{x_{\mathrm{c}}} H_{\mathrm{d}}(\xi),\end{aligned} \tag{A.0.6}$$

$$\begin{aligned}\dot{x}_{\mathrm{c}} =& F_{31}(x_{\mathrm{c}}, y(q))\nabla_q H_{\mathrm{d}}(\xi) + F_{32}(x_{\mathrm{c}}, y(q))\nabla_p H_{\mathrm{d}}(\xi)\\ &+ F_{33}(x_{\mathrm{c}}, y(q))\nabla_{x_{\mathrm{c}}} H_{\mathrm{d}}(\xi),\end{aligned} \tag{A.0.7}$$

Noting that

$$\begin{aligned}\nabla_q H(q,p) &= \frac{\partial}{\partial q}\left(\frac{1}{2}p^\top M(q)^{-1}p\right) + \frac{\partial V(q)}{\partial q},\\ \nabla_p H(q,p) &= M(q)^{-1}p,\\ \nabla_p \bar{H}(x_{\mathrm{c}}, y(q)) &= 0_{n\times 1},\\ \nabla_{x_{\mathrm{c}}} H(q,p) &= 0_{m\ell\times 1},\end{aligned}$$

comparison of (A.0.2) and (A.0.5) yields

$$\begin{aligned}0_{n\times 1} =& F_{11}(x_{\mathrm{c}}, y(q))\frac{\partial}{\partial q}\left(\frac{1}{2}p^\top M(q)^{-1}p\right)\\ &+ F_{11}(x_{\mathrm{c}}, y(q))\frac{\partial V(q)}{\partial q}\\ &+ F_{11}(x_{\mathrm{c}}, y(q))\nabla_q \bar{H}(x_{\mathrm{c}}, y(q))\\ &+ (F_{12}(x_{\mathrm{c}}, y(q)) - I_n)M(q)^{-1}p\\ &+ F_{13}(x_{\mathrm{c}}, y(q))\nabla_{x_{\mathrm{c}}} \bar{H}(x_{\mathrm{c}}, y(q)).\end{aligned} \tag{A.0.8}$$

Since $M(q)^{-1}$ is not constant, (A.0.8) is a quadratic equation for p, and the coefficients of the quadratic term and the linear term have to be zero so that (A.0.8) holds for any p. Thus, we have the following relation.

$$F_{11}(x_{\mathrm{c}}, y(q)) = 0_{n\times n}, \tag{A.0.9}$$

$$F_{12}(x_{\mathrm{c}}, y(q)) = I_n, \tag{A.0.10}$$

$$F_{13}(x_{\mathrm{c}}, y(q)) = 0_{n\times m\ell}. \tag{A.0.11}$$

In the same way, by comparing (A.0.3) and (A.0.6), we have

$$\begin{aligned}0_{n\times 1} =&(F_{21}(x_{\mathrm{c}}, y(q)) + I_n)\left(\frac{\partial}{\partial q}\left(\frac{1}{2}p^\top M(q)^{-1}p\right)\right)\\ &+ (F_{21}(x_{\mathrm{c}}, y(q)) + I_n)\left(\frac{\partial V(q)}{\partial q}\right)\\ &+ F_{21}(x_{\mathrm{c}}, y(q))\nabla_q \bar{H}(x_{\mathrm{c}}, y(q))\\ &+ F_{22}(x_{\mathrm{c}}, y(q))M(q)^{-1}p\\ &+ F_{23}(x_{\mathrm{c}}, y(q))\nabla_{x_{\mathrm{c}}} \bar{H}(x_{\mathrm{c}}, y(q)) - Gh^{\mathrm{c}}(x_{\mathrm{c}}, y(q)),\end{aligned}$$

and this yields the following relation.

$$F_{21}(x_{\mathrm{c}}, y(q)) =- I_n \tag{A.0.12}$$

$$F_{22}(x_{\mathrm{c}}, y(q)) =0_{n\times n} \tag{A.0.13}$$

$$\begin{aligned}Gh^{\mathrm{c}}(x_{\mathrm{c}}, y(q)) =& - \nabla_q \bar{H}(x_{\mathrm{c}}, y(q))\\ &+ F_{23}(x_{\mathrm{c}}, y(q))\nabla_{x_{\mathrm{c}}} \bar{H}(x_{\mathrm{c}}, y(q))\end{aligned} \tag{A.0.14}$$

As for the (A.0.4) and (A.0.7), the equality

$$\begin{aligned}0_{m\ell\times 1} =&F_{31}(x_{\mathrm{c}}, y(q))\frac{\partial}{\partial q}\left(\frac{1}{2}p^\top M(q)^{-1}p\right)\\ &+ F_{31}(x_{\mathrm{c}}, y(q))\frac{\partial V(q)}{\partial q}\\ &+ F_{31}(x_{\mathrm{c}}, y(q))\nabla_q \bar{H}(x_{\mathrm{c}}, y(q))\\ &+ F_{32}(x_{\mathrm{c}}, y(q))M(q)^{-1}p\\ &+ F_{33}(x_{\mathrm{c}}, y(q))\nabla_{x_{\mathrm{c}}} \bar{H}(x_{\mathrm{c}}, y(q)) - f^{\mathrm{c}}(x_{\mathrm{c}}, y(q))\end{aligned}$$

holds, and thus we have

$$F_{31} = 0_{m\ell\times n}, \tag{A.0.15}$$

$$F_{32} = 0_{m\ell\times n}, \tag{A.0.16}$$

$$f^{\mathrm{c}}(q, x_{\mathrm{c}}) = F_{33}(x_{\mathrm{c}}, y(q))\nabla_{x_{\mathrm{c}}} \bar{H}(x_{\mathrm{c}}, y(q)). \tag{A.0.17}$$

At the last thing, it follows from (A.0.9)-(A.0.17) that the parametrized closed-loop system is rewritten as (A.0.1), and since the closed-loop system is a pH system, we have

$$\begin{pmatrix} 2D(q,p) & -F_{23}(x_{\mathrm{c}},y(q)) \\ -F_{23}(x_{\mathrm{c}},y(q))^\top & -F_{33}(x_{\mathrm{c}},y(q))-F_{33}(x_{\mathrm{c}},y(q))^\top \end{pmatrix} \succeq 0. \tag{A.0.18}$$

The conditions (A.0.9)-(A.0.18) equal to (6.2.3) and (6.2.4), which completes the proof. □

Bibliography

[1] K. Zhou and J. C. Doyle, *Essentials of robust control.* Prentice hall Upper Saddle River, NJ, 1998, vol. 104.

[2] X. Zhang, M. Kamgarpour, A. Georghiou, P. Goulart, and J. Lygeros, “Robust optimal control with adjustable uncertainty sets,” *Automatica*, vol. 75, pp. 249–259, 2017.

[3] C. E. Garcia, D. M. Prett, and M. Morari, “Model predictive control: Theory and practice—a survey,” *Automatica*, vol. 25, no. 3, pp. 335–348, 1989.

[4] T. Ohtsuka, “A continuation/gmres method for fast computation of nonlinear receding horizon control,” *Automatica*, vol. 40, no. 4, pp. 563–574, 2004.

[5] K. Hamada, I. Maruta, K. Fujimoto, and K. Hamamoto, “On hands-off trajectory generation for a two-wheeled rover based on l^1/l^2-optimal control,” in *IECON 2018 - 44th Annual Conference of the IEEE Industrial Electronics Society*, 2018, pp. 2601–2606.

[6] S. Saban and S. Swaminathan, “Real time trajectory optimization of l1 optimal control problem using gauss-pseudo-spectral method,” *IFAC-PapersOnLine*, vol. 53, no. 1, pp. 258–265, 2020.

[7] Y. Kayama, “Optimal trajectory design and control for low-thrust spacecraft in multi-body dynamics,” Ph.D. dissertation, Kyusyu University, 2021.

[8] A. V. Rao, “A survey of numerical methods for optimal control,” *Advances in the Astronautical Sciences*, vol. 135, no. 1, pp. 497–528, 2009.

[9] H. G. Bock and K.-J. Plitt, “A multiple shooting algorithm for direct solution of optimal control problems,” *IFAC Proceedings Volumes*, vol. 17, no. 2, pp. 1603–1608, 1984.

[10] G. Elnagar, M. A. Kazemi, and M. Razzaghi, “The pseudospectral legendre method for discretizing optimal control problems,” *IEEE transactions on Automatic Control*, vol. 40, no. 10, pp. 1793–1796, 1995.

[11] J. Lan and J. Li, “Newton-kantorovich/radau pseudospectral solution rightarrow rigid spacecraft time-optimal three-axis reorientation,” *Advances in Space Research*, 2020.

[12] Y. Kanai, T. Kodama, K. Hamada, K. Fujimoto, and I. Maruta, “On sparse trajectory planning via newton ’ s method for under-determined systems (in japanese),” in *Proceedings of the 65th Annual Conference of the Institute of Systems, Control and Information Engineers (ISCIE)*, 2021, pp. 88–94.

[13] H. P. Geering, *Optimal control with engineering applications.* Springer, 2007.

[14] S. N. Ha, “A nonlinear shooting method for two-point boundary value problems,” *Computers & Mathematics with Applications*, vol. 42, no. 10-11, pp. 1411–1420, 2001.

[15] R. Bertrand and R. Epenoy, “New smoothing techniques for solving bang-bang optimal control problems–numerical results and statistical interpretation,” *Optimal Control Applications and Methods*, vol. 23, no. 4, pp. 171–197, 2002.

[16] G. Vossen and H. Maurer, “On l1-minimization in optimal control and applications to robotics,” *Optimal Control Applications and Methods*, vol. 27, no. 6, pp. 301–321, 2006.

[17] D. Garg, M. Patterson, W. W. Hager, A. V. Rao, D. A. Benson, and G. T. Huntington, “A unified framework for the numerical solution of optimal control problems using pseudospectral methods,” *Automatica*, vol. 46, no. 11, pp. 1843–1851, 2010.

[18] S. Roberts and J. Shipman, “Continuation in shooting methods for two-point boundary value problems,” *Journal of mathematical analysis and applications*, vol. 18, no. 1, pp. 45–58, 1967.

[19] W. Bosarge, “Iterative continuation and the solution of nonlinear two-point boundary value problems,” *Numerische Mathematik*, vol. 17, no. 4, pp. 268–283, 1971.

[20] P. Deuflhard, H.-J. Pesch, and P. Rentrop, "A modified continuation method for the numerical solution of nonlinear two-point boundary value problems by shooting techniques," *Numerische Mathematik*, vol. 26, no. 3, pp. 327–343, 1976.

[21] S. N. Chow, J. Mallet-Paret, and J. A. Yorke, "Finding zeroes of maps: homotopy methods that are constructive with probability one," *Mathematics of Computation*, vol. 32, no. 143, pp. 887–899, 1978.

[22] J. F. Bonnans and A. Hermant, "Stability and sensitivity analysis for optimal control problems with a first-order state constraint and application to continuation methods," *ESAIM: Control, Optimisation and Calculus of Variations*, vol. 14, no. 4, pp. 825–863, 2008.

[23] M. Mehrpouya, M. Shamsi, and M. Razzaghi, "A combined adaptive control parametrization and homotopy continuation technique for the numerical solution of bang–bang optimal control problems," *The ANZIAM Journal*, vol. 56, no. 1, pp. 48–65, 2014.

[24] B. Pan, P. Lu, X. Pan, and Y. Ma, "Double-homotopy method for solving optimal control problems," *Journal of Guidance, Control, and Dynamics*, vol. 39, no. 8, pp. 1706–1720, 2016.

[25] K. Bergman and D. Axehill, "Combining homotopy methods and numerical optimal control to solve motion planning problems," in *2018 IEEE Intelligent Vehicles Symposium (IV)*. IEEE, 2018, pp. 347–354.

[26] B. Polyak and A. Tremba, "Sparse solutions of optimal control via newton method for under-determined systems," *Journal of Global Optimization*, vol. 76, no. 3, pp. 613–623, 2020.

[27] D. K. Wilde, "Computing clothoid segments for trajectory generation," in *IEEE/RSJ The International Conference on Intelligent Robots and Systems 2009*. IEEE, 2009, pp. 2440–2445.

[28] C. Alia, T. Gilles, T. Reine, and C. Ali, "Local trajectory planning and tracking of autonomous vehicles, using clothoid tentacles method," in *IEEE Intelligent Vehicles Symposium (IV) 2015*. IEEE, 2015, pp. 674–679.

[29] V. Schneider, P. Piprek, S. P. Schatz, T. Baier, C. Dörhöfer, M. Hochstrasser, A. Gabrys, E. Karlsson, C. Krause, P. J. Lauffs, *et al.*, "Online trajectory generation using clothoid segments," in *The 14th International Conference on Control, Automation, Robotics and Vision (ICARCV) 2016.* IEEE, 2016, pp. 1–6.

[30] D. H. Shin, S. Singh, and W. Whittaker, "Path generation for a robot vehicle using composite clothoid segments," *IFAC Proceedings Volumes*, vol. 25, no. 6, pp. 443–448, 1992.

[31] A. Kelly and B. Nagy, "Reactive nonholonomic trajectory generation via parametric optimal control," *The International Journal of Robotics Research*, vol. 22, no. 7-8, pp. 583–601, 2003.

[32] A. J. van der Schaft and D. Jeltsema, *Port-Hamiltonian Systems Theory: An Introductory Overview*, 2014, vol. 1, no. 2-3.

[33] V. Duindam, A. Macchelli, S. Stramigioli, and H. Bruyninckx, *Modeling and control of complex physical systems: the port-Hamiltonian approach.* Springer Science & Business Media, 2009.

[34] R. Ortega, A. J. van der Schaft, I. Mareels, and B. Maschke, "Putting energy back in control," *IEEE Control Systems Magazine*, vol. 21, no. 2, pp. 18–33, 2001.

[35] R. Ortega, J. A. Loría-Perez, P. J. Nicklasson, and H. J. Sira-Ramirez, *Passivity-based control of Euler-Lagrange systems : mechanical, electrical and electromechanical applications.* Springer Science & Business Media, 2013.

[36] S. Sakai and S. Stramigioli, *Passivity based force control of hydraulic robots.* IFAC, 2009, vol. 42, no. 16.

[37] R. Ortega, M. W. Spong, F. Gómez-Estern, and G. Blankenstein, "Stabilization of a class of underactuated mechanical systems via interconnection and damping assignment," *IEEE transactions on automatic control*, vol. 47, no. 8, pp. 1218–1233, 2002.

[38] J. A. Acosta, R. Ortega, A. Astolfi, and A. D. Mahindrakar, "Interconnection and damping assignment passivity-based control of mechanical systems with underactuation degree one," *IEEE Transactions on Automatic Control*, vol. 50, no. 12, pp. 1936–1955, 2005.

[39] J. G. Romero, A. Donaire, and R. Ortega, “Robust energy shaping control of mechanical systems,” *Systems & Control Letters*, vol. 62, no. 9, pp. 770–780, 2013.

[40] J. G. Romero, A. Donaire, R. Ortega, and P. Borja, “Global stabilisation of underactuated mechanical systems via pid passivity-based control,” *Automatica*, vol. 96, pp. 178–185, 2018.

[41] K. Fujimoto, S. Sakai, and T. Sugie, “Passivity based control of a class of hamiltonian systems with nonholonomic constraints,” *Automatica*, vol. 48, no. 12, pp. 3054–3063, 2012.

[42] H. Vazquez-Leal, A. Marin-Hernandez, Y. Khan, A. Yıldırım, U. Filobello-Nino, R. Castañeda-Sheissa, and V. M. Jimenez-Fernandez, “Exploring collision-free path planning by using homotopy continuation methods,” *Applied Mathematics and Computation*, vol. 219, no. 14, pp. 7514–7532, 2013.

[43] T. Ohtsuka and H. Fujii, “Stabilized continuation method for solving optimal control problems,” *Journal of Guidance, Control, and Dynamics*, vol. 17, no. 5, pp. 950–957, 1994.

[44] M. Nagahara, D. E. Quevedo, and D. Nešić, “Maximum hands-off control: a paradigm of control effort minimization,” *IEEE Transactions on Automatic Control*, vol. 61, no. 3, pp. 735–747, 2015.

[45] D. Liberzon, *Calculus of Variations and Optimal Control Theory: A Concise Introduction.* Princeton University Press, 2011. [Online]. Available: https://doi.org/10.1515/9781400842643

[46] F. Clarke, *Functional analysis, calculus of variations and optimal control.* Springer Science & Business Media, 2013, vol. 264.

[47] D. Chatterjee, M. Nagahara, D. E. Quevedo, and K. M. Rao, “Characterization of maximum hands-off control,” *Systems & Control Letters*, vol. 94, pp. 31–36, 2016. [Online]. Available: https://www.sciencedirect.com/science/article/pii/S0167691116300330

[48] R. Howard, “The gronwall inequality,” *lecture notes*, 1998.

[49] M. Elad, *Sparse and redundant representations: from theory to applications in signal and image processing.* Springer Science & Business Media, 2010.

[50] B. Polyak and A. Tremba, “Sparse solutions of optimal control with l^1-objective,” in *2020 European Control Conference (ECC)*, 2020, pp. 1707–1712.

[51] W. H. Press, S. A. Teukolsky, W. T. Vetterling, and B. P. Flannery, *Numerical Recipes in C: Japanese Edition.* Gijutsu Hyoron Sha, Tokyo, 1993.

[52] B. Polyak, “Gradient methods for solving equations and inequalities,” *USSR Computational Mathematics and Mathematical Physics*, vol. 4, pp. 17–32, 12 1964.

[53] B. Polyak and A. Tremba, “New versions of newton method: step-size choice, convergence domain and under-determined equations,” *Optimization Methods and Software*, vol. 35, no. 6, pp. 1272–1303, 2020.

[54] M. Grant and S. Boyd, “CVX: Matlab software for disciplined convex programming, version 2.1,” http://cvxr.com/cvx, Mar. 2014.

[55] ——, “Graph implementations for nonsmooth convex programs,” in *Recent Advances in Learning and Control*, ser. Lecture Notes in Control and Information Sciences, V. Blondel, S. Boyd, and H. Kimura, Eds. Springer-Verlag Limited, 2008, pp. 95–110, http://stanford.edu/ boyd/graph_dcp.html.

[56] S. Miura, I. Kuronuma, and K. Hamamoto, “Next generation construction production system: On automated construction machinery,” in *Proceedings of the seventh civil engineering conference in the Asian region*, 2016.

[57] T. Narumi, S. Aoki, T. Yokoshima, N. Uyama, S. Wakabayashi, G. Tabuchi, and H. Kanamori, “Preliminary system design for unmanned building construction in extreme environments,” in *The International Conference on Research and Education in Mechatronics (REM) 2017.* IEEE, 2017, pp. 1–6.

[58] H. Delingette, M. Hebert, and K. Ikeuchi, “Trajectory generation with curvature constraint based on energy minimization,” in *IEEE/RSJ The International Workshop on Intelligent Robots and Systems Intelligence for Mechanical Systems, Proceedings of IROS’91.* IEEE, 1991, pp. 206–211.

[59] R. M. Murray and S. S. Sastry, “Nonholonomic motion planning: Steering using sinusoids,” *IEEE Transactions on Automatic Control*, vol. 38, no. 5, pp. 700–716, 1993.

[60] Y. J. Kanayama and B. I. Hartman, "Smooth local-path planning for autonomous vehicles1," *The International Journal of Robotics Research*, vol. 16, no. 3, pp. 263–284, 1997.

[61] J. Reuter, "Mobile robots trajectories with continuously differentiable curvature: an optimal control approach," in *IEEE/RSJ 1998 The International Conference on Intelligent Robots and Systems. Innovations in Theory, Practice and Applications (Cat. No. 98CH36190). Proceedings*, vol. 1. IEEE, 1998, pp. 38–43.

[62] B. Nagy and A. Kelly, "Trajectory generation for car-like robots using cubic curvature polynomials," *Field and Service Robots*, vol. 11, 2001.

[63] T. M. Howard and A. Kelly, "Optimal rough terrain trajectory generation for wheeled mobile robots," *The International Journal of Robotics Research*, vol. 26, no. 2, pp. 141–166, 2007.

[64] P. Tokekar, N. Karnad, and V. Isler, "Energy-optimal trajectory planning for car-like robots," *Autonomous Robots*, vol. 37, no. 3, pp. 279–300, 2014.

[65] M. Athans and P. L. Falb, *Optimal control: an introduction to the theory and its applications.* Courier Corporation, 2013, ch. 3, 6.

[66] M. Nagahara, D. E. Quevedo, and D. Nesic, "Maximum hands-off control and l^1 optimality," in *IEEE 52nd Annual Conference on Decision and Control (CDC) 2013.* IEEE, 2013, pp. 3825–3830.

[67] D. Jeltsema and J. M. A. Scherpen, "Tuning of Passivity-Preserving Controllers for Switched-Mode Power Converters," *IEEE Transactions on Automatic Control*, vol. 49, no. 8, pp. 1333–1344, 2004.

[68] D. A. Dirksz and J. M. A. Scherpen, "Tuning of dynamic feedback control for nonlinear mechanical systems," in *2013 European Control Conference (ECC)*, 2013, pp. 173–178.

[69] D. A. Dirksz, J. M. A. Scherpen, A. J. van der Schaft, and M. Steinbuch, "Notch filters for port-hamiltonian systems," *IEEE Transactions on Automatic Control*, vol. 60, no. 9, pp. 2440–2445, 2015.

[70] C. Chan-Zheng, P. Borja, and J. M. A. Scherpen, "Tuning rules for a class of passivity-based controllers for mechanical systems," *IEEE Control Systems Letters*, pp. 1–1, 2020.

[71] K. Ogata, *Modern Control Engineering.* Prentice Hall, 2002, vol. 4.

[72] K. J. Astrom and L. Rundqwist, "Integrator windup and how to avoid it," in *1989 American Control Conference.* IEEE, 1989, pp. 1693–1698.

[73] D. A. Dirksz and J. M. Scherpen, "On tracking control of rigid-joint robots with only position measurements," *IEEE Transactions on Control Systems Technology*, vol. 21, no. 4, pp. 1510–1513, 2012.

[74] J. Ferguson, A. Donaire, R. Ortega, and R. H. Middleton, "Matched disturbance rejection for a class of nonlinear systems," *IEEE Transactions on Automatic Control*, vol. 65, no. 4, pp. 1710–1715, 2020.

[75] T. C. Wesselink, P. Borja, and J. M. A. Scherpen, "Saturated control without velocity measurements for planar robots with flexible joints," in *2019 IEEE 58th Conference on Decision and Control (CDC)*, 2019, pp. 7093–7098.

[76] H. K. Khalil and J. W. Grizzle, *Nonlinear systems.* Prentice hall Upper Saddle River, NJ, 2002, vol. 3.

[77] *2 DOF Serial Flexible Joint, Reference Manual*, 1st ed., Quanser, 2013.

List of Publications

Peer-reviewed journal articles

1. Kiyoshi Hamada, Pablo Borja, Jacquelien MA Scherpen, Kenji Fujimoto, and Ichiro Maruta, “Passivity-Based Lag-Compensators With Input Saturation for Mechanical Port-Hamiltonian Systems Without Velocity Measurements,” IEEE Control Systems Letters, vol. 5, no. 4, pp. 1285-1290, 2021. **Chapter 5** (©2020 IEEE. “ In reference to IEEE copyrighted material which is used with permission in this thesis, the IEEE does not endorse any of Kyoto University ’ s products or services. Internal or personal use of this material is permitted. If interested in reprinting/republishing IEEE copyrighted material for advertising or promotional purposes or for creating new collective works for resale or redistribution, please go to http://www.ieee.org/ publications_standards/publications/rights/rights_link.html to learn how to obtain a License from RightsLink. If applicable, University Microfilms and/or ProQuest Library, or the Archives of Canada may supply single copies of the dissertation. ”)

2. Kiyoshi Hamada, Ichiro Maruta, Kenji Fujimoto, and Kenniti Hamamoto, “Locally deforming continuation method based on a shooting method for a class of optimal control problems,” SICE Journal of Control, Measurement, and System Integration, vol. 14, no. 2, pp. 80-89, 2021. **Chapter 2** (©2021 The Author(s). Published by Informa UK Limited, trading as Taylor & Francis Group. This is an Open Access article distributed under the terms of the Creative Commons Attribution License (http://creativecommons.org/licenses/by/4.0/), which permits unrestricted use, distribution, and reproduction in any medium, provided the original work is properly cited.)

3. Kiyoshi Hamada, Ichiro Maruta, Kenji Fujimoto, and Kenniti Hamamoto, “On the Method of Generating a Circular-Clothoid Trajectory for Front-Steering

Vehicles Based on L1/L2-Optimal Control," SICE Journal of Control, Measurement, and System Integration, vol. 13, no. 3, pp. 107-113, 2020. **Chapter 4**

Peer-reviewed conference proceedings

1. Kiyoshi Hamada, Pablo Borja, Kenji Fujimoto, Ichiro Maruta, and Jacquelien M. A. Scherpen, "On Passivity-Based High-Order Compensators for Mechanical Port-Hamiltonian Systems Without Velocity Measurements," In Preprints of the Third IFAC Conference on Modelling, Identification and Control of Nonlinear Systems, pp. 306–311, 2021. **Chapter 6** (©2021 The Authors. This is an open access article under the CC BY-NC-ND license. Peer review under responsibility of International Federation of Automatic Control. 10.1016/j.ifacol.2021.10.367)

2. Kiyoshi Hamada, Ichiro Maruta, Kenji Fujimoto, and Kenniti Hamamoto, "On Trajectory Planning for Hydraulic Excavators Based on Time-varying Lp-Optimal Control," In Proceedings of the SICE Annual Conference 2020, pp. 1523–1526, 2020.

3. Kiyoshi Hamada, Ichiro Maruta, Kenji Fujimoto, and Kenniti Hamamoto, "On Circular-Clothoid Trajectory Generation for Front Steering Vehicles Based on L1/L2-Optimal Control", In Proceedings of the SICE Annual Conference 2019, pp. 1741–1744, 2019. **Chapter 4**